A photophysical study of novel silicon and zinc phthalocyanines

FitzGerald, Simon

A Photophysical Study of Novel Silicon and Zinc Phthalocyanines

Simon FitzGerald

Department of Chemistry,
University of Durham,
Durham, U.K.

Submitted in partial fulfilment of the requirements for the degree of Doctor of Philosophy, University of Durham.

August 2002

DECLARATION

The work described in this thesis was carried out in the Chemistry Department of the University of Durham between October 1999 and August 2002. The thesis is the work of the author except where acknowledged by reference, and has not been submitted for any other degree.

STATEMENT OF COPYRIGHT

ABSTRACT

Phthalocyanines are an important class of compounds with many commercial applications. The core macrocycle is chemically robust, such that a wide variety of substituted species with interesting properties can be synthesised. The work reported in this thesis represents a detailed photophysical study of both known and novel substituted silicon and zinc phthalocyanines.

The behaviour of tetrasulfonated zinc phthalocyanine ($ZnPcS_4$) in aqueous acetonitrile is investigated. This work shows the sensitivity of $ZnPcS_4$ to pH, caused by protonation of the phthalocyanine on the bridging azomethine nitrogen atoms. The spectral perturbation that results includes red shifted absorption and emission bands, with a reduced fluorescence lifetime relative to the unprotonated species.

Axially substituted silicon phthalocyanines functionalised through bis-esters have highly resolved spectral features due to reduced ring interactions, whilst the light core atom results in excellent fluorescence quantum yields and lifetimes. Electron rich axial substituents (in this case methoxybenzenes) cause quenching of the phthalocyanine fluorescence through an electron transfer mechanism, and the extent of quenching is related to both the oxidation potential of the quencher and the chain length/flexibility.

A number of silicon phthalocyanines with tetrathiafulvalene (TTF) containing substituents are also investigated. TTF is known to quench phthalocyanine fluorescence very efficiently, but this current work shows that the degree of quenching is strongly distance dependent. The oxidation potential of TTF is low, and this allows the selective electrochemical oxidation of TTF without affecting the phthalocyanine. It is shown that such oxidation causes a reversal of the electron transfer mechanism.

The phenomenon of fluorescent dimers in phthalocyanine chemistry is rarely observed, and most reports arise from spectral and experimental artefacts. However a solketal substituted zinc phthalocyanine and some of its derivatives are conclusively shown to demonstrate this behaviour. At low temperature a broadened absorption profile is observed, with new emission centred at ~750 nm - such spectral behaviour agrees with Exciton Theory for a clamshell dimer. Flash photolysis studies at intermediate temperatures highlights the dynamic nature of the dimer species - absorption of a photon results in the separation of the dimer, followed by fast recombination.

ACKNOWLEDGEMENTS

First and foremost sincere thanks go to Andy Beeby who has encouraged, cajoled and supported me, as and when required, throughout my research at Durham. Without him this thesis most certainly would not exist. Memories of his kind friendship and hospitality will always remain with me, wherever I am. I also extend deep gratitude to him for allowing me open access to his delightful office window – such views I shall probably never encounter again, alas!

Those who have had to suffer my very real eccentricities whilst working in an often rather crowded research environment deserve medals for surviving. Fellow postgraduates Allison, Lisa, Sylvia and Karen have all made it through the FitzGerald Era, but sadly won't be receiving medals. This honourable mention of thanks will have to suffice.

Chris Farren, phthalocyanine synthesiser extraordinaire, made possible the majority of work outlined in this thesis, and proved a good friend in the process. Our delight at various shades of blue, green and blue-green kept us going through thick and thin. As a team we were "mint" and definitely the "top banana".

For useful discussion and helpful advice thanks go to Steve Faulkner, Paul Low and Martin Bryce. In addition, there are many people in the department who provided help and advice on all manner of topics – in particular the workshop technicians (Kelvin, Barry, Jimmy and Neil) fixed and built nameless devices vital for the work in this thesis.

My parents have provided so much support whilst I've been at Durham, and are largely responsible for my having managed not just four years, but seven in this city. As with many of the people mentioned here, without them, there would be no thesis.

Last, but quite definitely not least, enormous thanks go to my wife, Kay, who has kept me sane throughout many years of chemistry at Durham. She held my hand when things got bad, and held my hand when things went well – what more could I ask? If this thesis is for anyone, it is for her.

CONTENTS

Chapter 2 - Experimental Techniques

Chapter 3 - Protonation of Phthalocyanines

Appendix A - LabVIEW Computer Programming

Appendix B - Visual Basic Computer Programming

Appendix C - Publications, Posters Presented, Conference and Seminars Attended

LIST OF FIGURES

Chapter 1

Chapter 2

Chapter 3

Chapter 4

Chapter 5

Chapter 6

Appendix A

Appendix B

LIST OF SCHEMES

LIST OF TABLES

COMMON ABBREVIATIONS

Phthalocyanines

Pc	Phthalocyanine
$ZnPcS_4$	Tetrasulfonated zinc phthalocyanine
BuO_8ZnPc	1,4,8,11,15,18,22,25-Octabutoxy zinc phthalocyanine

Others

CTAB	Cetyltrimethylammonium bromide
EPA	Diethyl ether : 2-methylbutane : ethanol (5:5:2 v/v/v)
HOMO	Highest occupied molecular orbital
LUMO	Lowest unoccupied molecular orbital
PDT	Photodynamic therapy
UV	Ultraviolet

Symbols

ε	Extinction coefficient, $dm^3\ mol^{-1}\ cm^{-1}$
ε_r	Relative permittivity
ε_{TT}	Triplet-triplet extinction coefficient, $dm^3\ mol^{-1}\ cm^{-1}$
k_f	Rate constant for fluorescence, s^{-1}
k_{IC}	Rate constant for internal conversion, s^{-1}
k_{ISC}	Rate constant for intersystem crossing, s^{-1}
k_{VR}	Rate constant for vibrational relaxation, s^{-1}
Φ_f	Fluorescence quantum yield
λ_{em}	Emission wavelength, nm
λ_{ex}	Excitation wavelength, nm
λ_{max}	Maximum wavelength, nm
λ_{probe}	Probe wavelength in flash photolysis, nm
τ_f	Fluorescence lifetime, ns
τ_T	Triplet state lifetime, μs

Chapter 1

Introduction

1.1 Background

The discovery of phthalocyanine is assigned to the chance formation of a side product during the industrial production of phthalimide by a Scottish dye company.[1a] Passing ammonia through molten phthalic anhydride held in an iron container caused traces of a dark blue compound to be formed which was later identified as iron phthalocyanine. The first synthesis was recorded in 1907,[2] but it was not until 1934 and ensuing years that the structure of the deep blue compound was determined and its properties studied comprensively. In a series of papers[1] Linstead and co-workers described the new class of organic compound, named phthalocyanine because of its intense blue colour. The work of 1934 looked at the properties and synthesis of phthalocyanine and its derivatives, and it was proposed that the parent molecule possessed a macrocyclic structure with four isoindole units linked by azomethine bridges (see Figure 1.1 below). X-ray diffraction work by Robertson confirmed this structure,[3] and its similarity to naturally occurring porphyrins with four pyrrole rings linked by methine bridges was not missed.

This initial work marked the start of extensive research into the colourful and extraordinarily versatile chemistry of phthalocyanines* which continues to the present day. The uses of such compounds are widespread, perhaps the most obvious being as blue/green dyes. Of rather more than aesthetic use is the application of phthalocyanine derivatives to Photodynamic Therapy (PDT), a treatment for cancer. PDT initially used porphyrin compounds, which were shown to accumulate preferentially in tumour cells.[4] Photo-excitation of the sensitiser causes localised tissue damage as a result of singlet oxygen ($^1\Delta_g$ O_2, $^1O_2$) formation (due to interactions between the porphyrin triplet state and ground state oxygen). Investigation continued into the mid 1980s when it was realised that there were some complications associated with skin retention of the porphyrins. Phthalocyanines were proposed as a second generation PDT sensitiser in 1985[5] and since then there has been considerable work in the field.[6]

Another application lies in optical limiting, which is used to protect eyes from damage by laser radiation. The transmittance of the compound is required to be large in normal conditions, but if subjected to radiation of potentially dangerous intensity (for

* Phthalocyanine is both the name of the unsubstituted, non-metallated compound and of the class of compounds, which all possess the 18 membered, isoindole-based macrocycle.

example, from a laser weapon) an excited state is formed that has an extremely high transient absorbance. Heavy metal containing phthalocyanines have been shown[7] to have excellent properties, reducing incident radiation energies by over 300 times. The incorporation of such material into goggles and visors has applications in industry, research and defence agencies.

The catalytic properties of phthalocyanines have also been noted, and derivatives are currently used to catalytically remove thiols from petroleum fuels.[8] Additionally there has been considerable interest in their suitability for catalysing the photoreduction of water into hydrogen gas,[9,10] a process that would allow clean and energy efficient production of renewable fuel, and also in the four electron reduction of oxygen to form water.[11,12]

Material chemists also display interest in phthalocyanines in the synthesis of one dimensional conductors,[13,14] self-organising transport systems,[15] and within the field of second-order non-linear optics.[16]

These and many other applications, together with the properties and synthesis of phthalocyanine and its derivatives are discussed in full detail in the excellent series of books by Leznoff and Lever[17] and many review articles (for example, ref. 18) The size and depth of these volumes detail how phthalocyanines have quickly been shown to be far more than simple dye molecules. The wealth of information already available shows that phthalocyanines are becoming increasingly important in the world, and continued research is vital so that the full potential of these beautifully coloured molecules can be realised.

1.2 Structure

1.2.1 Chemical

The general structure of phthalocyanine is shown in Figure 1.1. The four isoindole rings joined by azomethine bridges comprise an extensively delocalised π-electron system which results in the strong blue/green colour (see Section 1.2.2.1). The planar structure of phthalocyanines make them strongly susceptible to aggregation (see Section 1.4). Many metallic and metalloid elements can be coordinated at the centre of the phthalocyanine ligand, the most common being zinc, copper and aluminium. The ligand groups (R) can be wide ranging, to which the following references are a small

selection: macrocyclic structures,[19,20] alkoxy and aryloxy,[16,21] carboxylates and analogues such as sulfonates,[22] oligomers,[15] alkyl and alkynyl,[13,23,24] bridge links between two phthalocyanine macromolecules,[25] or side strapped to individual isoindole rings.[26] The macrocycles can undergo a range of substitution, from mono- to hexadecasubstituted species[13,21,27,28,29] although synthetic techniques favour symmetrical substitution patterns and selective syntheses are generally difficult.

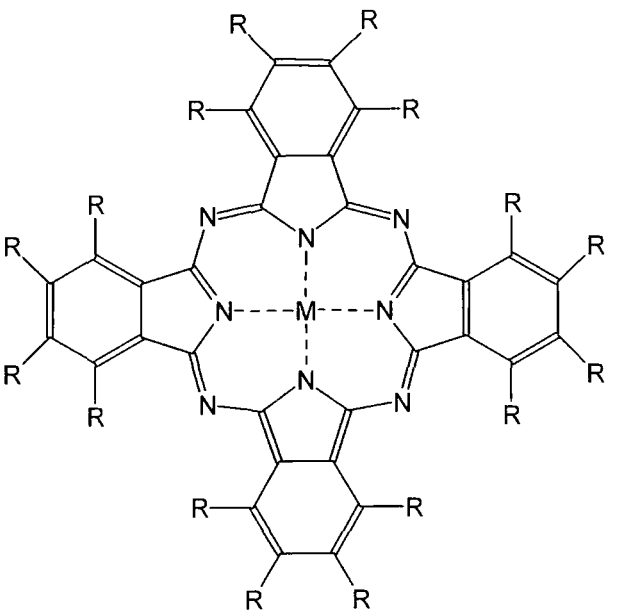

Figure 1.1 Structure of phthalocyanine (M = H_2, R = H) and metallophthalocyanine (M = metal, R = H)

Phthalocyanines are planar molecules as a result of the ring aromaticity. However, in certain metallated species the size of the metal guest precludes complete inclusion within the macrocycle core; for example, theoretical calculations have shown that for tin and lead phthalocyanine complexes the central metal ion is displaced from the molecular plane, and the whole molecule is distorted into a 'bowl' shape.[30] Where the metal is exceptionally large (for example the 5d metal ion, lutetium) its inclusion into the core is so minimal that it is bound by two macrocycles in a sandwich type complex.[31,32,33]

1.2.2 Electronic

1.2.2.1 UV-Visible Absorption

Typical UV-visible absorption spectra are shown in Figure 1.2. The intense peak centred for most phthalocyanines between 650-700 nm is labelled the Q band, whilst the broader peak between 300-400 nm is labelled the Soret or B band. There is a dramatic change in the spectrum upon demetallation of the phthalocyanine – removal of the metal ion causes a decrease in the molecule's symmetry which alters the degeneracy of the electronic states as discussed below. The result is to split the single Q band of metallated phthalocyanine into two component peaks Q_x and Q_y. To fully understand these transitions it is essential to consider the molecular orbitals of phthalocyanines

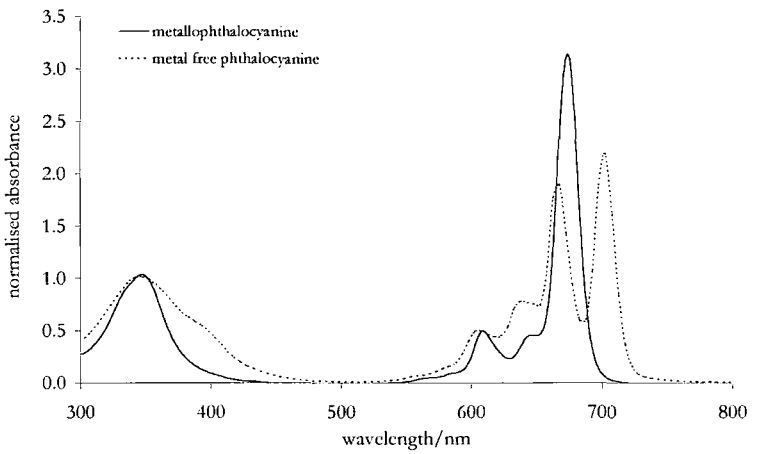

Figure 1.2 UV-visible absorption spectra of a typical monomeric metallophthalocyanine and free base phthalocyanine.

1.2.2.2 Molecular Orbital Description

The conjugated π-system of the phthalocyanine molecule comprises 40 atoms. Metallophthalocyanines possess D_{4h} group symmetry, whereas the unmetallated parent compound is of D_{2h} symmetry because of the two central hydrogen atoms which replace the metal.[18] This symmetry change has an important effect in the electronic spectra of phthalocyanines as will be seen below. The general model theory that is used to describe the molecular orbitals of phthalocyanines is the Four Orbital Model, developed by Gouterman[34] for porphyrins, and based upon previous simpler models.

The electronic core of metalloporphyrin is the inner 16 atom ring, which possesses 18 electrons. The simplest model treats this 16 member ring as a free electron wire, and correctly predicts the relative energies of the Soret and Q bands, and implies the Soret transition to be allowed, whilst the Q transition is forbidden as a result of an angular momentum selection rule. Similar to this model is the Cyclic Polyene Theory, which now treats the inner ring of the metalloporphyrin as being comprised of 16 CH units, with a total of 18 π-electrons (ie, 4n+2 π-electrons, implying aromaticity). Similar excited states to those in the Electron Wire Model are obtained, but the Polyene Model also provides a simple explanation why the Q band splits on going from metallo- to free base porphyrin.

The first model that took into account the detailed porphyrin shape was the Hückel Model and, whilst proving inaccurate in calculating transition dipole magnitudes, it did explain how variation in ring structure affects optical transitions.[35]

The Four Orbital Model unites the Hückel Model, which allows consideration of the macrocycle skeleton, with the Electron Wire and Polyene Models, which are sufficient to model the electron interactions with reasonable success. It uses the top two occupied molecular orbitals (MO), a_{2u} and a_{1u}, and the degenerate lowest unoccupied MO, e_g, to account for the allowed transitions within the UV-visible region. For simplicity the HOMOs are labelled b_1 (a_{2u}) and b_2 (a_{1u}) whilst the two LUMOs are labelled c_1 and c_2. The Soret or B band transition is assigned $c \leftarrow b_2$ and the Q band $c \leftarrow b_1$ (see Figure 1.3).

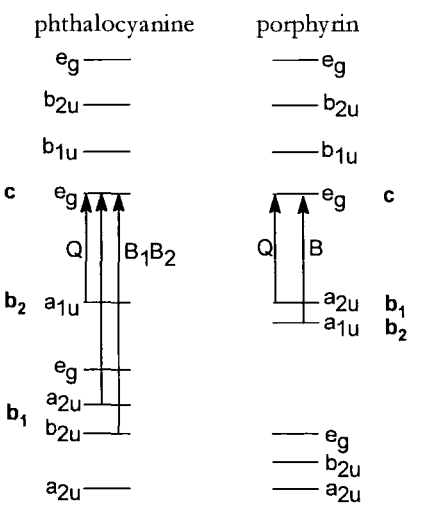

Figure 1.3 Origin of absorption in the region of the first two π-π* transitions, the Q and B bands, in porphyrins and phthalocyanines.[17a]

It so happens for porphyrins that the two HOMOs (b_1 and b_2) are accidentally degenerate, so that there occurs considerable electron interaction and mixing, as shown in Equation 1.1.

$$B_x^{\circ}Q_x^{\circ} = [(b_1 \rightarrow c_2) \pm (b_2 \rightarrow c_1)](2)^{-1/2}$$

$$B_y^{\circ}Q_y^{\circ} = [(b_1 \rightarrow c_1) \mp (b_2 \rightarrow c_2)](2)^{-1/2} \qquad (1.1)$$

As the orbital energies are shifted from degeneracy (as happens when moving from porphyrin through tetraazaporphyrin and tetrabenzporphyrin to tetraazatetrabenzporphyrin, otherwise known as phthalocyanine) it can be shown[34] that the x-polarised state remains virtually unchanged, whilst the y-polarised state becomes more and more weighted in favour of the lower energy state, Q_y. The b_2 level now lies well above the b_1 state, and so the lowest energy π-π^* transition is considerably red shifted, and as a result of the weighting, considerably more intense than the higher Soret transition.

1.2.2.3 Assignment of UV-Visible Transitions

Edwards and Gouterman prescribed a labelling scheme for porphyrins which has been successfully transferred to phthalocyanines.[36] Thus, in ascending energy order the transitions are labelled as Q, B, N, L, C. Whilst the first two are easily identified between 600-700 nm and 300-400 nm respectively the remaining three are generally hidden in solution state spectra by solvent absorption, although Caughey *et al.* have observed porphyrin N and L bands in solution.[37] However, gas-phase[36,38] and matrix isolated[39,40] spectra are reported in the literature which allow these transitions to be seen. Numerous theoretical studies have been carried out to study the electronic structure of phthalocyanines.[30,31,33,41,42,43]

The absorption spectra of phthalocyanines have long presented problems to those wishing to assign individual transitions to the bands, particularly because below 500 nm the bands overlap continuously towards the solvent cutoff. Further confusion is added by the presence of charge transfer bands in spectra of certain metallophthalocyanines.[44] These were assigned in 1974 by Stillman and Thomson[45] and discussed further by Gouterman[34] who also characterised the porphyrins in terms of their absorption and

emission spectra as normal, hyper or hypso. This characterisation can also, to a certain extent, be applied to phthalocyanines.[46] Briefly, normal spectra have the standard π-π* Q and B bands. Hypso spectra are similar to normal ones but with a noticeable blue shift, and are shown by transition metal complexes where the octahedral metal t_{2g} (d_π) orbitals are filled – the metal of greatest interest in this class is iron (II). Hyper spectra show prominent extra bands in the UV-visible region and are further categorised into p-types and d-types. The former occur mainly with low oxidation main group metals, and CT bands arise from e_g(ring)←a_{2u}(metal), that is, metal to ligand CT (MLCT). d-type CT bands are present when the complexing metal is from the transition series, with configuration d^m where $1 \leq m \leq 6$ (that is, possessing holes within the t_{2g} (d_π) orbitals). The transition is then from the ligand to the metal (LMCT), e_g(metal)←a_{1u},a_{2u}(ring). In addition to adding new bands to the spectrum mixing can also occur (generally between metal orbitals and phthalocyanine B orbitals – the Q usually remains unperturbed) which thus further increases the complexity in assigning transitions to the observed absorption bands. More recent work by Lever's group[47] has correlated the energies of CT bands for a wide range of phthalocyanine spectra, and Stillman and Nyokong give a useful summary of CT spectra.[44]

The two main bands of interest, Q and B, are both considered to be π-π* transitions.[31,41,48] The Q band is straightforward, consisting of the e_g←a_{1u} transition (see Figure 1.3) accompanied by vibrational satellites at higher energy.[48,49] Three peaks are generally observed, relating to the Q(0,0), Q(1,0) and Q(2,0) transitions. In the unmetallated phthalocyanine the lowering of symmetry ($D_{4h} \rightarrow D_{2h}$) causes the degeneracy of the excited state (e_g) to be relaxed, and so two individual transitions are observed, labelled as Q_x and Q_y. By convention Q_x lies to lower energy of Q_y. Proof of this change from a degenerate to a non-degenerate state has been demonstrated by MCD studies.[50]

The B band remains somewhat more complicated. Again, the π-π* nature of the e_g←a_{2u} state is generally assumed correct, but it has been suggested that there is additional n-π* character.[51,52] The notation of this band is also questioned, some suggesting the presence of two B transitions, labelled B_1 and B_2.[53,54] These individual bands remain unresolved in Edwards' and Gouterman's gas phase work,[36] but have been identified in a magnetic circular dichroism study.[55] Hollebone and Stillman[56] suggested

that B_1 and B_2 are both of π-π^* character, albeit with considerable configuration interaction. The transitions for B_1 and B_2 are thus assigned to $e_g \leftarrow a_{2u}$ and $e_g \leftarrow b_{2u}$ respectively. Additionally, the n-π^* transition has been labelled B_3.[40] Rosa and Baerends suggest, on the evidence of density functional calculations, that the Soret band consists of a mixture of several π-π^* and n-π^* transitions.[57]

1.3 Synthesis

1.3.1 General Methods

The very first synthesis of phthalocyanine (**1a**) involved the condensation of o-cyanobenzamide (**2**) in refluxing ethanol (Scheme 1.1).[2] The pioneering investigations of Linstead and co-workers[1b] showed that yields could be dramatically improved by heating **2** to temperatures greater than 230°C in the presence of antimony or magnesium metal or magnesium salts. Demetallation could be simply effected by dissolution in cold, concentrated sulfuric acid. Linstead's first paper on phthalocyanine mentioned its chance discovery during a reaction involving phthalimide and ammonia[1a] and the brief study of the compound suggested the possibility of using phthalonitrile (**3**) as an alternative to **2** (Scheme 1.1).[1b] At that time phthalonitrile was not easily prepared, but techniques have improved, and it is now possible to prepare a whole range of substituted phthalonitriles.

A widely used method is the displacement of a nitro group from 4-nitrophthalonitrile, first reported by Keller *et al.* in 1980,[58] and further studied by Siegl.[59] The two nitrile groups activate the nitro group towards nucleophilic substitution, and in the presence of moderate base (potassium carbonate) it can be displaced by a range of nucleophiles including alkoxy and malonate. There are a number of different reactions utilising phthalonitriles which all yield phthalocyanine as product, and these are discussed together with other synthetic techniques elsewhere.[60]

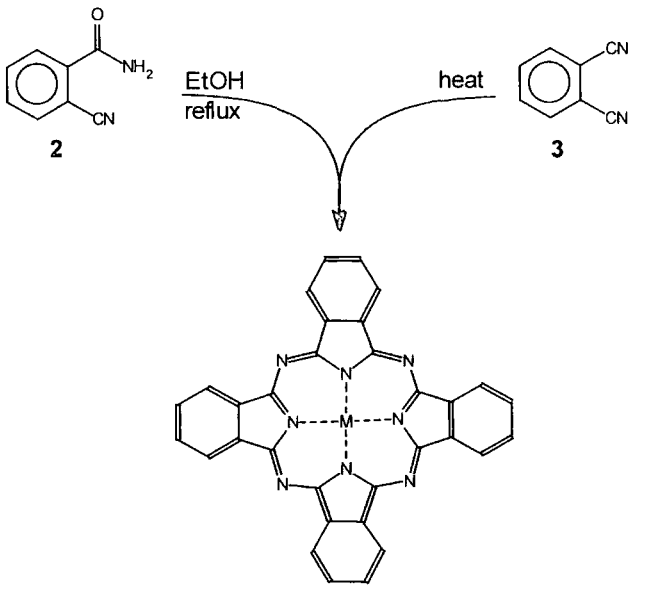

Scheme 1.1 Early synthetic strategies to form phthalocyanine

Metallated phthalocyanines are generally relatively easy to synthesise by templating to the central metal ion. However, free base phthalocyanines are more difficult, and most of the syntheses involve preparation of the metallated compound followed by liberation of the metal using concentrated sulfuric acid. Brach *et al.* showed that high yields (in excess of 75%) could be obtained directly by either heating the phthalonitrile (**3**) in an atmosphere of ammonia or the 1,3-diiminoisoindoline (**4**) alone with substantial amounts of lower N-alkylalkanolamines (Scheme 1.2).[61] In general, 2-dimethylaminoethanol (**5**) is used as the solvent. The simpler diiminoisoindoline method lends support to the hypothesis that phthalocyanine formation occurs via a diiminoisoindoline. The presence of ammonia in the phthalonitrile method is thought to result in the formation of the diiminoisoindoline *in situ*. The diiminoisoindoline route is now perhaps the most common route to phthalocyanines; Leznoff *et al.* have suggested that synthesis of metal free phthalocyanine in this way, followed by metal insertion, is the most successful technique for acquiring pure metallophthalocyanine.[25] As well as the more usual compounds,[62] silicon phthalocyanine and silicon naphthalocyanine have both been prepared via diiminoisoindolines.[63] The 1,3-diiminoisoindolines are generally prepared by bubbling anhydrous ammonia through a refluxing solution of phthalonitrile for several hours.[61]

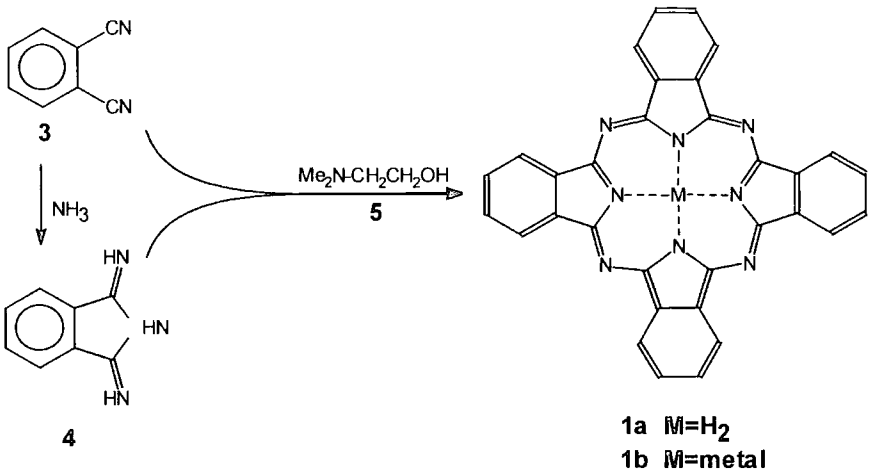

Scheme 1.2 Common synthetic strategies to form phthalocyanine.

1.3.2 Methods for Unsymmetrical Phthalocyanines

The methods described above result in identically substituted phthalocyanines, but the real challenge of phthalocyanine synthesis lies in being able to prepare unsymmetrically substituted compounds. Crossed condensation of different diiminoisoindolines is the most straightforward technique, but even with the use of suitable ratios of starting materials a statistical mixture of the mono-, di-, tri- and tetra- isomers* is obtained. This method has been reported, but requires careful chromatographic separation to obtain the desired isomer, and yields are usually low.[64] A more successful synthesis utilising solid phase techniques was reported in 1982.[65] This involved fixing a phthalonitrile unit to a solid phase polymer bead, followed by conversion to the corresponding diiminoisoindoline. A different diiminoisoindoline was then allowed to condense onto the fixed species, resulting in a monosubstituted phthalocyanine linked to the polymer bead. By ensuring that the self-condensation product was sufficiently soluble it was possible to remove this simply by washing the polymer beads with solvent. Finally cleavage in acid conditions yielded the monosubstituted product.

In the last ten years there has been a number of papers published concerning the use of subphthalocyanines in unsymmetrical synthesis. Subphthalocyanine is the lowest homologue of phthalocyanine-type compounds, and contains just three isoindole rings.

* For the purposes of this discussion, the prefix of mono, di, tri and tetra indicates the individuality of the isoindole rings. A mono-substituted macrocycle will contain one A isoindole and three B isoindoles. The actual isoindole rings themselves could be mono-, di-, tri- or tetrasubstituted.

The most common examples contain a central boron atom (see Figure 1.4). The preparation, reactivity and physical properties of these compounds have been comprehensively discussed by Geyer *et al.*[66] The first report of a subphthalocyanine being used for the synthesis of phthalocyanine appeared in 1990.[28] The synthesis of tri-*tert*-butylphthalocyanine was effected by inserting an unsubstituted diiminoisoindoline into the tri-*tert*-butylated boron subphthalocyanine chloride.

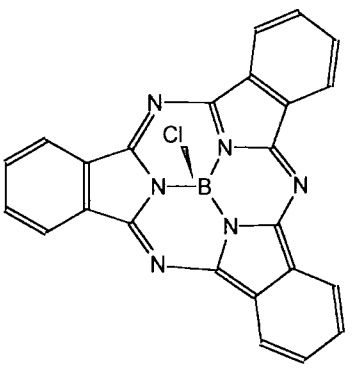

Figure 1.4 Boron subphthalocyanine chloride

Whilst the relatively high yield (20% for the tri-*tert*-butylphthalocyanine mentioned above) remains undisputed for this technique, the efficacy in producing monosubstituted phthalocyanine has been challenged, although earlier work does agree with this statement.[19,29] Whilst the process was originally believed to involve a one step insertion of a diiminoisolindoline into the subphthalocyanine structure, Sastre *et al.* suggested that the insertion step is not as selective as first thought, being instead a multistep process.[67] The mechanism they proposed involved the cleavage of the subphthalocyanine structure by the diiminoisoindoline to yield an open structure containing four isoindole rings, which then undergoes various reactions, including ring closure to form the desired phthalocyanine, and cleavage to create a number of different dimer and trimer fragments. These fragments can then rejoin to create zero-, di- and tetrasubstituted phthalocyanines.

1.3.3 Methods for Binuclear Phthalocyanines

The synthesis of dimeric phthalocyanines has been dominated by the work of Leznoff, Lever and co-workers. They have successfully prepared a number of binuclear compounds with covalent bridges containing –1 (that is, two phthalocyanine rings

joined by a common benzene ring),[68] 0 (that is, linked directly),[69] 1,[70] 2,[71] 4,[71] and 5[25,72] bridging atoms. In addition, alkyne and alkene,[73] 1,8-naphthalene[74] and 1,8-anthracene[69] bridges have been used. Outside of this group, Gaspard *et al.* have prepared a mixed phthalocyanine-porphyrin dimer,[75] whilst Kobayashi *et al.* report a broad near infra-red absorber consisting of a –1 linked phthalocyanine-naphthalocyanine dimer.[76] Although the main emphasis of research is placed with dimeric species, trinuclear,[70] tetranuclear,[11] and pentanuclear[77] species have also been reported.

The most usual method for preparing these compounds is to use 1,3-diiminoisoindolines in a similar fashion to monomer synthesis. Treatment of nitrophthalonitrile with a diol in the presence of base yields a bisphthalonitrile compound[58] which can then be converted to the diiminoisoindoline in the usual fashion. Phthalocyanine formation is in effect a crossed condensation, with various possible products. However, the distinct properties of the dimer relative to the monomer mean that separation by column chromatography is feasible, and Hall *et al.* report the unusual mixture of 2-methoxyethanol and toluene in various ratios as a particularly good eluant.[65]

1.4 Aggregation

Phthalocyanines have long been known to aggregate,[78,79,80,81,82] a phenomenon which occurs due to interactions between the π-systems of the rings - the larger phthalocyanine systems show enhanced aggregation relative to the closely related porphyrins.[15] The tendency to aggregate is affected by many factors including temperature, solvent and substituents, all of which will be discussed below. Aggregated species are readily distinguished in the UV-visible absorption spectrum by the appearance of extra peaks to the blue and/or red of the monomer peak. Fluorescence is generally not seen from the aggregated systems. The spectroscopic changes observed from aggregates are explained by Exciton Theory.

1.4.1 Exciton Theory

Exciton Theory is applicable to molecular aggregates with strong monomer electronic transitions and negligible electron overlap between the monomer units, which includes such species as porphyrins,[83] cyanine dyes,[84] rhodamines,[85] arylazonaphthols,[86,87] as well

as phthalocyanines.[17a] The theory was first developed by Kasha *et al.* in 1965[88] and there have been later discussions.[83,85]

The theory is based upon the assumption that the transition dipole moment for an electronic transition can be considered localised at the centre of the chromophore, that is, the dipoles are considered as vectors only. It has been shown for porphyrins however that this assumption fails when the distance between monomers is comparable with monomer dimensions. By assuming also negligible overlap of the monomer units it is possible to describe the wave functions of the aggregate species in terms of the monomer wave functions. Interaction between the monomer units results in a splitting of the excited state energy level, and this splitting is dependent upon the geometry of the monomers, in particular the inter-monomer distance, r, and the angles between the transition moments, θ and (where necessary) α. There are a number of different classes of dimer, as shown in Figure 1.5.

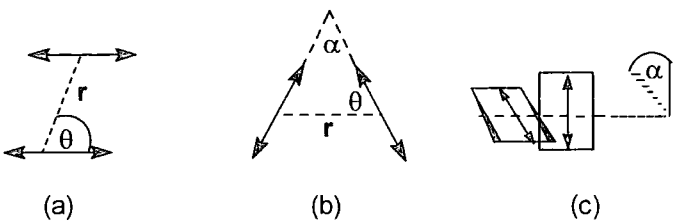

Figure 1.5 Classes of dimers described in Exciton Theory.[88] (a) slipped co-facial (b) oblique (clamshell) and (c) out-of-plane dimers.

Consider the slipped co-facial dimers (Figure 1.5a). With θ = 0° the monomer units lie in the same plane, in a head-to-tail fashion; there are two limiting configurations. The lower energy arrangement has the two dipoles aligned, whilst the higher energy arrangement has them opposed. In the former vector addition results in a finite dipole moment, whilst the latter results in a zero net dipole. For an allowed transition the net dipole moment must be non-zero, so a transition to the lower energy level is allowed, whilst that to the upper level is forbidden. With θ = 90° the monomer units now lie stacked one upon the other, and again there are two limiting cases. The lower energy arrangement is due to the two dipoles being opposed, resulting in a zero net dipole term. The higher energy configuration arises from the dipoles being aligned, giving a finite net dipole moment. Thus, converse to the θ = 0° case, the lower level is now forbidden, and the allowed transition is now between the upper level and the

ground state. Both the ground and excited state levels experience a small shift in their energetic centres of gravity.

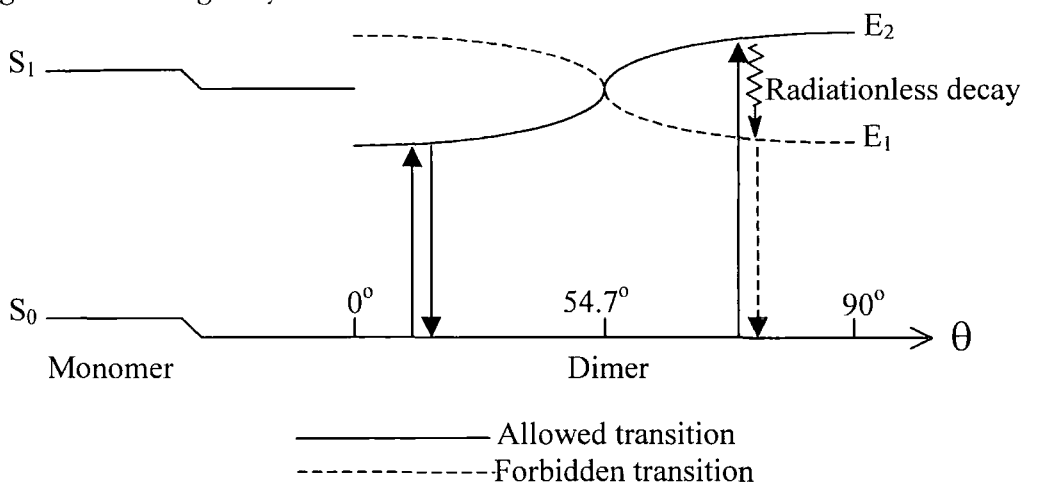

Figure 1.6 Energy diagram showing exciton splitting for co-facial phthalocyanine dimers.

The splitting between the two levels, ΔE (= E_2-E_1) is given by Equation 1.2. It can easily be seen that the exciton splitting is zero when $\theta = 54.7°$.

$$\Delta E = \frac{2|M|^2}{r^3}(1-3\cos^2\theta) \qquad (1.2)$$

Thus, depending upon the angle at which the monomers lie (in other words, the extent of slippage) the absorption spectrum of the dimer will be red (for $\theta < 54.7°$) or blue shifted (for $\theta > 54.7°$). Kasha's well-known rule[89] concerning the origin of fluorescence states that emission occurs from the lowest excited state, thus the red shifted dimer absorption peak will be fluorescent (since transitions to and from the lower level are allowed) whilst the blue shifted absorption peak will be non-fluorescent. In the latter case, absorption to the upper level is allowed, but rapid vibrational relaxation to the lower level means that fluorescence would originate from the lower level – the state is deactivated by non-radiative processes instead. It should be noted that for a D_{2h} metal free phthalocyanine, which already possesses a split excited state (Q_x and Q_y) the exciton splitting is extra, resulting in four levels, Q_{x+}, Q_{x-}, Q_{y+} and Q_{y-}.[90]

The oblique or clamshell dimers (Figure 1.5b) show a similar splitting, but one which is independent of the angles between the monomers. Both exciton levels are

accessible by allowed transitions, so the absorption spectrum is characterised by the appearance of both red and blue shifted absorption, and emission is seen via excitation at either peak (although Kasha's rule dictates the emission originates from the lower level (E_1) only).

Finally, the out-of-plane dimer (Figure 1.5c) has non-planar transition dipole moments. The lower level becomes increasingly forbidden as $\alpha \rightarrow 90°$, and the splitting increases as $\theta \rightarrow 0°$. The upper level remains an accessible state. Thus, absorption to the upper level is allowed, and a blue shifted, non-fluorescent dimer is expected.

1.4.2 Aggregation Studies

1.4.2.1 Mononuclear Species

Kroon *et al.* have studied the self-assembling properties of both porphyrins and phthalocyanines substituted with oligo(ethylene oxide)alkyl or alkoxy units.[15] They showed that aggregation of the porphyrins resulted in head-to-tail dimers, whereas phthalocyanines formed co-facial species, characterised by a blue shifted Q band. For the latter, aggregation displayed complex dependence upon solvent relative permettivity. This concurs with earlier work[91] upon linear stacks of octasubstituted phthalocyanine in dodecane solution, which showed that aggregation in polar solvents (high ε_r) is due to dominant solvent-solvent interactions excluding the macrocycle from solution. In solvents with low ε_r values (for example, pentane) aggregation is truly due to phthalocyanine-phthalocyanine interactions. Further work on a number of systems concurs with these hypotheses.[81,86,87,92]

Kobayashi and Lever[20] synthesised free base and metallophthalocyanine with four 15-crown-5 units fused onto the isoindole ring systems. Addition of K^+, NH_4^+, Na^+ and Ca^{2+} ions caused a reduction in intensity of the Q band, with a growing peak at ~630 nm (the blue shifted dimer Q band). It must be stressed that the observed aggregration is wholly due to the crown ether moieties of neighbouring phthalocyanines forming sandwich-type structures with the cations, rather than intrinsic phthalocyanine-phthalocyanine interaction. Perhaps more interesting is the work of Stanley on chloroaluminium phthalocyanine[93] which shows ion induced aggregation. Addition of small amounts of fluoride ions induced changes in the absorption spectrum which are

typical of co-facial aggregation. Once the concentration of ions reached a certain critical value further addition of F^- no longer caused aggregation of the phthalocyanine, but rather disaggregation. The concentrations of phthalocyanine used in the study were such that the parent ClAlPc was monomeric with no F^- added, so the aggregation seen was assumed to arise only from the added ions. It was suggested that at intermediate concentrations of F^- a number of different dimers were formed ([ClPcAl-F-AlPcF]$^-$, $[AlPcF]_2F^-$ and $[AlPcCl]_2F^-$) whilst increased presence of F^- resulted in the monomer $AlPcF_2^-$. The fluoride ion acts as a bridge at low concentration, but disaggregates at high concentration.

The substituents on the phthalocyanine macrocycle can also increase susceptibility to aggregation - strong aggregation properties of naphthalocyanines were reported by Tai and Hayashi.[94] Moderate aggregation was seen for tetrabutyl and tetrabutoxy compounds, but the novel ester substituents $-CO_2C_8H_{17}$ caused aggregation even at concentrations as low as 10^{-7} mol dm^{-3}. It has also been shown that the position of the substituent can effect aggregation.[95] Substituents in the α-position were shown to prevent aggregation because of steric effects, whilst β-substituted phthalocyanines showed the usual tendency to form dimers and higher aggregates.

One particular group of phthalocyanines which are well-known to exhibit strong aggregation are the water soluble sulfonated metallophthalocyanines. Their water solubility makes them strong candidates for Photodynamic Therapy, and the cobalt compounds have been demonstrated to bind oxygen reversibly.[96] Dimerisation of cobalt tetrasulfonated phthalocyanine ($CoPcS_4$) was shown to be temperature dependent, increasing as the temperature of the solution falls.[80] Further thermodynamic investigation in this study precluded hydrophobic bonding as the major factor for dimerisation, suggesting the strong tendency to aggregation is due to electrostatic interactions between the charged sulfonate groups. Blagrove and Gruen also studied the thermodynamics of dimerisation of both $CoPcS_4$ and $CuPcS_4$.[79] The copper derivative showed a higher degree of association and this was attributed to an entropy effect, although its origin was not given. By testing the samples in a number of different aqueous solutions (including urea, alcohols, and formamide) it was concluded that additives regarded as 'structure makers' enhanced both the enthalpy and entropy of dissociation, whilst 'structure breakers' had the opposite effect.

Lowering the temperature is known to promote aggregation[90] by freezing out the range of conformations which exist dynamically at room temperature. Only a few preferred, more completely coupled, conformations remain.

1.4.2.2 Binuclear Species

Prior to discussing research carried out on a number of binuclear phthalocyanines, it is important to discuss the validity of exciton theory to these species. The theory assumes negligible overlap between the molecular orbitals of each component. With two individual monomers this is a reasonable assumption, but for two linked monomers (that is, a binuclear compound) the possibility of interaction must be considered. With longer bridges and open conformations orbital overlap is likely to be minimal, but with the short bridges and co-facial conformers overlap could well be relevant. There are reports of studies (on silicon phthalocyanine stacks) which assume both the presence[97] and absence[98] of overlap, but the lack of definitive information concerning this means that all the work on binuclears by Leznoff, Lever and co-workers reported below utilises the Exciton Theory without orbital overlap.[90]

Whilst Exciton Theory predicts a number of forbidden transitions for the D_{4h}/D_{2h} phthalocyanines, the presence of a bridging moiety between two phthalocyanines lowers the symmetry and transitions to both high and low energy levels are not unexpected.[99] In general there will be a number of conformations with differing energies, and spectra are broadened as a result. The main shift is to the blue of the mononuclear Q band, but the broadness of the absorption will result in a tail extending into the red. In addition to the dimer spectral envelope there will be visible the Q component of the independent, uncoupled units.[90]

The synthesis of binuclear phthalocyanines allows the investigation of intramolecular dimerisation, as opposed to the aggregation so far discussed which is intermolecular. Nevin *et al.* discussed the aggregation of mononuclear and binuclear cobalt phthalocyanines[100] in which the mononuclear species was found to behave quite normally, whilst the binuclear systems displayed blue shifted spectra typical of aggregation. Two binuclear compounds were studied, one with a five atom bridge (O-C_3-O) and the other with a two atom bridge (C_2). The latter, with its less flexible bridge, was shown to have an open conformation and appeared to aggregate more readily than the closed clamshell five atom bridge compound, in which the intramolecular coupling

was assumed to inhibit the intermolecular aggregation. A planar binuclear[68] (with a –1 atom bridge) was found to have an aggregation constant an order of magnitude higher than these two, presumably a result of enhanced intermolecular interactions aided by the extended π systems. A novel tetranuclear spiro linked cobalt phthalocyanine was reported to have an aggregation constant a further order of magnitude higher, possibly resulting from a pair of rings stacking with a pair from another molecule, creating a stack of four coupled phthalocyanine rings.[11] Such an interaction would be expected to be twice as strong as simple aggregation between monomers.

Leznoff *et al.* briefly discussed the photophysics of binuclears linked with an O-C_3-O bridge.[72] Typical aggregated absorption spectra were obtained, and such dimerisation was shown to be virtually unaffected by dilution, implying it to be an intra- rather than intermolecular phenomenon. A small amount of monomeric species could be determined, and the presence of an open-closed equilibrium was assumed. Addition of strong ligands (such as cyanide or n-octylamine) promoted dissociation in the cobalt species, by forming a six coordinate complex.

Work by Dodsworth *et al.* in 1985 looked at a number of zero, one, two, four and five atom bridged metal free binuclears, in addition to an analogous mononuclear compound.[90] At room temperature all the binuclears showed the typical broadened absorption spectrum overlaid with varying amounts of monomeric unit Q_x and Q_y bands, with emission corresponding to residual monomer contribution. This dimerisation was shown to be both intermolecular (for the planar compounds with zero and one atom bridges) and intramolecular (for the non-planar species with flexible linkers). Spectra at 77 K showed the dimer envelope more prominently, at the expense of the monomer profile, as expected. The emission spectra were unremarkable, save for the species with four and five atom bridges, which displayed a weak band (only visible at low temperature) centred at 750 nm. This observation was attributed to rare fluorescence of exciton coupled phthalocyanines in an oblique or clamshell conformation. This concept of the fluorescent phthalocyanine dimer will be discussed more fully below (Chapter 6).

1.5 Photophysics of Phthalocyanines

1.5.1 Background

The transitions observed in UV-visible absorption and emission spectroscopy are electronic in nature, and involve the excitation of an electron in a low energy occupied orbital to a higher energy, initially unoccupied, orbital. The two molecular states involved in this process are known as the ground and excited states respectively. The chemical and physical properties of electronically excited states may differ from the those of the ground state.

Electrons possess spin angular momentum ($s = \pm ½$), and polyelectronic molecules have a resulting total spin angular momentum S which is the sum of the individual electron spins. Most commonly encountered organic molecules display a net pairing of electronic spins ($\uparrow\downarrow$) such that $S = 0$, and are said to exist in a singlet state. The ground state is thus depicted by S_o.

A transition which occurs with no change in spin maintains the spin pairing and results in a singlet excited state, depicted by S_n, where S_1 is the lowest excited singlet ground state. A transition which occurs with a change in spin to give unpaired spins results in a triplet excited state, with $S = 1$. Triplet states are depicted by T_n, where T_1 is the lowest triplet state. A selection rule formally requires $\Delta S = 0$ for a radiative transition, such that singlet-singlet and triplet-triplet processes are allowed, whilst singlet-triplet processes are forbidden. The repulsion between two electrons is minimised if their spins are parallel ($\uparrow\uparrow$) rather than opposed ($\uparrow\downarrow$) which can be considered a consequence of the Pauli Principle. For the triplet state there is zero probability of finding both electrons in the same location, so the electrons avoid each other.[101] This spin correlation results in triplet states being lower in energy relative to their respective singlet states.

The various photophysical processes involving these singlet and triplet states can best be described using a Jabłoński diagram (Figure 1.7).

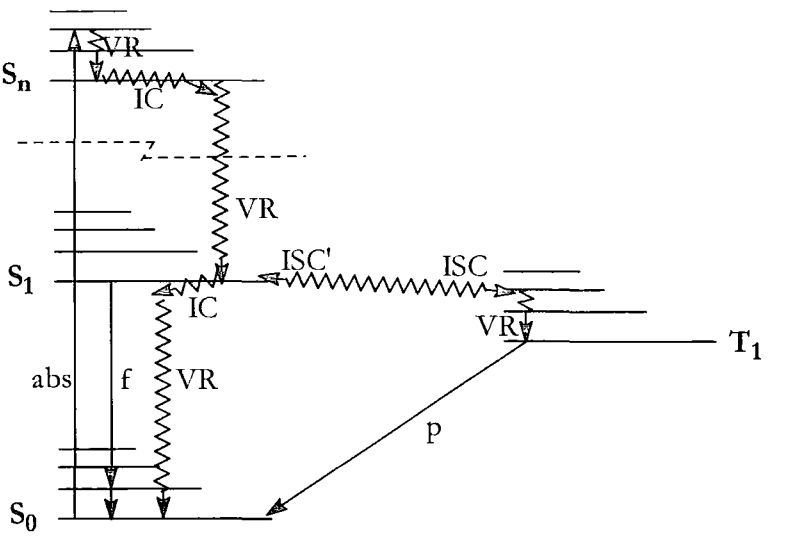

Figure 1.7 Jabłoński diagram showing common photophysical processes involving singlet and triplet states. Radiative and non-radiative processes are indicated by straight and zigzag arrows respectively. IC = internal conversion, ISC = intersystem crossing, ISC' = back intersystem crossing, VR = vibrational relaxation, abs = absorption, f = fluorescence, p = phosphorescence.

Absorption of a photon accesses an upper vibrational level of the excited singlet state, S_n. Rapid vibrational relaxation and internal conversion results in the loss of vibrational energy ($v = n \rightarrow v = 0$) and transition to a lower excited state ($S_n \rightarrow S_{n-1}$) respectively - the energy is lost as heat to the surrounding solvent molecules. The lowest vibrational level of the lowest excited state (S_1, $v = 0$) is quickly attained (typically in 10^{-12} s or less). This state is relatively long lived (typically 10^{-8} s) and there are a number of subsequent deactivation processes which are feasible. Relaxation to the ground state (S_o) can be non-radiative (vibrational relaxation and internal conversion) or radiative (fluorescence) - both of which are formally allowed processes. Alternatively, the formally forbidden process of intersystem crossing can occur, resulting in a change of spin and formation of the vibrationally excited lowest triplet state, T_1. The reverse process, back intersystem crossing, is possible, and competes with rapid vibrational relaxation which yields the vibrationally relaxed triplet state (T_1, $v = 0$). Transitions deactivating the T_1 state are formally forbidden, and so this state is extremely long lived (10^{-1}-10^{-6} s), and like the lowest excited singlet state it can be deactivated radiatively (phosphorescence) or non-radiatively to yield the lowest vibrational state of the ground state (S_o).

The quantum yield for a process affords useful information about that process in relation to others - for example, the quantum yield of fluorescence Φ_f gives the ratio of photons emitted to photons absorbed. In terms of rate constants, Φ_f can be represented as the ratio of k_f to the sum of the rate constants of *all* the deactivating rate constants ($\Phi_f = k_f/[k_f+k_{IC}+k_{VR}+k_{ISC}]$). The quantum yield of phosphorescence Φ_P has an analogous definition relating to the efficiency of phosphorescent emission. However, quantum yields are not restricted to radiative processes, for example, the triplet quantum yield Φ_T is the ratio of triplet molecules formed to photons absorbed.

The lifetime of a state is defined as the average time the molecule spends in that state prior to deactivation to another state. As stated above the lifetime for the first excited singlet state is typically 10 ns, but individual systems have characteristic lifetimes. This is in fact the *observed* fluorescence lifetime, τ_f, which corresponds to the reciprocal of all the deactivation rate constants ($\tau_f = 1/[k_f+k_{IC}+k_{VR}+k_{ISC}]$). The *natural*, or pure radiative, or intrinsic, lifetime τ_f° corresponds to the reciprocal of the rate constant for fluorescence ($\tau_f^\circ = 1/k_f$), and represents the average time the molecule spends in the S_1 state before fluorescence occurs. The natural lifetime can be calculated trivially if both the quantum yield of fluorescence and the observed fluorescence lifetime are known.

The intensity of fluorescence can be decreased by the presence of quenchers. These molecules interact with the fluorophore in such a way that an additional deactivation pathway is presented to the excited state (S_1), represented by the rate constant k_Q. The most common type of quenching is collisional in nature, where the excited state is deactivated during a collisional encounter with the quencher. In this case k_Q is bimolecular, and, if the concentration of quencher molecules ([Q]) is known, can be calculated from the Stern-Volmer equation

$$\tau_o/\tau = \Phi_o/\Phi = 1 + \tau_o k_q[Q] \qquad (1.3)$$

where Φ_o and Φ represent the unquenched and quenched quantum yields of fluorescence respectively, and τ_o and τ represent the unquenched and quenched observed fluorescence lifetimes respectively.

Full discussion of photophysical principles and techniques in general[101,102] and fluorescence spectroscopy in particular[103] can be found elsewhere.

1.5.2 Phthalocyanines

When monomeric, phthalocyanines generally behave as typical fluorophores, although their photophysical behaviour does depend upon the central atom within the macrocycle. Heavy atoms increase the triplet yield, at the expense of the fluorescence quantum yield and lifetime, and this is typified in the behaviour of aluminium and zinc phthalocyanines, the former typically having a lifetime of ~5 ns and quantum yield of ~0.4, the latter having values of ~3 ns and ~0.3 respectively. Copper, possessing one vacancy in its d shell, acts as a strong electron acceptor, and quenches the phthalocyanine emission such that copper phthalocyanines are generally non-fluorescent.

As mentioned previously phthalocyanines are important in their application as photodynamic therapeutic agents. This process involves energy transfer from the phthalocyanine to molecular oxygen, and due to its long lived nature this generally takes place via the triplet state. Phthalocyanines with paramagnetic ions such as copper or chromium possess very short triplet lifetimes, which severely limits their use as singlet oxygen generators.

1.6 Aims

The aim of this current study is to further investigate the photophysical properties of interesting phthalocyanine species. The phthalocyanine macrocycle is extremely robust, enabling wide and varied synthetic pathways to novel systems with unusual properties, and continued investigation into these properties will further enhance the knowledge base for these versatile compounds. A brief summary of the remaining chapters in this thesis is given below.

Chapter 2 This chapter describes the photophysical techniques and the experimental setups used to study the phthalocyanines. Where necessary background theory has been included to allow a basic understanding of the principles involved.

Chapter 3 The phenomenon of phthalocyanine ring protonation and its effect on the photophysical properties of tetrasulfonated zinc phthalocyanine is

explored. The potential application of this property to the design of photodynamic therapeutic agents with improved selectivity is considered, and in light of this, a brief study of octabutoxy zinc phthalocyanine is reported.

Chapter 4 The photophysical properties of a number of axially substituted silicon phthalocyanines with ester linkages are reported for the first time. The effect of intramolecular electron donors acting as fluorescence quenchers is related to their distance from the phthalocyanine core. Calculations based upon quencher oxidation potentials are used to elucidate the observed behaviour.

Chapter 5 This chapter contains a detailed study of novel silicon phthalocyanine - tetrathiafulvalene hybrids. Tetrathiafulvalene (TTF) is a strong quencher of phthalocyanine fluorescence, and the relative position of the TTF moiety with respect to the phthalocyanine core is related to the extent of quenching observed. Spectroelectrochemical studies of these compounds are described, and the application of this technique to creating switchable fluorescence is discussed.

Chapter 6 A detailed study of the photophysical properties of the novel fluorescent phthalocyanine dimers of a solketal substituted zinc phthalocyanine and its derivatives is presented. Time resolved transient absorption spectroscopy reveals the complex behaviour evident upon absorption of excitation light.

1.7 References

1 (a) R. P. Linstead, Phthalocyanines. Part I. A new type of synthetic colouring matters, *J. Chem. Soc.*, 1934, 1016 (b) G. T. Byrne, R. P. Linstead and A. R. Lowe, Phthalocyanines. Part II. The preparation of phthalocyanine and some metallic derivatives from o-cyanobenzene and phthalimide, *ibid.*, 1934, 1017 (c) R. P. Linstead and A. R. Lowe, Phthalocyanines. Part III. Preliminary experiments on the preparation of phthalocyanines from phthalonitrile, *ibid.*, 1934, 1022 (d) C. E. Dent and R. P. Linstead, Phthalocyanines. Part IV. Copper phthalocyanines, *ibid.*, 1934, 1027 (e) R. P. Linstead and A. R. Lowe, Phthalocyanines. Part V. The molecular weight of magnesium phthalocyanine, *ibid.*, 1934, 1031 (f) C. E. Dent, R. P. Linstead and A. R. Lowe, Phthalocyanines. Part VI. The structure of the phthalocyanines, *ibid.*, 1934, 1033.

2 A. Braun and J. Tcherniac, Products of the action of acetic anhydride on phthalamide, *Ber. Deut. Chem. Ges.*, 1907, 40, 2709.

3 (a) J. M. Robertson, An x-ray study of the structure of the phthalocyanines. I. The metal-free, nickel, copper and platinum compounds, *J. Chem. Soc.*, 1934, 615 (b) J. M. Robertson, An x-ray study of the phthalocyanines. II. Structure determination of the metal-free compounds, *ibid.*, 1936, 1195 (c) J. M. Robertson and I. Woodward, An x-ray study of the phthalocyanines. III. Quantitative structure determination of nickel phthalocyanine, *ibid.*, 1937, 219.

4 F. J. Figge, G. S. Weiland and L. O. J. Manganiello, Affinity of neoplastic, embryonic and traumatised tissue for porphyrins and metalloporphyrins, *Proc. of the Soc. Exp. Biol. and Med.*, 1948, **68**, 640.

5 E. BenHur and I. Rosenthal, Photochemical generation of superoxide radical and the cytotoxicity of phthalocyanines, *Int. J. Rad. Biol.*, 1985, **47**, 145.

6 E. BenHur and I. Rosenthal in *Phthalocyanines – Properties and Applications, Vol.1*, Eds. C. C. Leznoff and A. B. P. Lever, VCH Publishers, Inc., New York, 1989.

7 J. W. Perry, K. Mansour, S. R. Marder, K. J. Perry, D. Avlarez and I. Choong, Enhanced reverse saturable absorption and optical limiting in heavy-atom-substituted phthalocyanines, *Optics Lett.*, 1994, **19**, 625.

8 J. A. Alcaraz, B. J. Arena, R. D. Gillespie and J. S. Holmgren, Solid base catalysts for mercaptan oxidation, *Catalysis Today*, 1998, **43**, 89.

9 J. R. Darwent, Photoreduction of methyl viologen in micellar solutions sensitised by zinc phthalocyanine, *J. Chem. Soc., Chem. Comm.*, 1980, 805.

10 A. Harriman and M-C. Richoux, Attempted photoreduction of hydrogen using sulphophthalocyanines as chromophores for three-component systems, *J. Chem. Soc., Faraday II*, 1980, **76**, 1618.

11 W. A. Nevin, W. Liu, S. Greenberg, M. R. Hempstead, S. M. Marcuccio, M. Melnik, C. C. Leznoff and A. B. P. Lever, Synthesis, aggregation, electrocatalytic activity and redox properties of a tetranuclear cobalt phthalocyanine, *Inorg. Chem.*, 1987, **26**, 891.

12 (a) J. P. Collman, P. Denisevich, Y. Konai, M. Marrocco, C. Koval and F. C. Anson, Electrode catalysis of the four-electron reduction of oxygen to water by dicobalt face-to-face porphyrins, *J. Am. Chem. Soc.*, 1980, **102**, 6027 (b) J. P. Collman, P. Denisevich, Y. Konai, M. Marrocco, C. Koval and F. C. Anson, Potent catalysis of the electroreduction of oxygen to water by dicobalt porphyrin dimers adsorbed on graphite electrodes, *J. Electroanal. Chem. Interfacial Electrochem.*, 1979, **101**, 117 (c) J. P. Collman, F. C. Anson, C. E. Barnes, C. S. Bencosme, T. Geiger, E. R. Evitt, R. P. Kreh, K. Meier and R. B. Pettman, Further studies of the dimeric β-lined "face-to-face four" porphyrin, *J. Am. Chem. Soc.*, 1983, **105**, 2694.

13 (a) M. Hanack, F. Seelig and J. Strahle, Synthesis of properties of a new kind of one-dimensional conductors. 1. General aspects, *Z. Naturforsch. [a]*, 1979, **34**, 983 (b) F. Seelig, Synthesis and properties of a new kind of one-dimensional conductors. 2. Extended Hückel calculations on the energy band structure, *ibid.*, 1979, **34**, 986 (c) M. Hanack, K. Mitulla, G. Pawlowski and L. R. Subramanian, Synthesis and properties of new one-dimensional conductors. 3. Trans-Bis(1-

alkynyl) group IVA metallophthalocynanines, *Angew. Chem. Int. Ed. Engl.*, 1979, **18**, 322 (d) G. Pawlowski and M. Hanack, A convenient synthesis of octasubstituted phthalocyanines, *Synthesis*, 1980, 287.

14 J. Simon and P. Bassoul in *Phthalocyanines – Properties and Applications, Vol.2*, Eds. C. C. Leznoff and A. B. P. Lever, VCH Publishers, Inc., New York, 1993.

15 J. M. Kroon, R. B. M. Koehorst, M. van Dijk, G. M. Sanders and E. J. R. Sudhölter, Self-assembling properties of non-ionic tetraphenylporphyrins and discotic phthalocyanines carrying oligo(ethylene oxide) alkyl or alkoxy units, *J. Mater. Chem.*, 1997, **7**, 615.

16 M. Tian, T. Wada, H. Kimura-Suda and H. Sasabe, Novel non-aggregated unsymmetrical metallophthalocyanines for second-order non-linear optics, *J. Mater. Chem.*, 1997, **7**, 861.

17 C. C. Leznoff and A. B. P. Lever (Eds.), *Phthalocyanines – Properties and Applications*, VCH Publishers, Inc., New York, (a) Volume 1, 1989 (b) Volume 2, 1993 (c) Volume 3, 1994, (d) Volume 4, 1996.

18 A. B. Lever, The phthalocyanines, *Adv. Inorg. Radiochem.*, 1965, **7**, 27.

19 E. Musluoglu, A. Gürek, V. Ahsen, A. Gül and Ö. Bekaroglu, Unsymmetrical phthalocyanines with a single macrocyclic substituent, *Chem. Ber.*, 1992, **125**, 2337.

20 N. Kobayashi and A. B. P. Lever, Cation- or solvent-induced supermolecular phthalocyanine formation: crown ether substituted phthalocyanines, *J. Am. Chem. Soc.*, 1987, **109**, 7433.

21 C. C. Leznoff, S. Greenberg, B. Khouw and A. B. P. Lever, The syntheses of mono- and disubstituted phthalocyanines using a dithioimide, *Can. J. Chem.*, 1987, **65**, 1705.

22 M. Ambroz, A. Beeby, A. J. MacRobert, M. S. C. Simpson, R. K. Svensen and D. Phillips, Preparation, analytical and fluorescence spectroscopic studies of sulphonated aluminium phthalocyanine photosensitizers, *J. Photochem. Photobiol. B: Biol.*, 1991, **9**, 87.

23 C. C. Leznoff and S. Greenberg, The syntheses of a monosubstituted and an unsymmetrical tetrasubstituted phthalocyanine using binuclear phthalocyanines, *Tetrahedron Lett.*, 1989, **30**, 5555.

24 S. A. Mikhalenko, S. V. Barkanova, O. L. Lebedev and E. A. Luk'yanets, Phthalocyanines and related compounds. IX. Synthesis and electron absorption spectra of tetra-4-*tert*-butylphthalocyanines, *J. Gen. Chem. USSR*, 1971, **41**, 2770.

25 C. C. Leznoff, S. M. Marcuccio, S. Greenberg, A. B. P. Lever and K. B. Tomer, Metallophthalocyanine dimers incorporating five-atom covalent bridges, *Can. J. Chem.*, 1985, **63**, 623.

26 C. C. Leznoff and D. M. Drew, The use of bisphthalonitriles in the synthesis of side-strapped 1,11,15,25-tetrasubstituted phthalocyanines, *Can. J. Chem.*, 1996, **74**, 307.

27 J. G. Young and W. Onyebuagu, Synthesis and characterization of di-substituted phthalocyanines, *J. Org. Chem.*, 1990, **55**, 2155.

28 N. Kobayashi, R. Kondo, S-I. Nakajima and T. Osa, New route to unsymmetrical phthalocyanine analogues by the use of structurally distorted subphthalocyanines, *J. Am. Chem. Soc.*, 1990, **112**, 9640.

29 S. Dabak, A. Gül and Ö. Bekaroglu, Hexakis(alkylthio)-substituted unsymmetrical phthalocyanines, *Chem. Ber.*, 1994, **127**, 2009.

30 P. N. Day, Z. Wang and R. Pachter, Calculation of the structure and absorption spectra of phthalocyanines in the gas-phase and in solution, *J. Mol. Struct. (Theochem.)*, 1998, **455**, 33.

31 E. Ortí, J. L. Brédas and C. Clarisse, Electronic structure of phthalocyanines: theoretical investigation of the optical properties of phthalocyanine monomers, dimers and crystals, *J. Phys. Chem.*, 1990, **92**, 1228.

32 N. Ishikawa and Y. Kaizu, Exciton coupling and charge resonance in the lowest excited states of lutetium phthalocyanine dimer and trimer, *Chem. Phys. Lett.*, 1994, **228**, 625.

33 N. Ishikawa, O. Ohno and Y. Kaizu, Electronic states of bis(phthalocyaninato)lutetium radical and its related compounds: the application of localised orbital basis set to open-shell phthalocyanine dimers, *J. Phys. Chem.*, 1993, **97**, 1004.

34 M. Gouterman in *The Porphyrins, Volume III, Part A, Physical Chemistry*, Ed. D. Dolphin, Academic Press, New York, 1978.

35 H. C. Longuet-Higgins, C. W. Rector and J. R. Platt, Molecular orbital calculations on porphine and tetrahydroporphine, *J. Chem. Phys.*, 1950, **18**, 1174.

36 L. Edwards and M. Gouterman, Porphyrins XV. Vapor absorption spectra and stablility : phthalocyanines, *J. Mol. Spectrosc.*, 1970, **33**, 292.

37 W. S. Caughey, R. M. Deal, C. Weiss and M. Gouterman, Electronic spectra of substituted metal deuterioporphyrins, *J. Mol. Spectrosc.*, 1965 **16**, 451.

38 E. Ough, T. Nyokong, K. A. M. Creber and M. J. Stillman, Electrochemistry and spectroscopy of magnesium phthalocyanine. Analysis of the absorption and magnetic circular dichroism spectra, *Inorg. Chem.*, 1988, **27**, 2724.

39 L. Bajema, M. Gouterman and B. Meyer, Spectra of Porphyrins XI. Absorption and fluorescence spectra of matrix isolated phthalocyanines, *J. Mol. Spectrosc.*, 1968, **27**, 225.

40 T. C. van Cott, J. L. Rose, G. C. Misener, B. E. Williamson, A. E. Schrimpf, M. E. Boyle and P. N. Schatz, Magnetic circular dichroism and absorption spectrum of zinc phthalocyanine in an argon matrix between 14700 and 74000 cm^{-1}, *J. Phys. Chem.*, 1989, **93**, 2999.

41 E. Ortí and J. L. Brédas, Electronic structure of metal-free phthalocyanine: a valence effective Hamiltonian theoretical study, *J. Chem. Phys.*, 1988, **89**, 1009.

42 P. D. Hale, W. J. Pietro, M. A. Ratner, D. E. Ellis and T. J. Marks, On the electronic structure of substituted phthalocyanines: a Hartree-Fock-Slater study of octacyano- and octafluoro-substituted (phthalocyaninato)silicon dihydroxide, *J. Am. Chem. Soc.*, 1987, **109**, 5943.

43 L. K. Lee, N. H. Sabelli and P. R. Le Breton, Theoretical characterisation of phthalocyanine, tetraazoporphyrin, tetrabenzporphyrin and porphyrin electronic spectra, *J. Phys. Chem.*, 1982, **86**, 3926.

44 M. J. Stillman and T. Nyokong in *Phthalocyanines – Properties and Applications, Vol.1*, Eds. C. C. Leznoff and A. B. P. Lever, VCH Publishers, Inc., New York, 1989.

45 M.J.Stillman and A.J.Thomson, *J.Chem.Soc., Faraday Trans.II*, 1974, **70**, 790.

46 P. Sayer, M. Gouterman and C. R. Connell, Metalloid porphyrins and phthalocyanines, *Acc. Chem. Res.*, 1982, **15**, 73.

47 A.B.P.Lever, S.R.Pickens, P.C.Minor, S.Licoccia, B.S.Ramaswamy and K.Magnell, *J.Am.Chem.Soc.*, 1981, **103**, 6800.

48 P. C. Minor, M. Gouterman and A. B. P. Lever, Electronic spectra of phthalocyanine radical anions and cations, *Inorg. Chem.*, 1985, **24**, 1894.

49 M. Gouterman, Effects of substitution on the absorption spectra of porphin, *J. Chem. Phys.*, 1959, **30**, 1139.

50 M. J. Stillman and A. J. Thomson, Orbital reduction factors in the lowest excited state of the phthalocyanine ring and their measurement by magnetic circular dichroism spectroscopy, *J. Chem. Soc., Faraday Trans. II*, 1974, **70**, 805.

51 K. Jerwin and F. Wasgestian, Solvent dependence of the spin-allowed transitions in free base tetra-*t*-butylphthalocyanine, *Spectrochim. Acta A*, 1984, **40A**, 159.

52 L. J. Boucher in *Coordination Chemistry of Macrocyclic Compounds*, Ed. G. A. Melson, Plenum, New York, 1979.

53 M. G. Cory, H. Hirose and M. C. Zerner, Calculated structures and electronic absorption spectroscopy for magnesium phthalocyanine and its anion radical, *Inorg. Chem.*, 1995, **34**, 2969.

54 A. Henriksson, B. Roos and M. Sundbom, Semiempirical molecular orbital studies of phthalocyanines. II. Electronic structure and excited states of copper phthalocyanine, CuPc, *Theoret. Chim. Acta*, 1972, **27**, 303.

55 J. Mack, S. Kirkby, E. A. Ough, M. J. Stillman, Ground-state and optical spectrum of metallophthalocyanine radical anion from low-temperature magnetic circular dichroism spectroscopy, *Inorg. Chem.*, 1992, **31**, 1717.

56 B. R. Hollebone and M. J. Stillman, Assignment of absorption and magnetic circular dichroism spectra of solid, α phase metallophthalocyanine, *J. Chem. Soc., Faraday Trans. II*, 1978, **74**, 2107.

57 A. Rosa and E. J. Baerends, Metal-macrocycle interaction in phthalocyanines. Density functional calculations of ground and excited states, *Inorg. Chem.*, 1994, **33**, 584.

58 T. M. Keller, T. R. Price and J. R. Griffith, Synthesis of phthalonitriles by nitro displacement, *Synthesis*, 1980, 613.

59 W. O. Siegl, Metal-chelating 1,3-bis(2'-pyridylimino)isoindolines, *J. Heterocyclic Chem.*, 1981, **18**, 1613.

60 C. C. Leznoff in *Phthalocyanines – Properties and Applications, Vol.1*, Eds. C. C. Leznoff and A. B. P. Lever, VCH Publishers, Inc., New York, 1989.

61 P. J. Brach, S. J. Grammatica, O. A. Osanna and L. Weinberger, Improved synthesis of metal-free phthalocyanines, *J. Heterocyclic Chem.*, 1970, **7**, 1403.

62 (a) Z. Witkiewicz, R. Dabrowski and W. Waclawek, Properties of octamethoxyphthalocyanines. I. On their syntheses, electrical conductivity, and catalytic activity, *Mater. Sci.*, 1976, 39 (b) L. I. Solov'eva and E. A. Luk'yanets, Phthalocyanines and related compounds. XVII. Phthalocyaninetetra-t- and octa-4,5-carboxylic acids and their functional derivatives, *J. Gen. Chem. USSR*, 1980, **50**, 907 (c) D. Wöhrle and B. Wahl, Octasubstituted phthalocyanines from 1,2,4,5-tetracyanobenzene, *Tetrahedron Lett.*, 1979, **20**, 227 (d) M. J. Camenzind and C. L. Hill, Synthesis of 2,3,9,10,16,17,23,24-octaethylphthalocyanine, *J.Heterocyclic Chem.*, 1985, **22**, 575 (e) N. Kobayshi, M. Koshiyama, Y. Ishikawa, T. Osa, H. Shirai and N. Hojo, Electrolyte-induced spin-state transition of iron in iron(III) phthalocyanine, *Chem. Lett.*, 1984, 1633.

63 B. L. Wheeler, G. Nagasubramanian, A. J. Bard, L. A. Schechtman, D. R. Dininny and M. E. Kenney, A silicon phthalocyanine and a silicon naphthalocyanine: synthesis, electrochemistry, and electrogenerated chemiluminescence, *J. Am. Chem. Soc.*, 1984, **106**, 7404.

64 D. S. Lawrence and D. G. Whitten, Photochemistry and photophysical properties of novel, unsymmetrically substituted metallophthalocyanines, *Photochem. Photobiol.*, 1996, **64**, 923.

65 T. W. Hall, S. Greenberg, C. R. McArthur, B. Khouw and C. C. Leznoff, The solid phase synthesis of unsymmetrical phthalocyanines, *Nouv. J. Chim.*, 1982, **6**, 653.

66 M. Geyer, F. Plenzig, J. Rauschnabel, M. Hanack, B. del Rey, A. Sastre and T. Torres, Subphthalocyanines: preparation, reactivity and physical properties, *Synthesis*, 1996, 1139.

67 A. Sastre, B. del Rey and T. Torres, Synthesis of novel unsymmetrically substituted push-pull phthalocyanines, *J. Org. Chem.*, 1996, **61**, 8591.

68 C. C. Leznoff, H. Lam, S. M. Marcuccio, W. A. Nevin, P. Janda, N. Kobayashi and A. B. P. Lever, A planar binuclear phthalocyanine and its dicobalt derivative, e*J. Chem. Soc., Chem. Commun.*, 1987, 699.

69 H. Lam, S. M. Marcuccio, P. I. Svirskaya, S. Greenberg, A. B. P. Lever and C. C. Leznoff, Binuclear phthalocyanines with aromatic bridges, *Can. J. Chem.*, 1989, **67**, 1087.

70 S. Greenberg, S. M. Marcuccio and C. C. Leznoff, Selective synthesis of binuclear and trinuclear phthalocyanines covalently linked by a one atom oxygen bridge, *Synthesis*, 1986, 406.

71 S. M. Marcuccio, P. I. Svirskaya, S. Greenberg, A. B. P. Lever and C. C. Leznoff, Binuclear phthalocyanines covalently linked through two- and four-atom bridges, *Can. J. Chem.*, 1985, **63**, 3057.

72 C. C. Leznoff, S. Greenberg, S. M. Marcuccio, P. C. Minor, P. Seymour, A. B. P. Lever and K. B. Tomer, Binuclear 'clamshell' metallophthalocyanines, *Inorg. Chim. Acta*, 1984, **89**, L35.

73 S. Vigh, H. Lam, P. Janda, A. B. P. Lever, C. C. Leznoff and R. L. Cerny, Synthesis and electrochemistry of linear and co-facial conjugated binuclear phthalocyanines covalently linked by alkyne and alkene bridges, *Can. J. Chem.*, 1991, **69**, 1457.

74 C. C. Leznoff, H. Lam, W. A. Nevin, N. Kobayashi, P. Janda and A. B. P. Lever, 1,8-naphthalene-linked co-facial dimeric phthalocyanines, *Angew. Chem. Int. Ed. Engl.*, 1987, **26**, 1021.

75 S. Gaspard, C. Gianotti, P. Maillard, C. Schaeffer and T-H. Tran-Thi, The first synthesis of covalently linked mixed dimer complexes containing phthalocyanine and porphyrin, *J. Chem. Soc., Chem. Commun.*, 1986, 1239.

76 N. Kobayashi, Y. Higashi and T. Osa, A planar phthalocyaninylnaphthalocyanine as a broad near-infrared absorber, *Chem. Lett.*, 1994, 1813.

77 C. C. Leznoff, P. I. Svirskaya, B. Khouw, R. L. Cerny, P. Seymour and A. B. P. Lever, Syntheses of monometalated and unsymmetrically substituted binuclear phthalocyanines and a pentanuclear phthalocyanine by solution and polymer support methods, *J. Org. Chem.*, 1991, **56**, 82.

78 S. E. Sheppard and A. L. Geddes, Effect of solvents upon the absorption spectra of dyes. IV. Water as solvent: A common pattern, *J. Am. Chem. Soc.*, 1944, **66**, 1995.

79 R. J. Blagrove and L. C. Gruen, Thermodynamics of the dimerization of copper (II) phthalocyanine-4,4',4",4"'-tetrasulphonic acid, *Aust. J. Chem.*, 1973, **26**, 225.

80 Y-C. Yang, J. R. Ward and R. P. Seiders, Dimerization of cobalt (II) tetrasulfonated phthalocyanine in water and aqueous alcoholic solutions, *Inorg. Chem.*, 1985, **24**, 1765.

81 A. R. Monahan, J. A. Brado and A. F. De Luca, The dimerization of a copper(II)-phthalocyanine dye in carbon tetrachloride and benzene, *J. Phys. Chem.*, 1972, **76**, 446.

82 L. C. Gruen, Aggregation of copper phthalocyanine dyes, *Aust. J. Chem.*, 1972, **25**, 1661.

83 C. A. Hunter, J. K. M. Sanders and A. J. Stone, Exciton coupling in porphyrin dimers, *Chem. Phys.*, 1989, **133**, 395.

84 W. West and S. Pearce, The dimeric state of cyanine dyes, *J. Phys. Chem.*, 1965, **69**, 1894.

85 K. Kemnitz, N. Tamai, I. Yamazaki, N. Nakashima and K. Yoshihara, Fluorescence decays and spectral properties of rhodamine B in submono-, mono- and multilayer systems, *J. Phys. Chem.*, 1986, **90**, 5094.

86 A. R. Monahan and D. F. Blossey, The aggregation of arylazonaphthols. I. Dimerization of Bonadur Red in aqueous and methanolic systems, *J. Phys. Chem.*, 1970, **74**, 4014.

87 A. R. Monahan, N. J. Germano and D. F. Blossey, The aggregation of arylazonaphthols. II. Steric effects on dimer structure in water, *J. Phys. Chem.*, 1971, **75**, 1227.

88 M. Kasha, H. R. Rawls and M. A. El-Bayoumi, The Exciton Model in molecular spectroscopy, *Pure Appl.Chem.*, 1965, **11**, 371.

89 M. Kasha, Characterization of electronic transitions in complex molecules, *Disc. Faraday Soc.*, 1950, **9**, 14.

90 E. S. Dodsworth, A. B. P. Lever, P. Seymour and C. C. Leznoff, Intramolecular coupling in metal-free binuclear phthalocyanines, *J. Phys. Chem.*, 1985, **89**, 5698.

91 W. J. Schutte, M. Sluyters-Rehbach and J. H. Sluyters, Aggregation of an octasubstituted phthalocyanine in dodecane solution, *J. Phys. Chem.*, 1993, **97**, 6069.

92 M. Abkowitz and A. R. Monahan, ESR and electronic spectral investigation of the self-association of phthalocyanine dyes in solution, *J. Chem. Phys.*, 1973, **58**, 2281.

93 C. F. Stanley, *Photophysical evaluation of substituted zinc phthalocyanines as sensitisers for photodynamic therapy*, Ph.D. Thesis, University of Durham, 1997.

94 S. Tai and N. Hayashi, Strong aggregation properties of novel naphthalocyanines, *J. Chem. Soc., Perkin Trans. 2*, 1991, 1275.

95 R. D. George, A. W. Snow, J. S. Shirk and W. R. Barger, The alpha substitution effect on phthalocyanine aggregation, *J. Porphyrins Phthalocyanines*, 1998, **2**, 1.

96 E. W. Abel, J. M. Pratt and R. Whelan, Formation of a 1:1 oxygen adduct with the cobalt(II)-tetrasulfophthalocyanine complex, *J. Chem. Soc. D*, 1971, 449.

97 A. B. Anderson, T. L. Gordon and M. E. Kenney, Electronic and redox properties of stacked-ring silicon phthalocyanines from molecular orbital theory, *J. Am. Chem. Soc.*, 1985, **104**, 192.

98 N. S. Hush and I. S. Woolsey, Electronic absorption spectra of phthalocyanine monomers and dimers, *Mol. Phys.*, 1971, **21**, 465.

99 M. Gouterman, D. Holten and E. Lieberman, Porphyrins XXXV. Exciton coupling in μ-oxo scandium dimers, *Chem. Phys.*, 1977, **25**, 139.

100 W. A. Nevin, W. Liu and A. B. P. Lever, Dimerisation of mononuclear and binuclear cobalt phthalocyanines, *Can. J. Chem.*, 1987, **65**, 855.

101 A. Gilbert and J. Baggott, *Essentials of molecular photochemistry*, Blackwell Scientific Publishing, Oxford, 1991.

102 N. J. Turro, *Modern Molecular Photochemistry*, University Science Books, Mill Valley, California, 1991.

103 J. R. Lakowicz, *Principles of Fluorescence Spectroscopy*, Kluwer Academic/Plenum Press, New York, 1999, Second Edition.

Chapter 2

Experimental techniques

2.1 Introduction

The work discussed in this thesis makes use of a number of standard spectroscopic techniques, and the general theory of these techniques and required experimental setups are discussed briefly below. In addition, where necessary, individual chapters have specific experimental sections, and details of synthetic strategies for the compounds discussed within the chapters can be found in these sections.

2.2 UV-Visible Absorption Spectroscopy

Background corrected UV-visible absorption spectra were obtained on an ATI Unicam UV/VIS UV2 spectrometer. Spectra were generally acquired over an appropriate wavelength range using quartz cells with a 10 mm pathlength - where necessary, however, cuvettes with pathlengths of 1 mm, 2 mm, 25 mm and 50 mm were also utilised.

Molar extinction coefficients at a given wavelength, ε_λ, were obtained using the Beer-Lambert law:

$$A_\lambda = \varepsilon_\lambda c l \qquad (2.1)$$

where A_λ is the absorbance at the wavelength of interest, c is the concentration in units of mol dm^{-3}, and l is the pathlength of the cuvette in cm. The units of ε_λ are $dm^3 mol^{-1} cm^{-1}$. Beer-Lambert plots were generally obtained over the concentration range 10^{-4}-10^{-7} mol dm^{-3}.

2.3 Fluorescence Spectroscopy

2.3.1 Spectra

Emission and excitation spectra were recorded on a Perkin Elmer LS-50B luminescence spectrometer, a Spex Fluoromax 2 spectrofluorimeter and a Spex Fluorolog 3 spectrofluorimeter. In all cases the obtained spectra were corrected for the spectral response of the machines. Sample conditions were carefully chosen to avoid the effects of re-absorption as described by Dhami *et al.*[1] Excitation in the Q band region was used

without exception, to prevent the possibility of emission from upper excited states[2] and the presence of complex UV activated photochemistry.[3]

In the case of the 1,4,8,11,15,18,22,25-octabutoxy zinc phthalocyanine the extreme red shifted emission of the protonated species made necessary the use of a home built near infra-red fluorimeter. The chopped output of a xenon lamp (Bentham IL6 Illuminator) was used to excite the samples, and emission was collected at 90° to the excitation source, and focussed into a Jobin Yvon Triax 320 monochomator. The intensity of light at a given wavelength was measured by a silicon pin diode (Hamamatsu). The signal was demodulated using a lock in amplifier (Stanford SR510), and transferred to PC for analysis.

2.3.2 Quantum yields

The fluorescence quantum yield is defined as the ratio of the number of photons emitted as fluorescence to the number of photons absorbed. In terms of competing decay processes, and assuming steady state conditions (such that the rate of formation of singlet state equals the rate of decay) the quantum yield can be represented by Equation 2.2.

$$\Phi_f = k_f / (k_f + k_{ic} + k_{isc} + k_{nr}) \qquad (2.2)$$

where k_f, k_{ic}, k_{isc} and k_{nr} represent the rate constants for fluorescence, internal conversion, intersystem crossing and other non-radiative processes, respectively.

Fluorescence quantum yields reported in this work were obtained using the comparative method of Williams *et al.*[4] using cresyl violet in methanol (Φ_f = 0.54) and disulfonated aluminium phthalocyanine in water (Φ_f = 0.40) as standards. Relative to the standard compound, the quantum yield of the unknown sample is presented in Equation 2.3.

$$\Phi_X = \Phi_{ST}\left(\frac{A_{ST}}{A_X}\right)\left(\frac{I_X}{I_{ST}}\right)\left(\frac{\eta_X^2}{\eta_{ST}^2}\right) \qquad (2.3)$$

The subscripts X and ST represent the unknown and standard compounds respectively, Φ is the quantum yield, A the absorbance at the excitation wavelength, I the integrated area of fluorescence emission and η the refractive index of the solvent. Measurements were performed using at least five different concentrations of fluorophore to ensure the absence of concentration effects, and all solutions were prepared with absorbances below 0.1 in a 10 mm pathlength cell to minimise inner filter effects.[1] All spectra were corrected for the spectral response of the chosen fluorimeter prior to integration to obtain the area of emission, I.

2.4 Time Correlated Single Photon Counting

2.4.1 Introduction

The technique of time correlated single photon counting[5,6] was used to record fluorescence lifetimes of the phthalocyanines discussed in this work.

Decays are obtained using a sub-nanosecond pulsed excitation source to repeatedly excite the sample. For each excitation pulse, the system is so arranged that only a single randomly selected photon is detected following the pulse, and the time taken between pulse and photon arrival is recorded for each event. This time interval is measured using the voltage ramp of a time to amplitude converter (TAC). A histogram of the number of photons arriving versus time interval is built up by a pulse height analyser (PHA) – the histogram represents the probability of detecting a photon at a given time after the excitation pulse. At a short time interval after excitation the probability of photon emission is greater than at a large time interval when the fluorescence has decayed, and hence the resulting histogram represents directly the variation of fluorescence intensity with time. Further details can be found in reviews by O'Connor and Phillips[5] and Lakowicz.[6]

The TAC works by charging a capacitor during the time interval between start and stop pulses. In general the TAC is the rate-limiting component in the photon counting experiment. The capacitor discharge and TAC reset takes several microseconds, and so for a high repetition laser source (for example, a 1 MHz source) the TAC will be overloaded by start pulses. This problem is circumvented by operating the TAC in 'reverse mode,' in which the first photon detected provides the start pulse, and the signal from the subsequent excitation pulse is the stop signal. Hence the TAC is only

activated if an emitted photon is detected, rather than for every excitation pulse (in general, one photon is detected for every 50-100 excitation pulses). The resulting histogram appears reversed, but correction by software is trivial.

2.4.2 Data Analysis

The measured intensity decay obtained from a photon counting experiment is a convolution of the exponential decay with the excitation and instrument response functions.[5,6] In an ideal system in which both the excitation and instrument response are represented by true δ-functions the true decay, I(t), would be observed (see Figure 2.1). However, in reality, the excitation pulse can be considered as a series of δ-functions with varying amplitudes, such that each δ-function will yield one decay from the sample. The measured intensity decay will be the sum of these individual exponential decays.

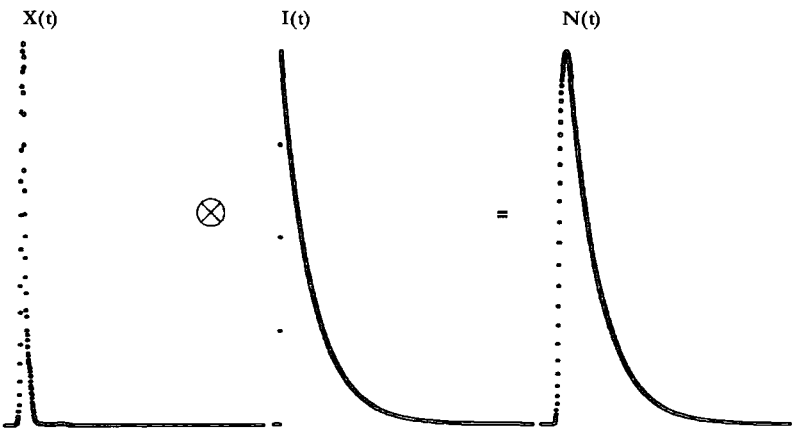

Figure 2.1 Convolution of a decay I(t) with the excitation profile X(t) to yield the measured intensity decay, N(t).

The most general and reliable method used for the analysis of the convolved data is that of non-linear least-squares analysis,[7] which involves iterative reconvolution of the instrument response function, X(t), with a chosen function and non-linear least-squares fitting. This entails recording an excitation pulse profile, convolving this instrument response function with a theoretical exponential decay, and then optimising the parameters of the decay to match the measured intensity decay. The fitting procedure is carried out using the Solver function in Microsoft Excel, and yields values for the amplitude (A) and lifetime (τ) of the fluorescence decay.

The first excited singlet state of a fluorophore usually decays (through fluorescence) via a first order process, and hence the decay may be represented by a single exponential decay. However, in cases where there is more than one emitting species the decay may be described more adequately by a sum of exponential terms,

$$I(t) = A_1\exp(-t/\tau_1) + A_2\exp(-t/\tau_2) + \ldots \quad (2.4)$$

where A_n represents the fluorescence intensity at time t = 0 for the n^{th} component, τ_n the lifetime for the n^{th} component and I(t) the total intensity of fluorescence at time t. The contribution of each component to the overall fluorescence intensity is represented by the yield.

$$\text{Yield of } n^{th} \text{ component} = \frac{A_n\tau_n}{\sum_i A_i\tau_i} \times 100 \quad (2.5)$$

The quality of the fit is an important factor to be considered when analysing fluorescence decays, since without it the validity of the results is unknown. The quality of fits obtained for this thesis was judged according to a number of parameters:

Parameter		Description
χ_R^2	Reduced chi squared[6]	If only random errors contribute to χ_R^2 the value is expected to be near unity. Typically, if $0.95<\chi_R^2<1.20$ the fit is judged to be good.
r(j)	Weighted residuals[6]	The residuals, weighted by their standard deviation, represent the difference between the raw and fitted data. Ideally the residuals should be small and randomly distributed about zero.
cr(j)	Autocorrelated residuals[8]	The autocorrelation function cr(j) is the extent of correlation between the deviations in the k^{th} and $(k+j)^{th}$ channel. For a good fit the autocorrelated residuals should be small and randomly distributed about zero. The function is more sensitive than r(j).
DW	Durbin Watson parameter[9]	Like cr(j) the DW parameter also tests for correlation between deviations, returning a discrete number. A good fit will yield DW values greater than 1.7 and 1.75 for single and double exponential models respectively.

The mathematical functions relating to these parameters and a description of the computer software for their calculation can be found in Appendix B.

The use of all these parameters when analysing a fluorescence decays allows the relevant amplitude(s) and lifetime(s) of the system under study to be obtained with good confidence in their values. An example decay with a good quality fit is presented in Figure 2.2.

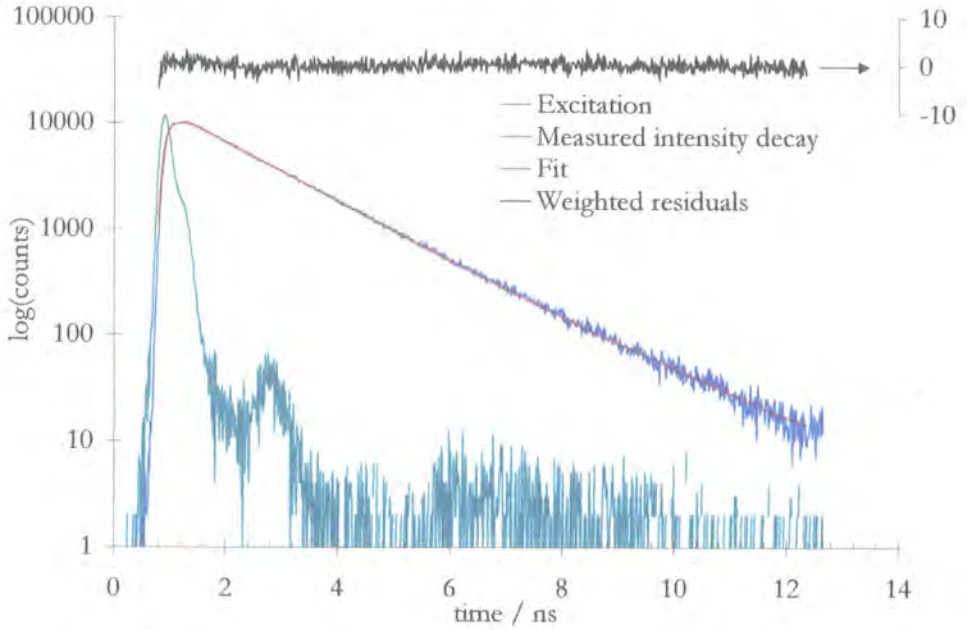

Figure 2.2 Example data and fit obtained by time correlated single photon counting for Rhodamine B in water, $\lambda_{ex} = 400$ nm, $\tau_f = 1.5$ ns.

2.4.3 Experimental Details

All solutions under study were prepared with a concentration so as to give to a maximum absorbance at the Q band of no greater than 0.05, in order to eliminate the effects of re-absorption.[1] The excitation source consists of a pulsed 635 nm diode laser (IBH NanoLED Model-02) providing output pulses of <200 ps at a repetition rate of 1 MHz. The fluorescence emission was collected at 90° to the excitation source (see Figure 2.3), and the emission wavelength selected using a monochromator (Jobin Yvon Triax 190). The fluorescence was detected using a cooled, red sensitive photomultiplier tube (IBH Model TBX-04) linked to a time-to-amplitude converter (Ortec 567) and multichannel analyser (E.G. & G. Trump Card and Maestro for Windows v.5.10). The instrument response function (IRF) of the apparatus was measured using a dilute suspension of milk powder in water as a scattering medium giving an IRF with a duration of 450 ps full width at half maximum (FWHM). The time per channel was typically ~50 ps giving a full range of ~50 ns over the 1,024 point data set. All

fluorescence decays were recorded to a minimum of 10,000 counts in the peak channel of the pulse height analyser. The data was transferred to computer and analysed by using the standard method of iterative reconvolution and non-linear least squares fitting in a Microsoft Excel spreadsheet[5] (see Appendix B).

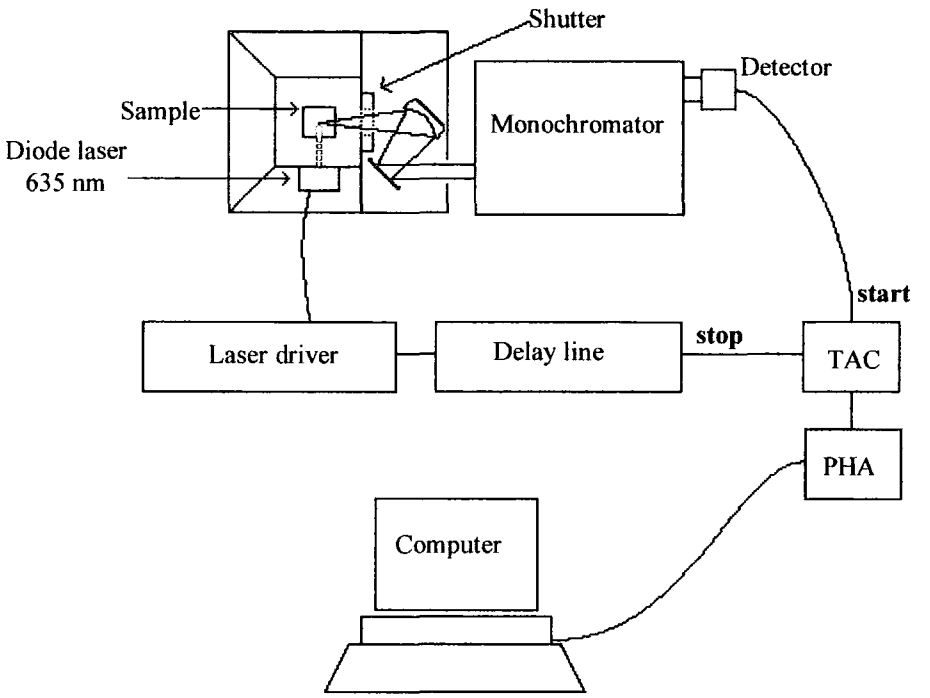

Figure 2.3 Experimental arrangement for time correlated single photon counting. TAC = time to amplitude converter; PHA = pulse height analyser.

2.5 Nanosecond Laser Flash Photolysis

2.5.1 Introduction

The technique of flash photolysis was first developed by Porter and Norrish in 1949,[10] and provides a technique of probing transient species with millisecond to sub-nanosecond lifetimes.

The sample is excited by an intense, temporally narrow pulse of light which generates the first excited singlet state, S_1. This state can decay by a number of processes, including fluorescence, internal conversion and intersystem crossing to access the triplet state, T_1 (Figure 2.4). A white light probe beam is then shone through the

sample to gain information specific to the triplet state. This probe light is absorbed by the T_1 state, and so changes in the probe beam intensity can be monitored to give information on the concentration of T_1 as a function of time. In the accompanying diagram (Figure 2.5), I_o represents the intensity of the incident probe beam, I(a) represents the intensity of *absorbed* probe light, and I(t) represents the intensity of *transmitted* radiation. The excitation pulse occurs at time t=0.

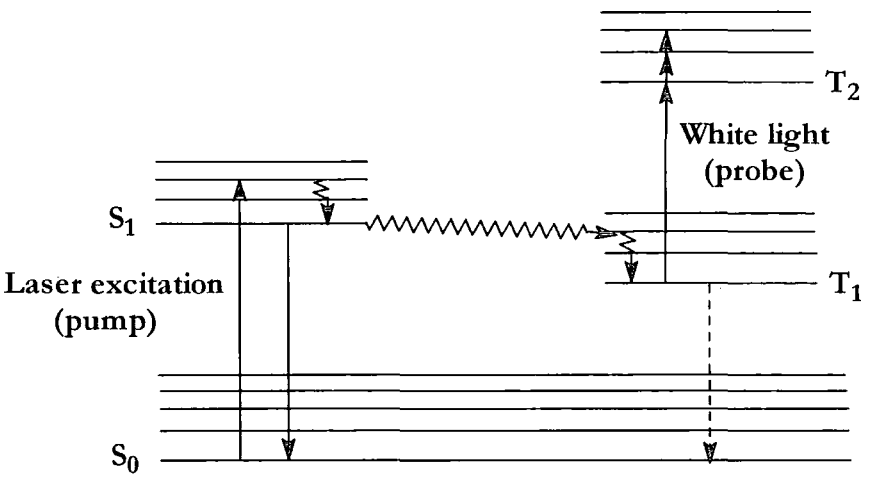

Figure 2.4 Jabłoński diagram outlining the processes involved in flash photolysis.

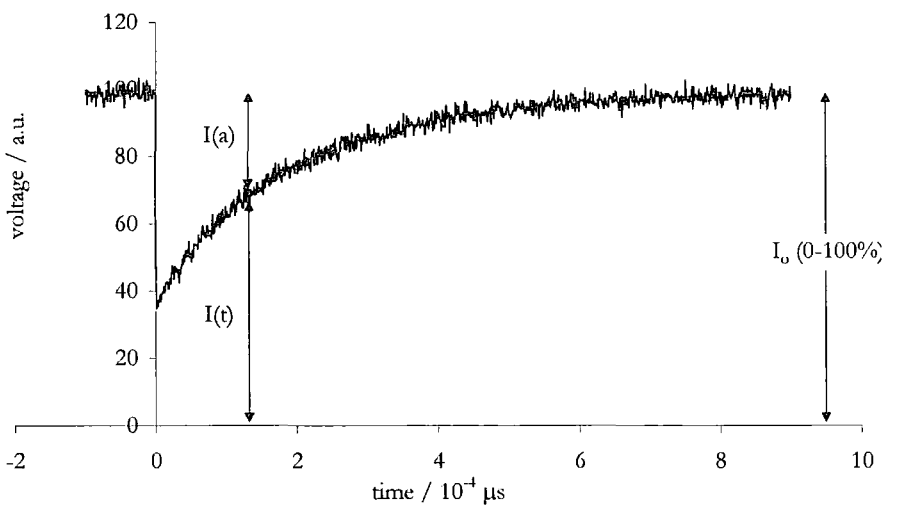

Figure 2.5 A typical transient decay.

It is trivial to calculate the absorbance of the transient species according to Equation 2.6 - I(a) is positive when an absorbing species is formed (that is, the intensity of the probe radiation *decreases* upon excitation), and negative when bleaching of the

ground state is observed (that is, the intensity of the probe radiation *increases* upon excitation).

$$\Delta A = \log_{10}\left(\frac{I_o}{I_o - I(a)}\right) \qquad (2.6)$$

This process of obtaining a ΔA decay is repeated whilst monitoring different probe wavelengths, allowing a three dimensional array of data to be obtained, containing both kinetic and spectral information about the transient species. It is thus possible to observe the decay of the T_1 state at any probe wavelength, or, by integrating the decays between set limits, to acquire the triplet state absorption spectrum.

2.5.2 Experimental Details

Studies of phthalocyanine triplet states were performed using a nanosecond laser flash photolysis system (see Figure 2.6). The apparatus consisted of a Q-switched Nd:YAG laser (Spectra Physics, Quanta Ray GCR-150-10) producing a 10 Hz train of pulses with a FWHM of ca 8 ns. The output was frequency doubled to produce 532 nm radiation which was used to pump a dye laser (Spectra Physics PDL-3) containing DCM (Lambda Physik) in methanol as the gain medium tuned to lase at 615 nm, providing a pulse energy at the sample of <3 mJ per pulse. A tungsten-halogen lamp (100W) was used to probe the transient species produced upon laser excitation; the probe beam was focussed through the sample, and subsequently into a monochromator (Jobin Yvon Triax 320) which was computer controlled. The intensity of light at a given wavelength was measured by a silicon avalanche diode (Hamamatsu), providing a steady state signal of ca 800 mV with transients of up to 50 mV. Transient decays were digitised and averaged by a digital storage oscilloscope (Tektronix TDS-340) over at least 64 laser pulses. The data were transferred to computer, converted into absorbance units and analysed using a programme written in LabVIEW (National Instruments)(see Appendix A). Triplet-triplet absorption spectra were obtained by adding a fraction of the ground state absorption spectrum to the difference spectrum:

$$T(\lambda) = D(\lambda) + \chi A(\lambda) \qquad (2.7)$$

where T(λ) = triplet-triplet absorption spectrum corrected for ground state bleach, D(λ) = difference spectrum, A(λ) = ground state absorption and χ is a constant. χ is chosen such that all ground state bleach evident in the difference spectrum, D(λ), is removed. At the point at which the removal of negative Δabsorbance is complete, A(λ) is only further added to remove any obvious trough still resulting from ground state bleach. This secondary addition of A(λ) is monitored using the first and second derivatives of the acquired ground state corrected transient spectrum, which allow much clearer indication of peak growth in the ground state bleach region. Such monitoring prevents excess addition of A(λ) to yield a transient spectrum with similar profile to that of the ground state.

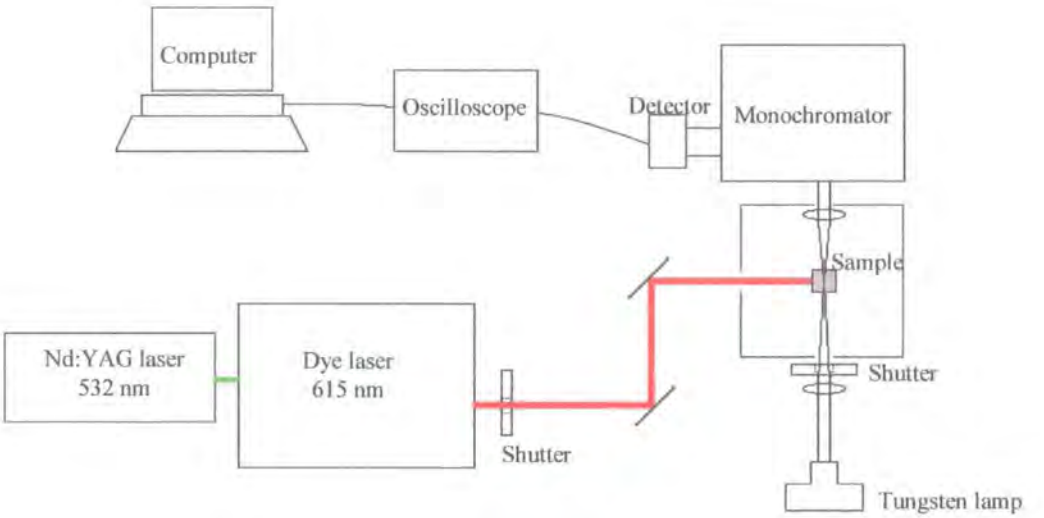

Figure 2.6 Experimental arrangement for flash photolysis.

2.6 Spectroelectrochemistry and Cyclic Voltammetry

Spectroelectrochemical studies were performed using an optically transparent thin layer electrode (OTTLE) cell,[11] comprising a 1 mm pathlength quartz cuvette, platinum mesh as the working electrode, and platinum wire reference and counter electrodes (Figure 2.7).[12] A home built potentiostat capable of supplying working voltages between +2 V and –2 V was used. Absorption studies were achieved by passing the probe beam through the working electrode (and solution of interest). For emission the Perkin Elmer LS-50B spectrometer was used - the cell was held at 45° to the excitation beam which

was focussed into the centre of the cell. The emission was collected from the opposite side of the cell (Figure 2.8).

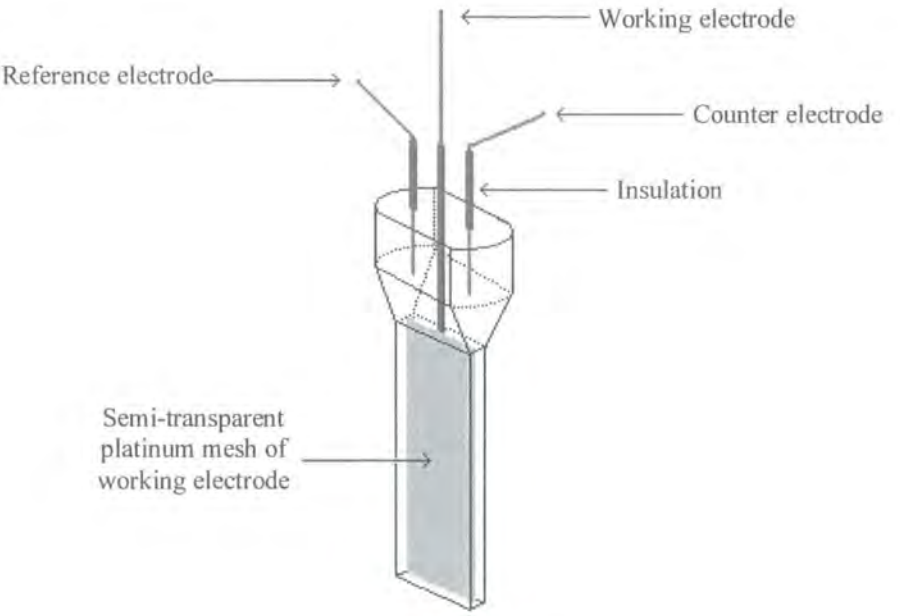

Figure 2.7 OTTLE cell used for spectroelectrochemistry.

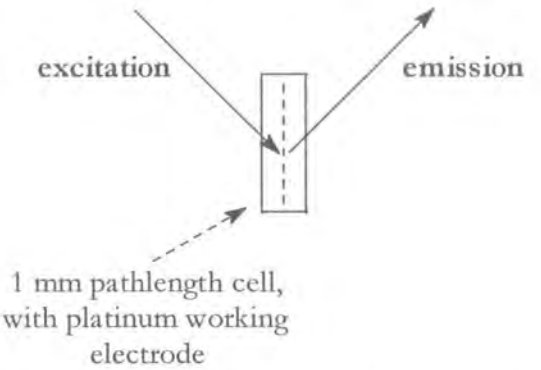

Figure 2.8 Experimental setup for emission spectroelectrochemical studies, viewed from above, looking down the cell.

Where oxidation potentials were required, cyclic voltammetry was used. Cyclic voltammetry experiments were recorded using an E.G. & G. Versastat II instrument, using $[NBu_4]BF_4$ as the electrolyte (0.1 mol dm^{-3} in acetonitrile). Solutions were purged with argon and experiments were conducted with a platinum working electrode and platinum wire reference and counter electrodes at room temperature. Oxidation

potentials obtained were referenced using the ferrocene-ferrocenium redox couple (0.40 V vs SCE).[13] All values are reported vs NHE, where E(SCE) = 0.24 V vs NHE.

2.7 Low Temperature Measurements

Low temperature measurements were performed in either EPA (5:5:2 v/v/v diethylether/2-methylbutane/ethanol) or 2-methyltetrahydrofuran, using a liquid nitrogen cooled cryostat (Oxford Instruments, DN 1704). Temperatures between 293 K and 77 K were obtained using a temperature controller (Oxford Instruments, Intelligent Instrument Controller, ITC 6). Samples were allowed to equilibrate for at least 30 minutes at each temperature. All spectrometers used were adapted to accommodate the cryostat.

2.8 References

1 S. Dhami, A. J. de Mello, G. Rumbles, S. M. Bishop, D. Phillips and A. Beeby, Phthalocyanine fluorescence at high concentration: dimers or reabsorption effect? *Photochem. Photobiol.*, 1995, **61**, 341.

2 S. Muralidharan, G. Ferraudi and L. K. Patterson, Luminescence from upper electronic excited states of phthalocyanines, *Inorg. Chim. Acta*, 1982, **65**, L235.

3 G. Ferraudi in *Phthalocyanines – Properties and Applications, Vol.1*, Eds. C. C. Leznoff and A. B. P. Lever, VCH Publishers, Inc., New York, 1989.

4 A. T. R. Williams, S. A. Winfield and J. N. Miller, Relative fluorescence quantum yields using a computer controlled luminescence spectrometer, *Analyst*, 1983, **108**, 1067.

5 D. V. O'Connor and D. Phillips, *Time Correlated Single Photon Counting*, Academic Press, London, 1984.

6 J. R. Lakowicz, *Principles of Fluorescence Spectroscopy*, Kluwer Academic/Plenum Press, New York, 1999, Second Edition.

7 D. V. O'Connor, W. R. Ware and J. C. Andre, Deconvolution of fluorescence decay curves, *J. Phys. Chem.*, 1979, **83**, 1333.

8 A. Grinvald and I. Z. Steinberg, On the analysis of fluorescence decay kinetics by the method of least-squares, *Anal. Biochem.*, 1974, **59**, 583.

9 (a) J. Durbin and G. S. Watson, Testing for serial correlation in least squares regression, I, *Biometrika*, 1950, **37**, 409; (b) J. Durbin and G. S. Watson, Testing for serial correlation in least squares regression, II, *ibid.*, 1951, **38**, 159.

10 G. Porter and R. G. W. Norrish, Chemical reactions produced by very high light intensities, *Nature*, 1949, **154**, 658.

11 P. A. Christensen and A. Hammett, *Techniques and mechanisms in electrochemistry*, Blackie Academic and Professional, Glasgow, 1994.

12 C. M. Huff and G. A. Heath, Step-wise ligand additivity effects on electrode potentials and charge-transfer spectra in hexahalide, mixed halide/nitrile and hexakis(nitrile) complexes of ruthenium(IV), -(III) and -(II), *Inorg. Chem.*, 1991, **30**, 2528.

13 N. G. Connelly and W. E. Geiger, Chemical redox agents for organometallic chemistry, *Chem. Rev.*, 1996, **96**, 877.

Chapter 3

Protonation of Phthalocyanines

3.1 Introduction

The phenomenon of protonation in phthalocyanines and its effect upon their photophysical and photochemical properties is one that has received very little attention in the literature. This is surprising, since it has been shown that acidic conditions can encourage localisation and retention of porphyrin photodynamic therapeutic agents within membranes in general[1] and tumour cells in particular.[2]

In 1983 Iodko *et al.* reported quantitative studies on the stepwise protonation of phthalocyanines,[3] occurring on the azomethine nitrogens.[4] Using an unusual solvent mixture of trifluoromethanesulfonic acid in benzotrifluoride with acid concentrations ranging from 0 to 5 mol dm^{-3}, it was shown that successive protonation of gallium tetra-butyl-phthalocyanine (Bu_4GaPc) could be monitored by absorption spectroscopy. The unprotonated species contains D_{4h} symmetry, and this is retained by the tetra-protonated form. The mono-, di- and tri-protonated forms however have a lower symmetry and the intense Q band splits into its x and y polarised transitions. Successive protonation steps are each accompanied by a bathochromic shift, the final tetra-protonated Q band being 170 nm red shifted. An almost identical effect was seen by Beeby *et al.*[5] looking at $^tBu_4ZnPc$ in acidified ethanolic solution. This work was considerably more detailed, and recorded emission and excitation spectra in addition to UV-visible. With tetra-protonation a 140 nm red shift was seen for the Q band absorption, and the emission peak was shifted by a similar amount, with decreased intensity. Excitation spectra mirrored those of absorption, confirming the presence of only one emitting species at each of the chosen acid concentrations. Kinetic studies showed a reduction in the rate of deactivation of the singlet excited state and a concomitant increase in the rate of internal conversion. The rate of intersystem crossing remained constant. As a result, it was shown that the overall rate of deactivation of the emitting state increased with protonation, which explained the decrease in quantum yield of fluorescence and hence the observed intensity.

Addition of a proton to the azomethine nitrogen removes electron density from the α-positions. A significant portion of the phthalocyanine electron density resides at these positions in the HOMO but not in the LUMO - hence removal of electron density favours the HOMO to LUMO transition, and leads to a reduction in the HOMO-

LUMO ($e_g \leftarrow a_{1u}$) energy gap.[6] The result is a continual red shift of both absorption and emission peaks upon protonation.

Investigation by Stanley[7] into protonation of disulfonated zinc phthalocyanine ($ZnPcS_2$) showed that protonation occurred under relatively mild conditions, resulting in a new absorption band at ~700 nm and emission band at ~707 nm (relative to ~675 and ~680 nm respectively).

Lang *et al.* studied the affect of mono-protonation upon the reactions of triplet-state sulfonated aluminium phthalocyanine chloride with dioxygen,[8] concluding that protonation substantially affects the triplet state lifetime and hence the rate of quenching by dioxygen. Such information is important when considering the efficacy of such compounds as PDT sensitisers. In 1982 Darwent *et al.* investigated electron transfer reactions of trisulfonated aluminium phthalocyanine, and although pH effects were not studied comprehensively, a reduction of the triplet state decay rate constant was observed on going from pH 8 to pH 5.[9]

The influence of substituents on the basicity of copper phthalocyanine derivatives was studied by Derkacheva *et al.*[10] who observed the stability constants for protonated species with a wide range of substituents in both the α- and β-positions. The bathochromic shift of the Q band was readily apparent, as expected. Their conclusions were that the basicity of the phthalocyanine ring decreased as the acceptor power of the substituent increased, with the α-substituents having more influence than the β-substituents. Substituents in the α-position containing donor atoms were shown to stabilise the protonated form by the formation of an intramolecular hydrogen bond between the donor atom and proton.

A complete study on the pH effect on the photophysics and photochemistry of disulfonated aluminium phthalocyanine has been reported.[11] The triplet state lifetime was found to reduce with decreasing pH, concurring with previous work mentioned above, but the fluorescence lifetime was found to be independent of pH, contrary to the observations for a zinc phthalocyanine.[5] It must be noted that spectral changes observed upon protonation in this work are assigned to ligand phenomena, seeing a change from $(H_3O^+)_2AlPcS_2$ at low pH to $(HO^-)AlPcS_2$ at high pH in a number of steps, rather than the macrocycle protonation discussed above. The changes in absorption spectrum with pH entailed increased intensity of a broad dimer-like peak at lower energy than the Q band, which was reasoned to be due to an interchange between a 'low-pH dimer' and a

'high-pH dimer,' identified (using *ab initio* calculations) as $[(H_3O^+)AlPcS_2]_2Cl^-$ and $[(H_2O)AlPcS_2]_2OH^-$ respectively. As such, this work appears to be unrelated to the rest of the literature on protonation, which is concerned with definite macrocycle protonation, as shown by a sharp peak to the red of the normal Q band.

There is a small number of reports in the literature that show a red shifted absorption band typical of protonation which have either not been commented upon, or else have been misassigned. Gaspard *et al.* reported the synthesis of a mixed phthalocyanine-porphyrin dimer[12] which included one step to demetallate the porphyrin moeity by acidifying the solution followed by neutralisation. Absorption spectra recorded to monitor the process were included in the report, and showed, in acid solution only, the appearance of a new band to the red of the phthalocyanine Q band. No mention concerning this spectral feature was made. Yoon *et al.* reported a fluorescent dimer of tetrasulfonated aluminium phthalocyanine chloride in aqueous alcoholic solution,[13] characterised by a red shifted absorption and emission peaks. The ratio of these peaks relative to the normal monomer bands were found to be dependent upon both solvent composition (proportional to volume percentage of ethanol) and concentration (increasing with increased concentration). This phenomenon was attributed by the authors to a new low energy (π-π^*) excited state, arising from slipped face-to-face overlap. Specifically the interaction was proposed to exist primarily between the metal in one monomer and nitrogen in the other. The disappearence of the peak with diminishing ethanol content was explained by the presence of increased water hydrogen bonding inhibiting the dimer interaction. The 'dimer' effect was re-interpreted by Dhami *et al.*[14] as a reabsorption effect on account of the high concentrations used, but this failed to completely explain the red shifted absorption peak. Stanley[7] suggested that the peak was typical of mono-protonation. A similar phenomenon was observed with tetrasulfonated zinc phthalocyanine in aqueous acetonitrile solution,[15] and this observation forms the basis of work reported in this chapter. An explanation of the new band being due to a slipped co-facial dimer was proposed.

The presence of a slipped co-facial aggregate is not impossible, for there has been reported an imidazolyl-porphyrin compound which displays a well characterised slipped co-facial dimer.[16] However, this was explained by an unusual interaction between the ligand and central metal ion, and should be considered the exception rather than the

rule. In the above cases, the reason for the so-called 'dimer' band can equally well be assigned to protonation, and work discussed in this report and elsewhere[5,7] serves to corroborate this. Yoon *et al.*[13] and Kaneko *et al.*[15] both worked with sulfonated phthalocyanines, so the presence of protons (originating from the sulfonic acid substituents) within the aqueous solution is not unexpected.

Given the interest in the use of sulfonated phthalocyanines as second generation PDT agents[17,18,19] it is vital that the protonation behaviour of such species is fully understood. This current work investigates more fully the report of unusual behaviour in tetrasulfonated zinc phthalocyanine, and discusses the results and their application to the design of new, enhanced PDT agents. With regard to this, a brief study of the effects of protonation on octabutoxy zinc phthalocyanine is reported.

3.2 Experimental

3.2.1 Synthesis of Tetrasulfonated Zinc Phthalocyanine

The condensation method used by Ambroz *et al.*[20] was followed for the synthesis, adapting the method to produce zinc rather than aluminium phthalocyanine. The product was isolated by chromatography on an alumina column (Brockmann I, activated, Aldrich) and further purified by dialysis (benzoylated cellulose tubing, Sigma). The product was isolated as a metallic, dark green, brittle solid.

Negative ion electrospray mass spectrometry* (ES^- MS) m/z: 448 $(M-2H)^{2-}$, 298 $(M-3H)^{3-}$, 223 $(M-4H)^{4-}$. High-performance liquid on a reverse-phase C_{18} column using gradient elution of methanol/phosphate buffer and UV-visible detection (λ = 300-800 nm) showed a single peak in the chromatogram, confirming the presence of only tetrasubstituted phthalocyanine.[21] A UV-vis spectroscopic assay was performed by dissolving a known mass of the solid in 1:1 ethanol : water solution. Taking the extinction coefficient ε as 10^5 dm^3 mol^{-1} cm^{-1} as cited in the literature[15] the purity of the sample was evaluated by comparing the experimental maximum absorbance to the calculated figure. The product was shown to be greater than 99% pure.

* The E.P.S.R.C. National Mass Spectrometry Service at Swansea is thanked for this work.

3.2.2 Synthesis of Octabutoxy Zinc Phthalocyanine

1,4,8,11,15,18,22,25-Octabutoxy phthalocyanine (39 mg, 35.7 μmol; Aldrich) was dissolved in 1% pyridine in toluene (2 ml). An excess of $Zn(OAc)_2$ (15 mg, 80 μmol) was added and the reaction stirred and heated at 300 K for 15 minutes, by which time the end point had been reached (monitored by UV-visible absorption spectroscopy). Dilute aqueous HCl was added, and the aqueous layer was discarded - this process was carried out three times in total. The remaining organic layer was dried (anhydrous K_2CO_3), and the product isolated by chromatography on an alumina column (Brockmann I, activated, Aldrich).

3.2.3 Chemicals and Sample Preparation

Potassium dihydrogen orthophosphate and acetonitrile (99.3%), purchased from BDH and Aldrich, respectively, were used as received. Deionised water was purified by the '$Purite_{STILL}$' method. Buffered solutions were prepared with a composition of 1:1 water/acetonitrile, 10 mmol dm^{-3} potassium dihydrogen orthophosphate (KH_2PO_4). A citrate buffer was prepared using 1:1 water:acetonitrile 12.5 mmol dm^{-3} in citric acid. Where required, cetyl trimethylammonium bromide (CTAB) ($C_{16}H_{33}NMe_3Br$) was added in 5 mmol dm^{-3} concentration to aid disaggregation. Potassium hydroxide and hydrochloric acid solutions (BDH) were used to adjust the pH.

1,4,8,11,15,18,22,25-Octabutoxy zinc phthalocyanine was studied in ethanolic solution, and solutions were acidified using sulfuric acid (BDH). Lithium chloride (Aldrich) was used as received.

3.3 Results and Discussion

3.3.1 Tetrasulfonated Zinc Phthalocyanine

In neutral solution tetrasulfonated zinc phthalocyanine ($ZnPcS_4$) tends to aggregate in water, as demonstrated by an absorption band centred at 635 nm. Thus, in this current work a mixed solvent system was used which prevents aggregation in dilute solution. A pH titration of $ZnPcS_4$ immediately shows the dependence of the red shifted band upon pH (Figure 3.1). At pH 7 the absorption spectrum is typical of a monomeric metallated phthalocyanine with the Q band maximum at 680 nm and vibrational satellites to higher

energy. As the pH is decreased this intense absorption band is reduced with a concomitant increase in absorbance at 635 nm, and the growth of a new peak at 705 nm. Emission spectra under similar conditions show the presence of the typical monomer fluorescence centred at 685 nm at neutral pH - on lowering the pH a new red shifted peak is observed at 710 nm (Figure 3.1), with reduced emission at 685 nm. Solutions at intermediate pH show contributions from nonprotonated and monoprotonated phthalocyanine, denoted as Pc and PcH^+ respectively.

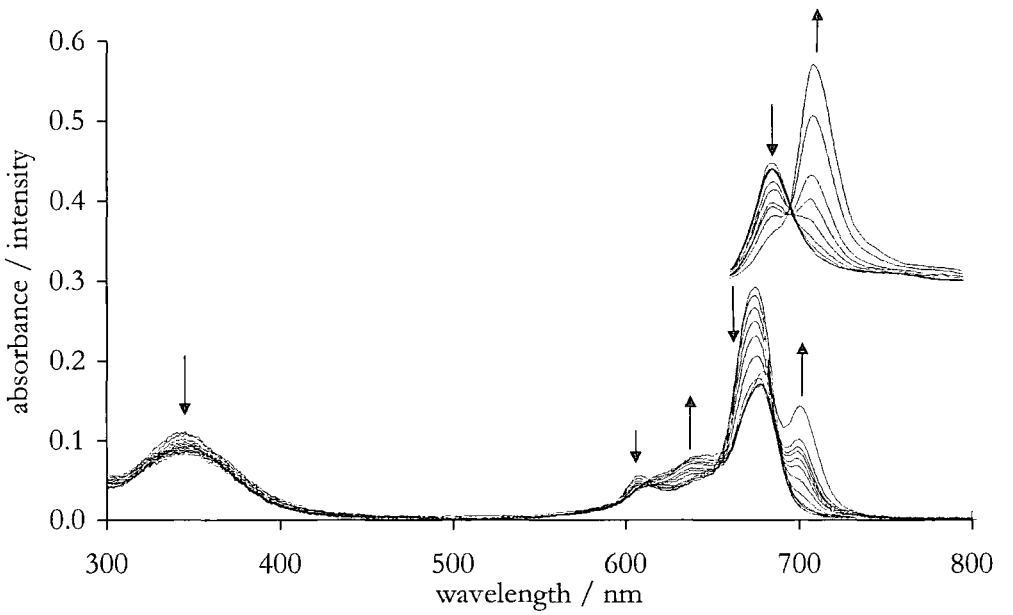

Figure 3.1 $ZnPcS_4$ in buffered solution. Absorption spectrum, pH 1-5 (0.5 unit steps), 6, 7 and 12. Emission spectrum (offset for clarity), pH 1-5 (0.5 unit steps) and 6, λ_{ex} = 640 nm. Arrows indicate changes in intensity with decreasing pH.

Dilute solutions of $ZnPcS_4$ in buffered solutions, pH 1 and 7 were used to probe the individual monomer and protonated monomer peaks. Excitation of the Pc absorption band shows principal emission centred at 685 nm, the intensity of which reduces on lowering the pH from 7 to 1 (Figure 3.2A). At pH 1 the presence of emission arising from the protonated monomer (PcH^+) is also visible despite exciting on the non-protonated absorption profile. This is attributed to additional excitation of the PcH^+ vibrational satellites lying beneath the Pc Q band. Excitation coinciding with the absorbance maximum of PcH^+ (705 nm) shows emission centred at 710 nm for the pH

1 solution, and negligible emission at pH 7. The presence of a small peak at 705 nm (marked 'x') shows the minimal amount of first order scattered light, and confirms the validity of scanning the emission wavelength through the excitation point (Figure 3.2B).

The excitation spectra recorded for a pH 3 solution (at which pH both Pc and PcH^+ exist) with λ_{em} = 685 nm (Pc) and 710 nm (PcH^+) are shown in Figure 3.3. Monitoring the emission at 685 nm shows a single Q band profile analogous to the absorption profile at pH 7. The excitation spectrum of the 710 nm emission band shows a split Q band, with its centre of gravity slightly to the red of the Pc absorption band, similar to that observed in the absorption profile of the dilute solutions at pH 1. Such a splitting of the Q band is expected as a result of the decrease in ring symmetry caused by protonation.[3,5]

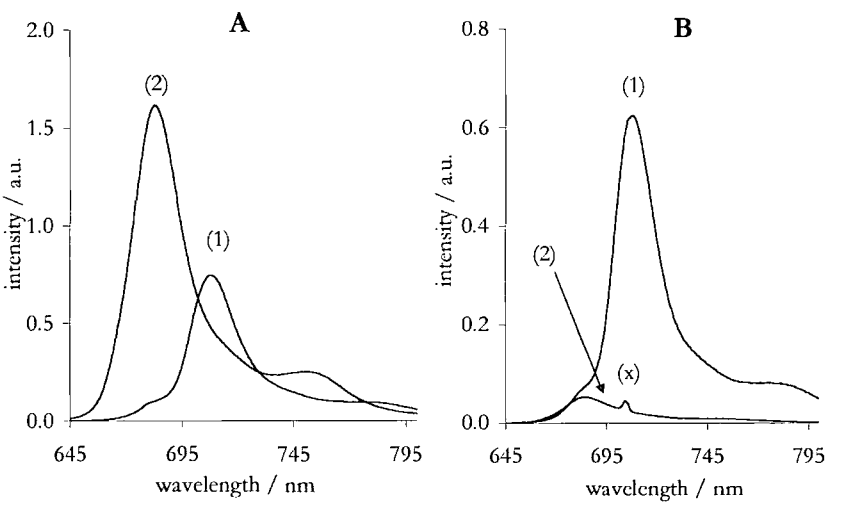

Figure 3.2 Emission spectra of $ZnPcS_4$ in buffered solution (A) λ_{ex} = 680 nm: (1) pH 1 and (2) pH 7; (B) λ_{ex} = 705 nm: (1) pH 1 and (2) pH 7.

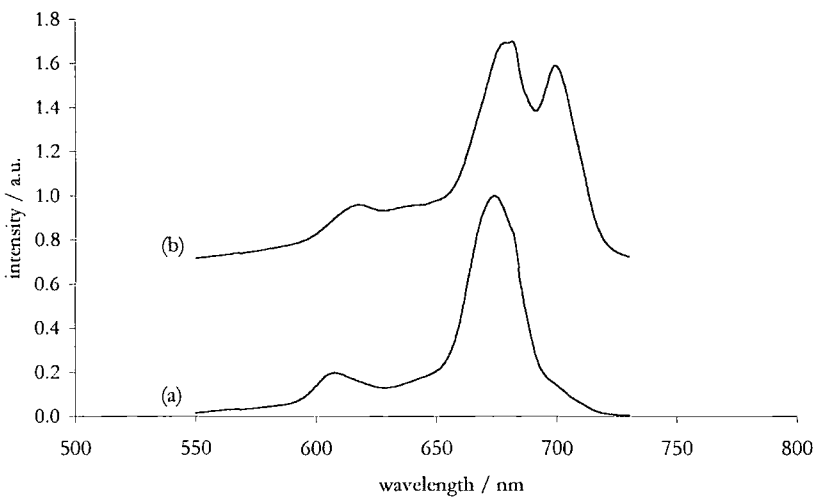

Figure 3.3 Normalised excitation spectra of $ZnPcS_4$ in buffered solution, pH 3 (a) λ_{em} = 685 nm (b) λ_{em} = 710 nm (offset for clarity).

The fluorescence lifetimes were found to be 3.3 ± 0.1 ns at pH 7 and 3.0 ± 0.1 ns at pH 1. Decays obtained at pH 1 show evidence of a minor contribution of a second component, with a yield of less than 2%. This second component is attributed to the presence of photodegradation products, for during the course of these studies the protonated species has proven to be extremely susceptible to photooxidation (a phenomenon not seen for the protonated forms of tetra-*tert*-butyl zinc phthalocyanine[5]). This decrease in lifetime is consistent with that reported elsewhere,[5] and it has been suggested that despite an increase in the intrinsic lifetime, concurrent increases in internal conversion pathways result in the observed lifetime decreasing.[7]

It is immediately apparent from this initial work that the red shifted absorption peak attributed to a slipped co-facial dimer by Kaneko *et al.*[15] is due to a pH effect, and based on the evidence of others[3,5] the probable cause is protonation of the phthalocyanine azomethine bridge. However, Kaneko *et al.* reported a positive correlation of red shifted peak intensity with increasing phthalocyanine concentration, and Yoon *et al.*[13] saw a similar relationship with $AlClPcS_4$. This dependence on concentration suggests the presence of a dimeric species, and the possibility that the red shifted peak is due to a novel protonation-induced dimer needs to be addressed. The above spectra show no evidence to the contrary, although the excitation spectra do confirm that the absorption at 635 nm can be attributed to a normal, blue shifted, non-fluorescent dimer, and is not related to the red shifted peak. The possibility of the buffer perturbing the system and causing the pH phenomenon has been addressed by using firstly a citrate buffer and secondly unbuffered solution - in both of these solutions, changes in pH cause the same effects as seen in phosphate buffer. Figure 3.4A shows the concentration effect clearly in unbuffered solution, with the prominent red shifted peak at 5.75×10^{-5} mol dm^{-3} disappearing on dilution by a factor of 100. However, in a buffered pH 7 solution (Figure 3.4B) no red shifted peak is seen even at the highest concentration. It is proposed that in the unbuffered solution, it is the phthalocyanine itself which is causing the protonation, on account of the four sulfonic acid groups – hence, as the concentration of $ZnPcS_4$ increases more acid groups are present in solution and more protonated molecules are formed, causing the increased 705 nm intensity. A pH titration of the most concentrated solution shows a similar trend as seen in Figure 3.1, albeit with increased presence of the blue shifted peak.

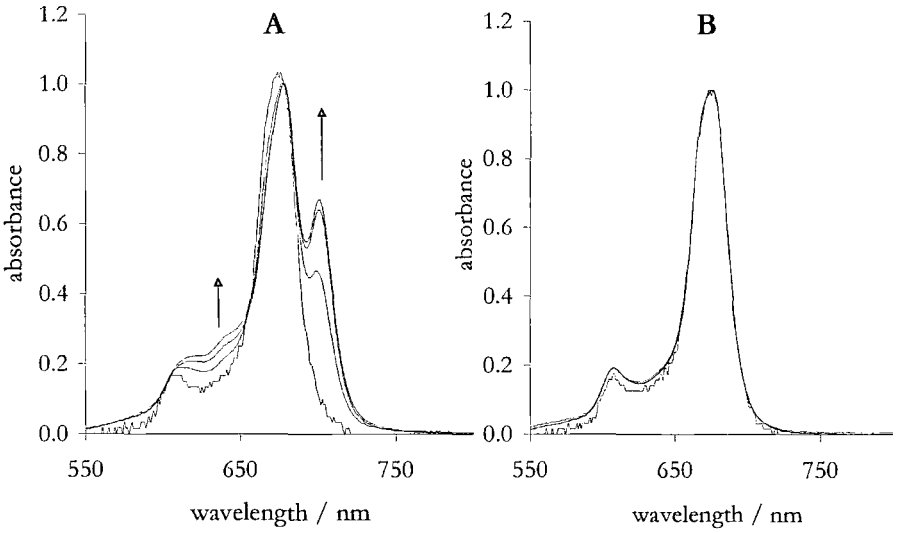

Figure 3.4 Normalised absorption spectra of [S], [S]/2, [S]/10 and [S]/100 $ZnPcS_4$ solutions ([S] = 5.75 x 10^{-5} mol dm^{-3}), pH 7 (A) unbuffered solution and (B) buffered solution. Arrows indicate changes in intensity with increasing concentration.

A further study on concentration looked at a number of solutions in buffer, adjusted to pH 2 (at which pH both Pc and PcH^+ exist). With increased concentration an increase in the absorption band of the aggregate at 635 nm with a concomitant decrease of the two maxima at greater wavelength is observed (Figure 3.5). The PcH^+ band at 705 nm can be seen to increase (relative to the normal Q band absorption at 680 nm) as the concentration is reduced, providing direct evidence that the phenomenon is not caused by aggregation.

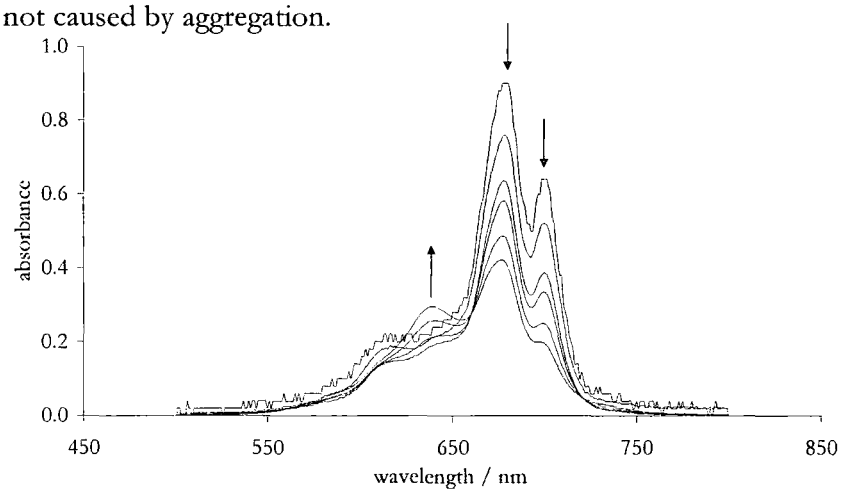

Figure 3.5 Fully normalised absorption spectra of [S], [S]/2, [S]/10, [S]/20, [S]/100, [S]/200 $ZnPcS_4$ solutions in buffered solution ([S] = 1.2 x 10^{-4} mol dm^{-3}). Arrows indicate changes in intensity with increasing concentration.

Evidence for the presence of non-fluorescent aggregates (indicated by absorption at 635 nm) at low pH is observed at surprisingly low concentrations. The excitation profiles obtained from such solutions exactly match the absorption spectrum of monomeric PcH^+, confirming that the aggregate is non-fluorescent, in common with virtually all other phthalocyanine dimers. As Figure 3.6A shows, the match between absorption and excitation spectra for a dilute solution of $ZnPcS_4$ at pH 7 is excellent, whereas the same solution at pH 1 shows considerable non-fluorescent aggregate (Figure 3.6B). Addition of the surfactant CTAB, $C_{16}H_{33}NMe_3Br$, to this solution reduces the presence of this aggregate considerably but not completely (Figure 3.6C), by partitioning the phthalocyanine molecules within the micelle core and hence reducing phthalocyanine-phthalocyanine interactions.[7] Only when the phthalocyanine concentration is reduced to 5 x 10^{-8} mol dm^{-3} in micellar solution is an excellent match between absorption and excitation spectra achieved (Figure 3.6D). The exact nature of this aggregate species is not known, although the blue shifted absorption band and non-fluorescence imply it has a co-facial geometry,[22] and it is suggested that it is of the form $Pc_nH_m^{m+}$.

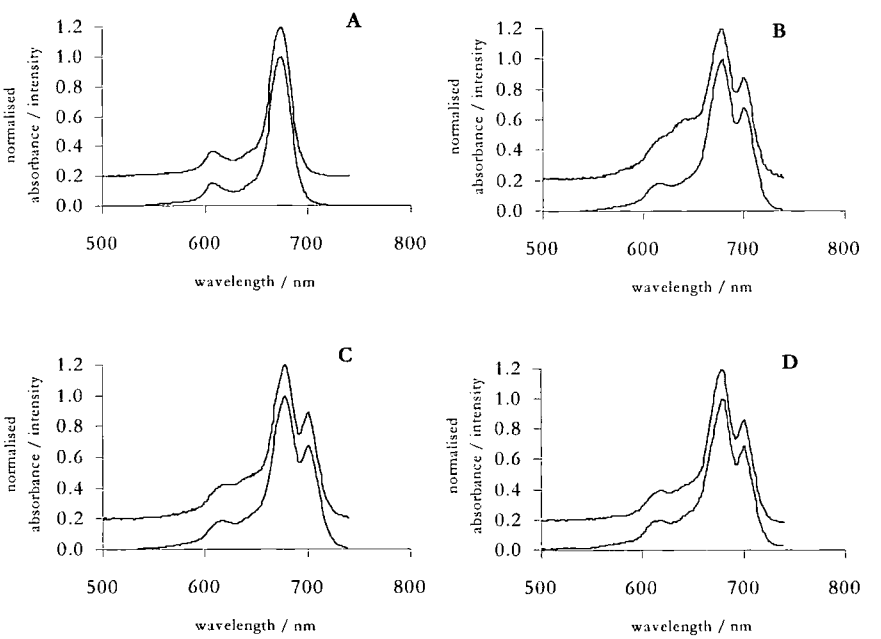

Figure 3.6 Normalised absorption and excitation profiles (λ_{em} = 750 nm) of $ZnPcS_4$ in buffered solution: (A) pH 7, 10^{-6} mol dm^{-3}; (B) pH 1, 10^{-6} mol dm^{-3}; (C) pH 1, 10^{-6} mol dm^{-3} with 5 mmol dm^{-3} CTAB; (D) pH 1, 5x10^{-8} mol dm^{-3} with 5 mmol dm^{-3} CTAB. Excitation spectra have been offset for clarity.

It was recently reported that macrocycle protonation reduces the singlet oxygen quantum yield,[5] and this fact would suggest protonation to be an unfavourable occurrence in the application of phthalocyanines as PDT agents. However, the efficacy of a PDT sensitiser depends upon a number of factors, including localisation and selectivity of uptake/retention by the tumour cells compared with the surrounding tissue, in addition to cytotoxic singlet oxygen generation. The red shifted absorption which results from protonation allows the protonated and unprotonated species to be distinguished spectroscopically with ease and the potential for improved selectivity in PDT agents as a result is of great interest. It is known that tumours have a lower pH than healthy tissue by up to 1.1 pH units[23,24] and the development of a pH-based model for the preferential uptake of porphyrins by tumours has previously been discussed.[1] Given the susceptibility of phthalocyanines to protonation, as demonstrated herein and elsewhere,[3,5] the extension of this model to phthalocyanines is not unreasonable. If the pK_a of the phthalocyanine can be increased by suitable chemical substitution to within the range of 5.5-7.0 then protonation would occur selectively in the tumour cell. The protonated form of the sensitiser can then be excited with excellent selectivity using red shifted wavelength radiation, at which wavelength the non-protonated form has no absorbance. On the basis of this current work the pK_a of $ZnPcS_4$ is estimated to be 4.0 ± 0.2, whilst that of tetra-*tert*-butyl zinc phthalocyanine is considerably lower at 2.9 ± 0.3.[5] Considerable variation in the basicity of copper phthalocyanines has been demonstrated,[10] with values ranging over three orders of magnitude depending on peripheral substitution - thus the design of a new therapeutic agent with a pK_a value within the biological range is not unfeasible. The enhanced selectivity brought about by the pH-sensitive agent could well compensate for the reduction in singlet oxygen quantum yield.

3.3.2 Octabutoxy Phthalocyanine

3.3.2.1 Introduction

In an attempt to further study the photophysical effect of macrocyclic protonation in phthalocyanines the properties of the α-substituted octabutoxy zinc species have been briefly investigated. Basic molecular modelling (CAChe, Oxford Molecular, Ltd.) shows three coordinate proton binding sites involving two butoxy oxygens and one

azomethine nitrogen each (Figure 3.7). It was felt that the presence of these sites with increased electron density would result in a raised pK_a value with respect to that of tetrasulfonated zinc phthalocyanine discussed above. A similar observation has previously been reported, and the presence of electron rich substituents in the α-positions was shown to have a profound effect on the pK_a of phthalocyanine systems.[10]

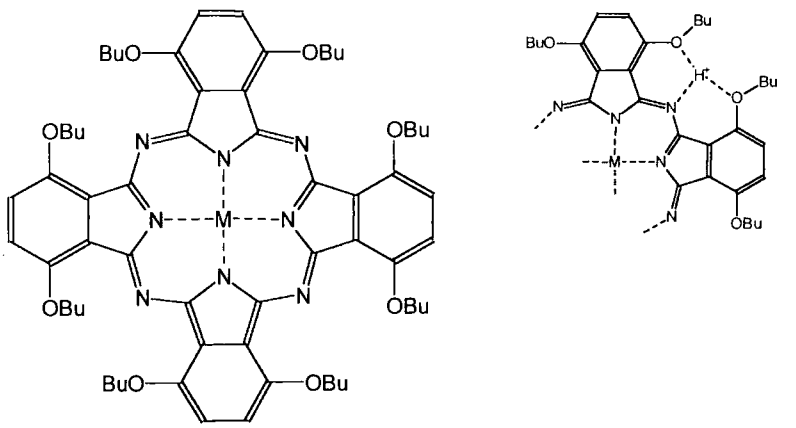

Figure 3.7 Structure of 1,4,8,11,15,18,22,25-octabutoxy zinc phthalocyanine, highlighting the high affinity proton binding site.

3.3.2.2 1,4,8,11,15,18,22,25-Octabutoxy zinc phthalocyanine

The α-substituted 1,4,8,11,15,18,22,25-octabutoxy zinc phthalocyanine shows strongly red shifted absorption and emission bands (λ_{max} = 735 nm and 760 nm respectively) in consequence of the strongly electron donating substituents perturbing the excited state energy.[6,25] The reason for this red shift is of a similar nature to that given above for protonation – substitution onto the phenyl rings, however, has a more powerful affect, since electron density can now be transferred to both the peripheral and inner nitrogens. The extinction coefficient was calculated to be 1.5 x 10^5 dm^{-3} mol^{-1} cm^{-1} in ethanol, with linear behaviour in the concentration range 10^{-4}-10^{-7} mol dm^{-3}. A fluorescence lifetime of 1.7 ns was recorded.

Addition of sulfuric acid results in reduction of the Q band absorption, with a concomitant increase in red shifted absorption centred at 825 nm (Figure 3.8A). The resulting profile is broadened, although evidence for a split Q band (as would be expected due to lowered symmetry caused by protonation) is ambiguous. Cook *et al.*[26] noted a correlation between the Q band energy and the energy splitting of the band in metal free species, such that the lower the energy the lower the splitting - thus, lack of

clear splitting in the red shifted octabutoxy zinc phthalocyanine is perhaps understandable. The di-protonated species, observed at higher acid concentrations, displayed a further 70 nm bathochromic shift (Figure 3.8B). The initial formation of the tri-protonated species could be detected but this species is unstable and continued addition of acid causes depletion of all phthalocyanine absorption bands. The conversions of non-protonated to mono-protonated, and mono-protonated to di-protonated were accompanied by clean isosbestic points, indicating sequential protonation with no competing side reactions. Interestingly the broad Soret band also undergoes considerable changes upon protonation, with new absorption evident between 400-600 nm and 500-700 nm for the mono- and di-protonated species respectively. As the Q band moves further into the near infra-red the Soret band becomes solely responsible for the colour observed by eye, and the solutions undergo dramatic colour changes, from green (unprotonated), through pink (mono-protonated) to purple (di-protonated). Note that tetrasulfonated zinc phthalocyanine discussed above showed only minor changes in Soret band profile, and the different behaviour may be due to the enhanced binding of the proton in octabutoxy species.

The spectral effect of protonation is rather more complex to explain, in comparison with the tetrasulfonated species previously discussed. In the current example there are a number of processes that must be considered. The electron rich α-substituents inject electron density into the ring system (and particularly onto the peripheral nitrogens), as explained above, resulting in the observed red shift for the parent compound. Protonation, considered as an isolated event, causes electron density to move from the phenyl rings to the peripheral nitrogens, with similar effect to the α-substituents. However, the peripheral substituents and proton are not isolated, and hence considerable interaction is observed in the proton binding site. The oxygen atoms of the butoxy substituents bind to the proton (see Figure 3.7) the effect of which is to *reduce* the extent of electron donation into the ring systems (and hence *reduce* the stabilisation of the LUMO the α-substituents cause), but *increase* the stability of the cationic PcH^+ species. That a red shift is still observed would suggest that the reduction in LUMO stabilisation from the α-substituents is small compared with the increased stability afforded by protonation.

It is interesting to compare the magnitude of the shift induced by protonation upon the Q band maximum in these two species. If the centres of gravity for the

protonated Q bands are estimated as being centrally placed between the Q_X and Q_Y components, the shifts (in *wavenumber*) are 265 cm^{-1} and 1360 cm^{-1} for the tetrasulfonated and octabutoxy species respectively. This indicates a clearly increased effect upon the phthalocyanine LUMO as a result of protonation for the octabutoxy species, and even given the ambiguity in locating the band centre for the mono-protonated octabutoxy zinc phthalocyanine, there is strong evidence to show that the three coordinate binding site in this species has a particularly strong proton affinity. If the equation pH = -log(2x[H_2SO_4]) is assumed to be valid at the concentrations required for mono-protonation, the pK_a can be estimated to be 4.2±0.2, compared with 4.0±0.2 for the tetrasulfonated species.

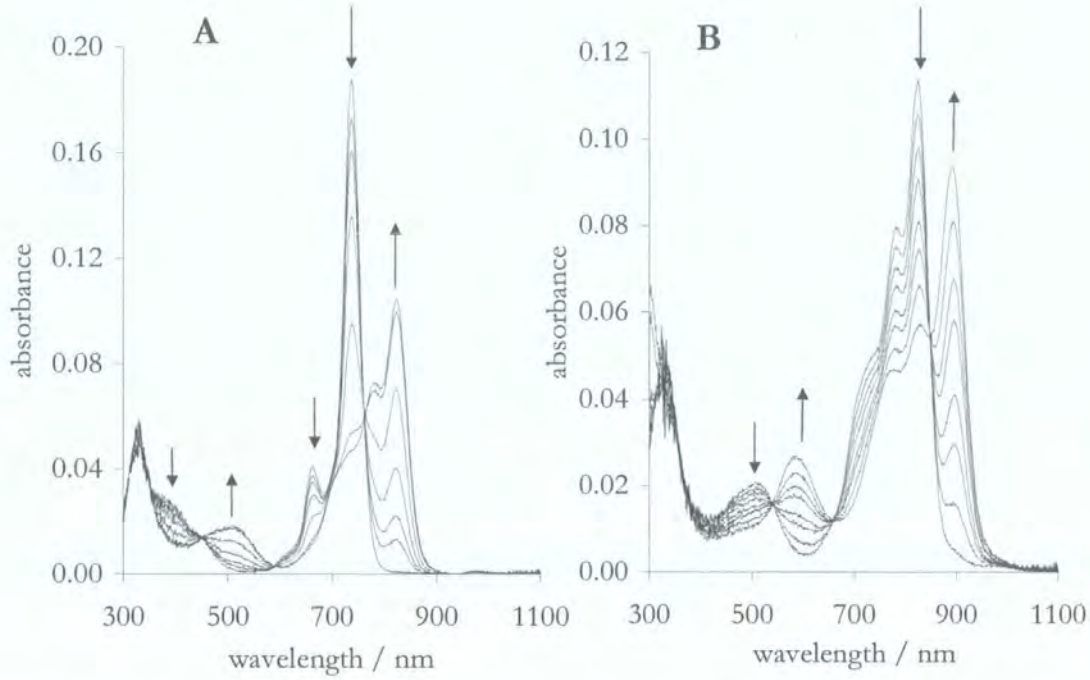

Figure 3.8 Absorption spectra of octabutoxy zinc phthalocyanine in ethanol. (A) 0→4 x 10^{-5} mol dm^{-3} H_2SO_4, Pc→PcH^+, (B) 7.5 x 10^{-5}→9.5 x 10^{-5} mol dm^{-3} H_2SO_4, PcH^+→PcH_2^{2+}. Arrows indicate spectral changes with increasing acid concentration.

The fluorescence spectra of the three species (BuO_8ZnPc, BuO_8ZnPcH^+ and $BuO_8ZnPcH_2^{2+}$) showed a similar band progression to lower energy, centred at 765 nm, 850 nm and 925 nm respectively (Figure 3.9 below), with a corresponding reduction in emission intensity. The energy shift caused by mono-protonation is 1308 cm^{-1}, in good agreement with the value calculated from the absorption data.

The pK_a value of octabutoxy zinc phthalocyanine remains too low for *in vivo* protonation, but the above work shows quite clearly that improvements can be achieved by using phthalocyanine with suitable substituents.

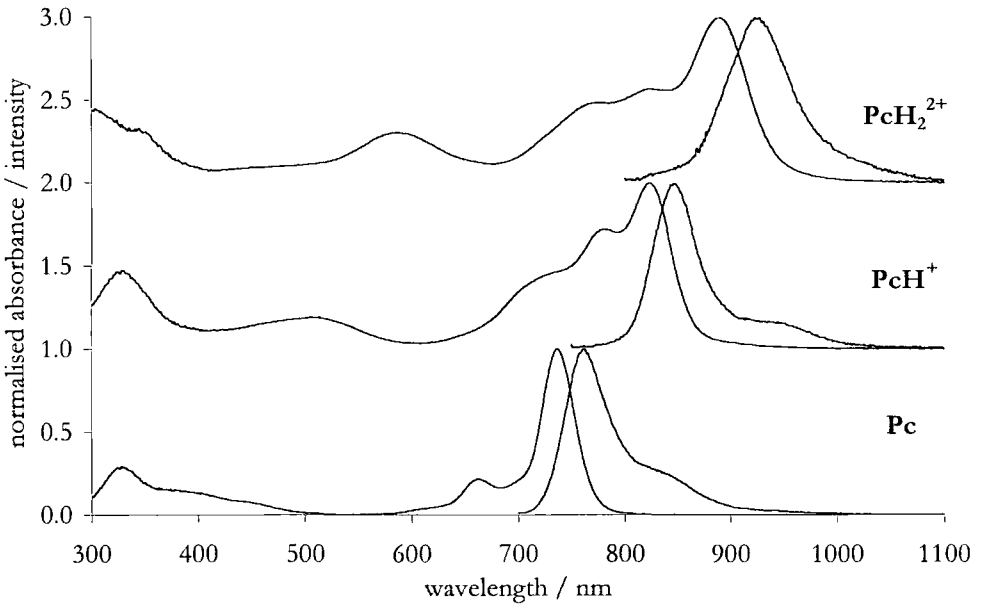

Figure 3.9 Absorption and emission spectra of protonated species, $BuO_8ZnPcH_n^{n+}$, n = 0-2.

Also of interest is the spectral sensitivity of the phthalocyanine to the presence of lithium ions. It was discovered in 1949 that small doses of lithium carbonate (Li_2CO_3) provide effective treatment for manic depression,[27] and use of this compound continues to the present day, despite the precise mode of action not being clearly understood - side effects, however, are minimal. Given this important use of lithium the development of a robust lithium sensor remains an important goal. Typical dosage maintains lithium levels in the blood at approximately 1 mmol dm^{-3}, so concentrations of 1-10 mmol dm^{-3} represent a realistic target for detection limits. In addition, a workable lithium detector for medicinal purposes must show excellent discrimination between the desired ion and and other Group I and II metals (particularly sodium).

Being the smallest of the unipositively charged metal ions (76 pm ionic radius[27]) lithium would be expected to bind in a similar fashion to a hydrogen ion in the 'proton binding site' of octabutoxy zinc phthalocyanine. Addition of aliquots of lithium chloride (in ethanol) to the phthalocyanine results in similar changes to those observed

previously, with a reduction of the Q band absorption at 740 nm and a concurrent increase at 815 nm (compared with 825 nm for the monoprotonated species), together with additional absorption apparent in the 400-600 nm window (Figure 3.10). The fluorescence emission band undegoes a corresponding bathochromic shift to 840 nm.

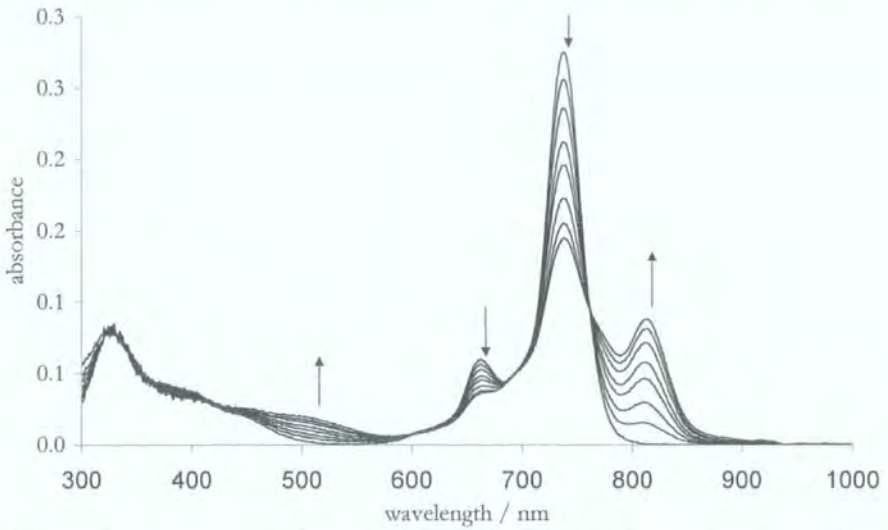

Figure 3.10 Absorption spectra of octabutoxy zinc phthalocyanine in ethanol. 0⟶1.0 mol dm^{-3} LiCl. Arrows indicate spectral changes with increasing lithium chloride concentration.

These spectroscopic changes are indicative of lithium ions perturbing the phthalocyanine electron density in a similar fashion to that caused by protonation, through the bridging azomethine nitrogens. However, the efficacy of binding is greatly reduced in comparison with hydrogen ions such that even at lithium ion concentrations as high as 1 mol dm^{-3} there is not complete conversion to the lithiated species. In addition, the selectivity of ion detection with respect to other unipositive ions such as sodium is poor. The application then of octabutoxy zinc phthalocyanine as a lithium sensor is unrealistic, but the results discussed here do show that lithium-phthalocyanine binding does occur, and with suitable molecular design lithium detectors based upon the phthalocyanine macrocycle could be possible.

3.4 Conclusions

The original observation of red shifted absorption and emission peaks of tetrasulfonated zinc phthalocyanine in aqueous acetonitrile solution has been shown to result from protonation.[28] Spectral changes indicate the site of protonation to be the bridging

azomethine nitrogen of the macrocycle. This assignment is of great importance, for previous work[15] assigned the phenomenon to the formation of a novel fluorescent dimer, the occurrence of which is extremely rare (see Chapter 6).

The application of the spectral changes resulting from protonation to the design of photodynamic therapeutic agents with enhanced selectivity has been discussed, and the photophysical properties of the α-substituted 1,4,8,11,15,18,22,25-octabutoxy zinc phthalocyanine were investigated in the light of this. This compound shows similar spectroscopic behaviour on protonation, and the presence of a three coordinate 'proton binding site' serves to raise the pK_a with respect to that of the tetrasulfonated species. The binding site also shows affinity for lithium, with similar spectroscopic changes upon lithiation as seen with protonation, albeit with greatly reduced efficacy.

3.5 References

1 D. Brault, C. Vever-Bizet and T. le Doan, Spectrofluorimetric study of porphyrin incorporation into membrane models - evidence for pH effects, *Biochim. Biophys. Acta*, 1986, **857**, 238.

2 A. J. Barrett, J. C. Kennedy, A. Jones, P. Nadeau and R. H. Pottier, The effect of tissue and cellular pH on the selective biodistribution of pophyrin-type photochemotherapeutic agents: a volumetric titration study, *J. Photochem. Photobiol. B: Biol.*, 1990, **6**, 309.

3 S. S. Iodko, O. L. Kaliya, N. V. Kondratenko, E. A. Luk'yanets, V. I. Popov and L. M. Yagupol'skii, Quantitative characteristics of the stagewise protonation of phthalocyanines, *J. Gen. Chem. USSR*, 1983, **53**, 791.

4 D. Berezin, *Coordination Compounds of Porphyrins and Phthalocyanines*, Wiley, New York, 1981.

5 A. Beeby, S. FitzGerald and C. F. Stanley, A photophysical study of protonated (tetra-*tert*-butyl phthalocyaninato) zinc, *J. Chem. Soc., Perkin Trans. 2*, 2001, 1978.

6 J. O. Morley and M. H. Charlton, Theoretical investigation of the structure and spectra of zinc phthalocyanines, *J. Phys. Chem.*, 1995, **99**, 1928.

7 C. F. Stanley, *Photophysical Investigation of Substituted Zinc Phthalocyanines as sensitisers for Photodynamic Therapy*, Ph.D. Thesis, University of Durham, 1997.

8 K. Lang, D .M. Wagnerová, P. Engst and P. Kubát, Influence of protonation on the reactions of triplet-state sulfonated chloro-aluminium (III) phthalocyanine with dioxygen, *J. Chem. Soc., Faraday Trans.*, 1992, **88**, 677.

9 J. R. Darwent, I. McCubbin and D. Phillips, Excited singlet and triplet state electron-transfer reactions of aluminium (III) sulphonated phthalocyanine, *J. Chem. Soc., Faraday Trans. II*, 1982, **78**, 347.

10 V. M. Derkacheva, S. S. Iodko, O. L. Kaliya and E. A. Luk'yanets, Influence of substituents on the basicity of copper phthalocyanines, *J. Gen. Chem. USSR*, 1981, **51**, 1998.

11 R. B. Ostler, A. D. Scully, A. G. Taylor, I. R. Gould, T. A. Smith, A. Waite and D. Phillips, The effect of pH on the photophysics and photochemistry of di-sulphonated aluminum phthalocyanine, *Photochem. Photobiol.*, 2000, **71**, 397.

12 S. Gaspard, C. Gianotti, P. Maillard, C. Schaeffer and T-H. Tran-Thi, The first synthesis of covalently linked mixed dimer complexes containing phthalocyanine and porphyrin, *J. Chem. Soc., Chem. Commun.*, 1986, 1239.

13 M. Yoon, Y. Cheon and D. Kim, Absorption and fluorescence spectroscopic studies on dimerization of chloroaluminum (III) phthalocyanine tetrasulfonate in aqueous alcoholic solutions, *Photochem. Photobiol.*, 1993, **58**, 31.

14 S. Dhami, A. J. de Mello, G. Rumbles, S. M. Bishop, D. Phillips and A. Beeby, Phthalocyanine fluorescence at high concentration: dimers or reabsorption? *Photochem. Photobiol.*, 1995, **61**, 341.

15 Y. Kaneko, T. Arai, K. Tokumaru, D. Matsunaga and H. Sakuragi, Observation of a novel fluorescent dimer of zinc tetrasulphonatophthalocyanine, *Chem. Lett.*, 1996, 345.

16 Y. Kobuke and H. Miyaji, Supramolecular organization of imidazolyl-porphyrin to a slipped cofacial dimer, *J. Am. Chem. Soc.*, 1994, **116**, 4111.

17 E. Ben-Hur and I. Rosenthal, Photosensitisation of Chinese hamster cells by water soluble phthalocyanines, *Photochem. Photobiol.*, 1986, **43**, 615.

18 E. BenHur and I. Rosenthal in *Phthalocyanines – Properties and Applications, Vol.1*, Eds. C. C. Leznoff and A. B. P. Lever, VCH Publishers, Inc., New York, 1989.

19 J. F. Marshall, W. S. Chan and I. R. Hart, Effect of photodynamic therapy on anti-tumour immune defences: Comparison of the photosensitisers hematoporphyrin derivative and chloroaluminium sulphonated phthalocyanine, *Photochem. Photobiol.*, 1989, **49**, 627.

20 M. Ambroz, A. Beeby, A. J. MacRobert, M. S. C. Simpson, D. Phillips and A. Beeby, Preparative, analytical and fluorescence spectroscopic studies of sulphonated phthalocyanine photosensitisers, *J. Photochem. Photobiol. B: Biol.*, 1991, **9**, 87.

21 S. M. Bishop, B. J. Khoo, A. J. MacRobert, M. S. C. Simpson, D. Phillips and A. Beeby, Characterisation of the photochemotherapeutic agent disulphonated aluminium phthalocyanine and its high-performance liquid chromatographic separated components, *J. Chromatogr.*, 1993, **646**, 345.

22 M. Kasha, H. R. Rawls and M. A. El-Bayoumi, The exciton model in molecular spectroscopy, *Pure Appl. Chem.*, 1965, **11**, 371.

23 D. Kessel, *Localisation Phenomena: pH effects in photodynamic therapy of neoplastic disease*, CRC Press, Boston, 1990.

24 P. M. Gullino, F. H. Grantham, S. H. Smith and H. C. Haggarty, Modifications of the acid-base status of the internal milieuof tumors, *J. Natl. Cancer Inst.*, 1965, **34**, 857.

25 M. J. Stillman and T. Nyokong, in *Phthalocyanines – Properties and Applications, Vol.1*, Eds. C. C. Leznoff and A. B. P. Lever, VCH Publishers, Inc., New York, 1989.

26 M. J. Cook, A. J. Dunn, S. D. Howe, A. J. Thomson and K. J. Harrison, Octa-alkoxy phthalocyanine and naphthalocyanine derivatives: dyes with Q-band absorption in the far red or near infrared, *J. Chem. Soc., Perkin Trans. 1*, 1988, 2453.

27 N. N. Greenwood and A. Earnshaw, *Chemistry of the Elements*, Butterworth-Heinemann Ltd., Oxford, 1984.

28 A. Beeby, S. FitzGerald and C. F. Stanley, Protonation of tetrasulfonated zinc phthalocyanine in aqueous acetonitrile, *Photochem. Photobiol.*, 2001, **74**, 566.

Chapter 4

Properties of Axially Substituted Silicon Phthalocyanines

4.1 Introduction

There exists in the literature a vast array of structurally modified phthalocyanine systems, with widely varied peripheral substituents and central atoms.[1] The most common core elements are zinc, copper and aluminium, but it is possible to synthesise an almost complete periodic table of phthalocyanines, including metalloid derivatives containing silicon, germanium, phosphorus, astatine and antimony.[2] This current work focuses on a number of new silicon phthalocyanines, with axial substituents - these compounds typically exhibit excellent photophysical properties, including higher quantum yields, longer fluorescence lifetimes and reduced aggregation with respect to zinc and aluminium species.[1] Most common axially substituted silicon phthalocyanines utilise bis-ether linkages, with simple[3] or dendritic[4] alcohols as the axial ligands, but the compounds discussed below are exclusively bis-*esters*. Reports of such compounds in the literature are extremely rare.

The first synthesis of a silicon phthalocyanine was reported in 1960,[5] and involved reaction of silicon tetrachloride with phthalonitrile. Since this first report many examples have been synthesised[1] and it has been shown that the spectral profile of monomeric silicon phthalocyanines show little variation from those of typical zinc phthalocyanines, with the dichloro and dihydroxy substituted silicon phthalocyanines showing Q band maxima at 699 nm (pyridine) and 667 nm (THF) respectively.[6] The Q band is generally extremely well resolved due to the prevention of ring interactions by the axial substituents.[7]

The six coordinate nature of phthalocyanine bound silicon allows the synthesis of dimeric and oligomeric phthalocyanine species linked through the central silicon atom. Many of these make use of a one atom oxygen bridge, of the form RO-SiPc-O-SiPc-OR. The first such compounds were observed for germanium and manganese compounds,[8] and similar behaviour for silicon containing species was reported in 1962.[9] The resulting excitonic interactions between the two phthalocyanine rings are strong, and yield a clearly defined blue shifted Q band at ~630 nm, with weaker broad tails to both the blue and the red. The main factors affecting the Q band blue shift are geometrical, including the interring separation and staggering angle - the latter, however, has been theoretically shown to have minimal effect.[10] Silicon phthalocyanine dimers with elongated, rigid bridging units incorporating dioxybiphenyl

and dioxynaphthalene units displayed absorption spectra typical of a *monomeric* phthalocyanine,[11] and this was attributed to a lack of exciton interactions as a result of the ~13 Å separation afforded by the large bridging units. A similar lack of exciton coupling was observed for terephthalate linked oligomers.[12]

The dimeric spectral profile is generally independent of concentration over a large range, indicating that the interactions are purely intramolecular. As the number of stacked rings increases from two to three the Q band blue shifts further to 600 nm, and its profile becomes much broader.[13] The Si-O-Si angle of a dimeric compound capped by $-OSi(CH_3)_2[C(CH_3)_3]$ groups was found to be 179.5°, clearly demonstrating that the phthalocyanine rings are held in a parallel conformation.[6] It is this co-facial arrangement which results in the blue shifted Q band absorption and the loss of fluorescence, as expected according to the Exciton Theory.[14] Trimers and tetramers displayed a similar lack of emission.[15]

Despite the generally observed non-fluorescence of the μ-oxo silicon phthalocyanines dimers, weak near infrared emission has been reported. This is attributed to emission from the lowest, formally forbidden exciton state, and study of an octa-alkoxy phthalocyanine dimer revealed a dimer emission quantum yield just 10^{-3} times that of the monomer, and an estimated lifetime of 24 ps.[16] Hybrid silicon, germanium and tin phthalocyanine dimers displayed similar broad emission in the range 800-1450 nm for silicon-germanium and silicon-tin species.[17]

This present study focusses on a number of interesting novel silicon phthalocyanine bis-esters and their photophysical properties are discussed. A robust reference compound has been spectroscopically characterised, and thereafter the photophysical behaviour of other silicon phthalocyanines is compared with it, and the results discussed in the light of the variation of axial substituent.

4.2 Experimental

Dr Chris Farren is thanked for providing the silicon phthalocyanine species discussed herein, which were synthesised by standard methodology, involving the reaction of silicon phthalocyanine dichloride with carboxylic acids in a polyether solvent. Full experimental data is reported elsewhere.[18]

4.3 Results and Discussion

The silicon phthalocyanine bis-(4-*tert*-butyl)benzoate **1** (Figure 4.1) was prepared as a robust, highly soluble compound for photophysical comparison purposes. This compound shows typical phthalocyanine absorption and emission (Figure 4.2 and Table 4.1), with an ε_{max} value of 2.9 x 10^5 dm^3 mol^{-1} cm^{-1} in dichloromethane. The Beer-Lambert law is obeyed across the concentration range 10^{-4}-10^{-7} mol dm^{-3}, indicating the excellent ability of the large axial substituents to prevent aggregation. There is, additionally, no evidence for aggregation even at 77 K and this is in line with the crystal structure of **1** which shows the axial substituents lying orthogonal to the plane of the macrocycle ring,[18] thus preventing any intermolecular interactions between the rings.

Table 4.1 Spectroscopic data for silicon phthalocyanine bis-esters, **1-11**.

Compound	λ_{max}(abs) / nm	λ_{max}(em) / nm	Φ_f ±10%	τ_f ±0.1/ ns [b]
1	685	691	0.62	6.7
2	685	691	0.39	6.7
3	685	693	0.66	6.8
4	685	693	0.64	6.8
5	686	694	0.64	6.8
6	688	693	0.64	6.5
7	687	694	0.57	6.4
8	685	693	0.50	5.6
9	686	693	0.57	6.2
10	687	694	0.08	0.96 [a]
11	686	696	0.33	3.8 [b]

[a] a second minor component was also detected: 5.1 ns (5%); [b] a second minor component was also detected: 2.4 ns (9%).

In concurrence with values obtained for other silicon phthalocyanines,[1] the fluorescence quantum yield and lifetime have values of 0.62 and 6.7 ns, considerably larger than typical values for zinc phthalocyanines as a result of the lighter core atom. With a low mass central atom the rate of intersystem crossing to the triplet manifold is decreased, and this reduction in deactivation of the first excited singlet state is reflected in the quantum yield and lifetime. The solubility of **1** is excellent in a number of organic

solvents, and in wet, aerated THF it proved stable to decomposition over a period of weeks when kept in the dark, whilst exposure to sunlight caused slow decomposition over a period of days, as monitored by absorption spectroscopy. As a reference compound the properties of **1** are thus excellent.

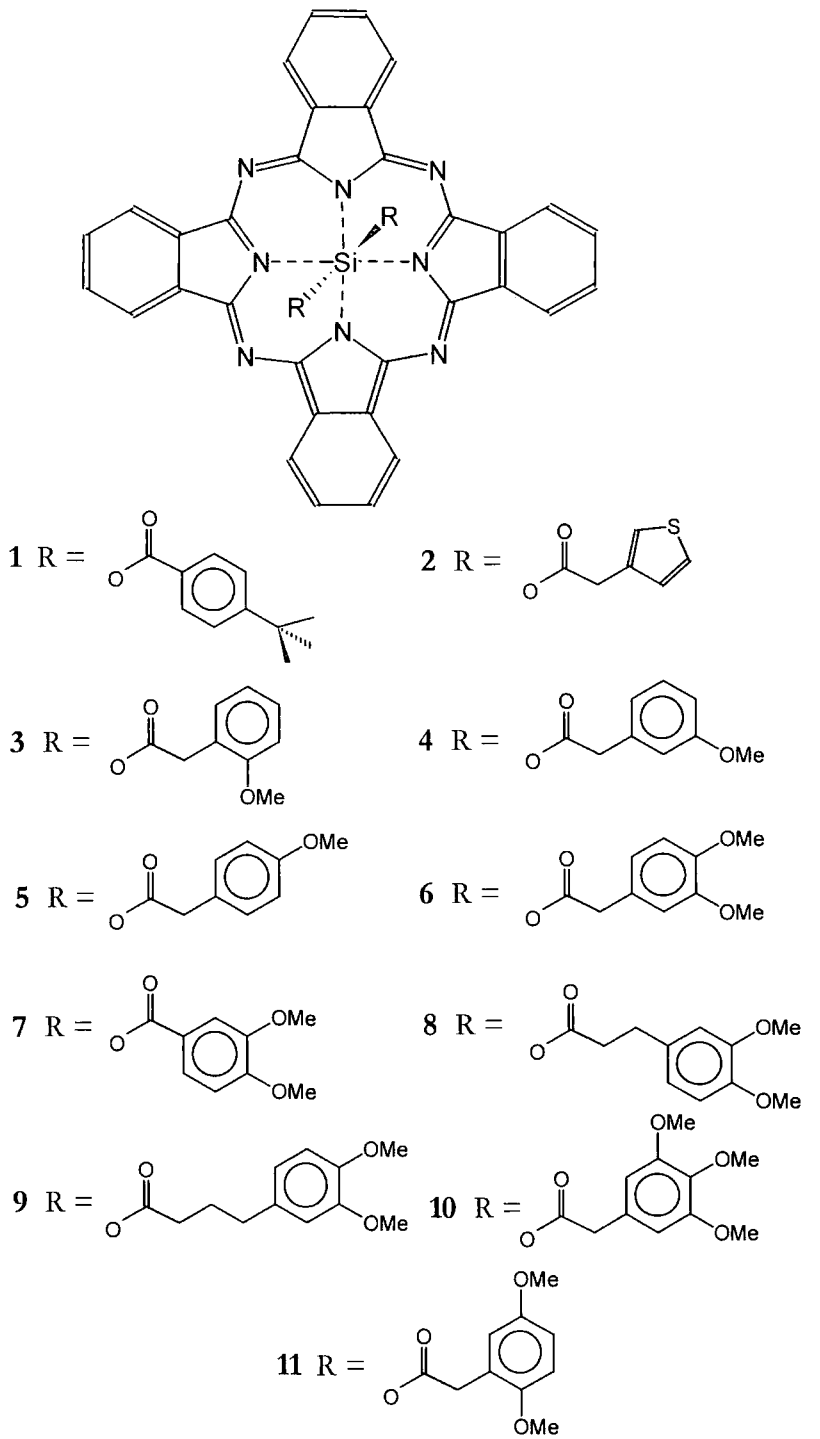

Figure 4.1 Structures of silicon phthalocyanine bis-esters, **1-11**.

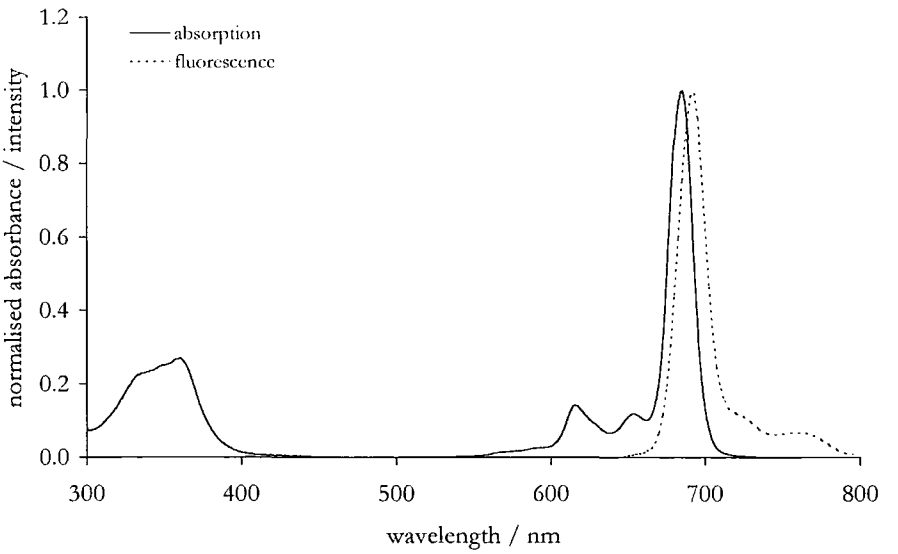

Figure 4.2 Absorption and fluorescence spectra of **1** in dichloromethane.

The thiophene containing phthalocyanine **2** showed almost identical behaviour to reference compound **1**, with unchanged spectral maximum and lifetime. An extinction coefficient of 2.4 x 10^5 dm^3 mol^{-1} cm^{-1} was recorded, just slightly lower than that of **1**. The fluorescence quantum yield is significantly reduced with a value of just 0.39, almost 40% lower than that of **1**. This quenching of the fluorescence is most probably a result of an electron transfer mechanism - the thiophene moiety possesses a large electron density and in **2** this is combined with the added flexibility that the acetic acid linker affords. This allows the thiophene ring to lie close to the phthalocyanine macrocycle (the crystal structure of **2** concurs, showing the thiophene almost parallel with the plane of the phthalocyanine ring[18]), enabling electron transfer to occur with ease. The phenomenon of electron transfer quenching of phthalocyanine emission is not unknown, and the process can occur both to and from the phthalocyanine excited state. For example, electron acceptors have been shown to quench either the singlet[19] or triplet excited state,[20] and electron donors too show quenching.[21] Metal free phthalocyanines with peripheral[22] and fused[23] thiophene moieties have been synthesised previously, displaying red shifted absorption and emission bands (indicating electronic interaction between phthalocyanine and thiophene groups) - unfortunately fluorescence quantum yields were not reported.

The unperturbed fluorescence lifetime of **2** is unusual - quenching generally results in a reduction of both the quantum yield *and* lifetime. The calculated rate constant of fluorescence, k_f ($= \Phi_f / \tau_f$) is reduced ($5.3 \pm 0.5 \times 10^7 s^{-1}$) compared with that

of **1** ($9.3 \pm 0.5 \times 10^7$ s^{-1}). The mechanism for this quenching is believed to involve two distinct states - an "on" state in which fluorescence is observed with a normal lifetime of 6.7 ns, and an "off" state in which the excited phthalocyanine singlet state is quickly and efficiently quenched. The lifetime of the "off" state is extremely rapid. It should be reiterated that the "off" state is not due to aggregation, for the axially substituted silicon phthalocyanines show no evidence of aggregation at concentrations up to 10^{-4} mol dm^{-3}.

Intermolecular quenching of the emission of reference compound **1** by the addition of thiophene-3-acetic acid was not observed in dichloromethane, even at quencher concentrations up to 0.1 mol dm^{-3}, yielding an upper limit for the quenching rate constant, k_Q, of 3×10^8 dm^3 mol^{-1} s^{-1}.

In the light of the unusual quenching by electron transfer seen in **2** the 2-, 3- and 4-methoxy substituted phenylacetic acid derivatives **3**, **4** and **5** were studied. The methoxyphenyl moieties are rich in electron density and it was hoped that similar quenching would be observed. However all three compounds possess lifetimes of 6.8 ns and quantum yields which match that of **1**, and it is evident that there is no quenching effect of the phthalocyanine excited state by the axial ligand. As a result these compounds are spectroscopically identical to **1**, with the exception of minor additional absorption below 300 nm due to the methoxybenzene chromophore.

The synthesis of the 3,4-dimethoxyphenylacetic acid substituted phthalocyanine **6** afforded a compound with increased electron density in the axial ligand with respect to the monomethoxy compounds. A small decrease in quantum yield and lifetime reflects this, indicating approximately 8% quenching by the axial ligand relative to **1**. The effect of the ligand arm length upon this quenching was investigated using the 3,4-dimethoxy substituted species with zero, two and three methylene spacer units - compounds **7**, **8** and **9** respectively - in addition to **6** with one methylene unit. With the shortest linker (zero methylene units) **7** shows quantum yield and lifetime values comparable with **1** (Table 4.1), whilst **6**, as just discussed, is partially quenched. The incorporation of another methylene group in **8** causes a significant increase in the quenching of the excited state with quantum yield and lifetime of 0.5 and 5.6 ns respectively. In contrast **9**, with three methylene spacer units, shows an increase in fluorescence relative to **8**, although the quantum yield and lifetime remain reduced in comparison with those of the reference compound **1**. Note that for all these quenched species both lifetime and quantum yield values are reduced, unlike the thiophene containing compound, **2**.

This behaviour indicates two contrasting effects - chain flexibility and quencher-phthalocyanine distance. As the crystallographic data for **1** confirms,[18] the axial ligand in a benzoic acid derivative is held perpendicular to the phthalocyanine macrocycle, and this means that the quenching dimethoxy unit in **7** will be held rigidly away from the fluorescent core. As a result, quenching does not proceed, and **7** shows identical photophysical behaviour to the reference compound **1**. As the ligand arm becomes more flexible (compounds **6** and **8**) the quenching moiety is more able to come into close contact with the phthalocyanine such that the fluorescence emission is quenched. However, in parallel to the increase in flexibility the addition of methylene spacer units results in lengthening of the ligand and hence the removal of the quenching unit from the phthalocyanine. Thus, addition of methylene units sets in competition the effects of chain flexibility and length, and a balance must be reached to observe the most quenching. The progression from **7** to **8** through **6** shows the dominance of the effect of the chain flexibility, and so quenching increases (Figure 4.3), but at this point the length of the chain becomes important, and addition of the final methylene unit to yield compound **9** pushes the quenching unit too far from the phthalocyanine core, and hence the extent of quenching is reduced again. This conclusion agrees with molecular modelling (CAChe, Oxford Molecular, Ltd.), in which optimised structures of the phthalocyanines clearly show the increase in flexibility allowing the quencher unit close proximity to the phthalocyanine core. The structure for **9** however, with three methylene units, shows the quencher unit to be only partially overlapping with the phthalocyanine ring, such is the length of the axial arm (Figure 4.4).

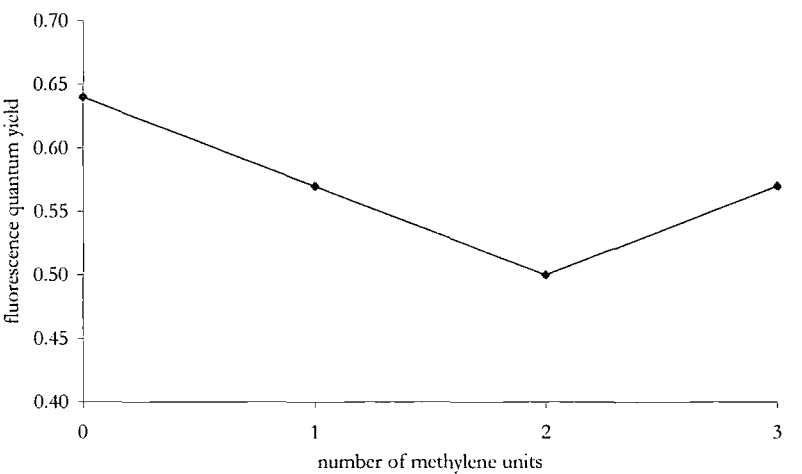

Figure 4.3 Quantum yields of compounds **6-9** showing competing effects of chain flexibility and length.

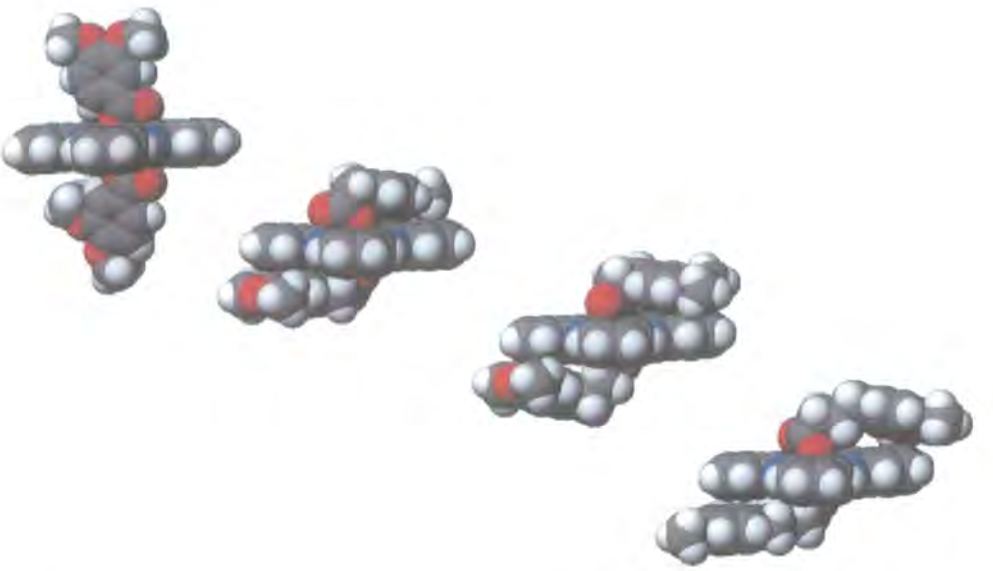

Figure 4.4 Optimised structures of compounds **6**-**9**.

The trimethoxy acetic acid substituted compound, **10**, shows significant quenching (fluorescence quantum yield = 0.33, lifetime = 3.8 ns), but it is **11**, isomeric with **6** with just two methoxy units which displays extensive quenching. The quantum yield and lifetime values of 0.08 and 0.96 ns respectively indicate greater than 85% reduction in emission relative to **1**. The change in substitution pattern of the two methoxy groups on the axial substituent proves an important factor in this electron transfer process. Investigation of the 2-, 3- and 4-substituted species **3**, **4** and **5** showed that the substitution position had no effect on the extent of quenching, but this new result would suggest something different. The important factor in moving from the 3,4-substituted **6** to the 2,5-substituted compound **11** is that the latter arrangement allows the existence of a quinoidal resonance canonical. The oxidation potentials of the 3,4- and 2,5-dimethoxyphenylacetic acids reflect this, that of the latter being considerably lower (+1.54 V *vs* NHE for **11**, +1.63 V *vs* NHE for **6**), making the electron transfer process more favourable.

When a phthalocyanine (or indeed any chromophore) absorbs a photon, generating an excited state, the redox potential of the compound is significantly changed. It is raised by an amount equal to the energy of the excited state, and the excited species is a better electron acceptor (because the original ground state energy level now possesses an electron 'hole') and concurrently a better electron donor

(because the promoted electron is now in a higher energy orbital and hence less tightly bound). As a result, an excited state phthalocyanine has a completely different redox chemistry and can undergo reactions which would not occur with ground state molecules (see Scheme 4.1).

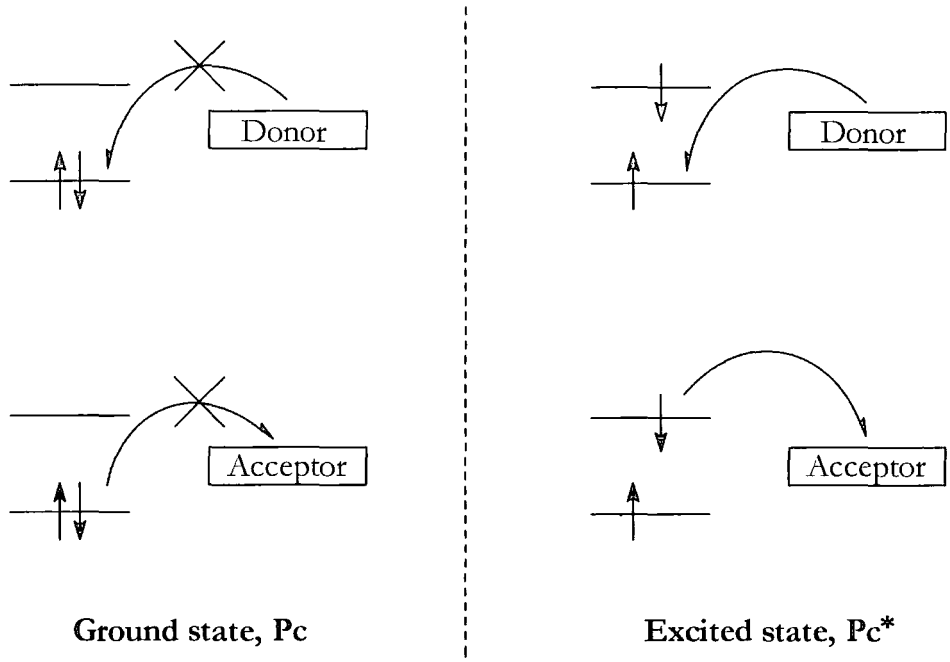

Scheme 4.1 Redox processes for ground and excited state phthalocyanine in the presence of electron donors and acceptors. Note that the donor and acceptor energy levels are intermediate to those of the phthalocyanine HOMO and LUMO.

Marcus first discussed the theory of electron transfer,[24] and related the rate of reaction, k_Q, to the transfer activation energy $\Delta G^{\#}$. Rehm and Weller[25] considered this result further and identified a plateau region occurring at high, negative ΔG - in this region k_Q becomes diffusion controlled, and so a maximum value for the rate constant is reached.

The free energy change for electron transfer depends upon a number of factors, including the reduction potentials of the donor (for the process $D^+ \rightarrow D$, in eV) and acceptor (for the process $A \rightarrow A^-$, in eV), the energy required to produce the excited state ($\Delta E_{0,0}$, in eV), and the free energy change for the two radical ions meeting at the encounter distance (described by $e_0^2/4\pi\varepsilon_0\varepsilon_r a$ in eV, where e_0 is the elementary charge, ε_0 the relative permittivity of a vacuum, ε_r the relative permittivity of the solvent and a the encounter distance). ΔG, in units of kJ mol^{-1}, can be calculated using Equation 4.1.

$$\Delta G / \text{kJ mol}^{-1} = 96.49\,[E^{\circ}_{D+/D} - E^{\circ}_{A/A-} - (e_0^2/4\pi\varepsilon_0\varepsilon_r a) - \Delta E_{0,0}] \quad (4.1)$$

The rate constant for quenching can be calculated using Equation 4.2.

$$k_Q = \frac{k_d}{1 + \frac{k_d}{\Delta V_d k_{deac}}\left(\exp\left(\frac{\Delta G^{\#} + \Delta G}{RT}\right)\right)} \quad (4.2)$$

where k_d is the rate of diffusion through the solvent medium, according to the equation $k_d = 8RT/3\eta$ (R is the gas constant, 8.314 J K^{-1} mol^{-1}, T the temperature in K and η the solvent viscosity),[26] ΔV_d is the ratio of forward to backward diffusion (k_d/k_{-d}), k_{deac} is the rate constant of deactivation of the radical pair, and $\Delta G^{\#}$ is the activation free enthalpy. $\Delta G^{\#}$ is related to ΔG in terms of Equation 4.3, where $\Delta G^{\#}_0$ is the activation enthalpy when $\Delta G = 0$.

$$\Delta G^{\#} = ((\tfrac{1}{2}\Delta G)^2 + (\Delta G^{\#}_0)^2)^{\frac{1}{2}} + \tfrac{1}{2}\Delta G \quad (4.3)$$

For ease of calculation the terms $k_d/\Delta V_d k_{deac}$ (Equation 4.2) and $\Delta G^{\#}_0$ (Equation 4.3) are approximated to the values determined by Rehm and Weller[25] for acetonitrile, 0.25 and 10 kJ mol^{-1} respectively.

Use of these equations allows the calculation of the rate constant for quenching by electron transfer, and subsequent comparison with the experimentally obtained fluorescence quantum yields for the silicon phthalocyanine bis-esters **5**, **6**, **10** and **11** previously described. For these calculations the following parameters were used:

E° [$(RO)_2SiPc/(RO)_2SiPc^{\bullet-}$] = -0.69 V (experimentally obtained for **1**).
E° [$Quencher^{\bullet+}$/Quencher] = values according to Table 4.2 (experimentally obtained for the free carboxylic acid).
$\Delta E_{0,0}$ = 1.81 eV (experimentally obtained for **1**, λ_{max}(abs) = 685 nm).
η = 0.4 cp for dichloromethane.[27]
T = 298 K.
a = 0.34 nm for intramolecular quenching (calculated from optimised structures, using CAChe – see text below for comment), 1.0 nm for intermolecular quenching.

Table 4.2 Rehm-Weller calculations for compounds **2**, **5**, **6**, **10** and **11**.

	Quenching Unit	E_{ox}/V [a]	ΔG/kJmol^{-1}	k_Q/dm^{3}mol^{-1}s^{-1} (calc.) [b]	Φ_f (expt) [c]
2	Thiophene	+1.58[28]	-0.62	1.2 x 10^9	0.39
5	4-(MeO)$C_6H_4CH_2CO_2H$	+1.93 [d]	33.2	2.4 x 10^4	0.64
6	3,4-(MeO)$_2C_6H_3CH_2CO_2H$	+1.63 [d]	4.2	4.3 x 10^8	0.57
10	3,4,5-(MeO)$_3C_6H_2CH_2CO_2H$	+1.58 [d]	-0.62	1.2 x 10^9	0.33
11	2,5-(MeO)$_2C_6H_3CH_2CO_2H$	+1.54 [d]	-4.4	4.4 x 10^9	0.08

[a] *vs* NHE; [b] Rate constant for quenching of phthalocyanine by quenching unit, intramolecular separation distance a = 0.34 nm (see text for comment); [c] Phthalocyanine fluorescence quantum yield; [d] obtained experimentally – see Chapter 2.

The results of the Rehm-Weller calculations for these methoxy containing silicon phthalocyanines immediately show the direct relation of the quencher unit oxidation potential and the extent of observed quenching. Despite the small difference in oxidation potential for the 3,4- and 2,5-dimethoxy substituted systems there is a calculated five-fold increase in the rate constant k_Q for the 2,5-substituted compound (Table 4.2). The experimental results concur qualitatively, with **11** showing a ten-fold increase in quenching relative to **6**. The mono-substituted species, **5**, displayed no observable quenching, and the calculation shows good agreement with this, the obtained value of k_Q for **5** being 10^5 times smaller than that of **6**. The 3,4,5-trimethoxy substituted **10** has an oxidation potential of +1.58 V, intermediate to those of **6** and **11**, and, whilst demonstrating emission quenching, the quantum yield and lifetime values of 0.33 and 3.8 ns respectively indicate this to be only partial with respect to the unquenched mono-substituted **5**. The calculated k_Q value of 1.2 x 10^9 dm^3 mol^{-1} s^{-1} reflects this partial quenching. The thiophene containing species, **2**, discussed above also shows a reduced quantum yield, corroborated by the Rehm-Weller calculations.

The importance of the separation distance between the quenching and fluorescing units has already been discussed in terms of ligand arm length, but the calculations also stress this point. For the intramolecular quenching calculations discussed thus far a quencher-fluorophore separation distance of 0.34 nm was used, which value was obtained from the modelled optimised structures (Figure 4.4). The distance was taken from the centre of the quenching moiety to the nearest point of the phthalocyanine ring, and the value was obtained directly from the CAChe software. The value of 0.34 nm

should, however, not be considered as a strict separation distance, but rather used as a measure of the *intra*molecular nature of the quenching. Given the non-static nature of the axial ligands in these compounds the error involved in this value is necessarily quite large, in the order of 10-20%. The *inter*molecular process should also be considered, and for these calculations a separation distance of 1.0 nm was estimated.[29] Intermolecular quenching of phthalocyanine fluorescence by the methoxyphenylacetic acids shown in Table 4.2 is calculated to be unfavourable with quenching rate constants of 0.22 $dm^3 mol^{-1} s^{-1}$ or less - a stark contrast to the behaviour of **11**, for example, where k_Q takes the value of 2.2 x 10^9 dm^3 mol^{-1} s^{-1} and greater than 85% *intra*molecular quenching is observed relative to the reference compound **1**. Experiment concurs with the reduced intermolecular rate constants, and no intermolecular quenching between ligand and **1** is observed at quencher concentrations up to 0.1 mol dm^{-3}, inferring $k_Q < 3$ x 10^8 dm^3 mol^{-1} s^{-1}. A similar lack of quenching was obtained for a zinc phthalocyanine in the presence of 1,4-dimethoxybenzene.[29]

4.4 Conclusions

The photophysical properties of a number of novel silicon phthalocyanine bis-esters have been investigated.[18] The reference compound silicon phthalocyanine bis-(4-*tert*-butyl)benzoate **1** shows excellent properties with a long fluorescence lifetime and high quantum yield typical of silicon phthalocyanines. The absorption spectrum displays a sharp Q band with well defined vibrational satellites which results from reduction in intermolecular interaction due to the axial ligands. A thiophene containing compound shows a reduced quantum yield due to quenching by the electron rich thiophene moiety. However, the lifetime remains unperturbed and a two state system ("on"/"off") is proposed.

The remaining bis-esters all contain electron rich moieties, and demonstrate normal fluorescence quenching (reduced quantum yield and lifetime) by intramolecular electron transfer from the ligand to the excited state of the phthalocyanine. The extent of quenching is related to the chain length between the phthalocyanine core and the aromatic nucleus of the ligand, with competing effects between chain flexibility and length. However, the ease of oxidation of the ligand which has most affect upon the observed reductions in fluorescence, and calculations according to Rehm-Weller theory of electron transfer quenching show good agreement with the experimental results.

4.5 References

1 C. C. Leznoff and A. B. P. Lever (Eds.), *Phthalocyanines – Properties and Applications*, VCH Publishers, Inc., New York, (a) Volume 1, 1989 (b) Volume 2, 1993 (c) Volume 3, 1994, (d) Volume 4, 1996.

2 P. Sayer, M. Gouterman and C. R. Connell, Metalloid porphyrins and phthalocyanines, *Acc. Chem. Res.*, 1982, 15, 73.

3 R. D. Joyner and M. E. Kenney, Phthalocyaninosilicon compounds, *Inorg. Chem.*, 1962, 236.

4 M. Brewis, G. J. Jackson, V. Goddard, M. Helliwell, A. M. Holder and N. B. McKeown, Silicon phthalocyanines with axial dendritic substituents, *Angew. Chem. Int. Ed.*, 1998, **37**, 1092.

5 R. D. Joyner, J. Cekada, Jr., R. G. Linck and M. E. Kenney, Diphenoxysilicon phthalocyanine, *J. Inorg. Nucl. Chem.*, 1960, **15**, 387.

6 E. Ciliberto, K. A. Doris, W. J. Pietro, G. M. Reisner, D. E. Ellis, I. Fragala, F. H. Herbstein and M. A. Ratner, π-π interactions and bandwidths in "molecular metals". A chemical, structural, photoelectron spectroscopic and Hartree-Fock-Slater study of monomeric and cofacially joined dimeric silicon phthalocyanines, *J. Am. Chem. Soc.*, 1984, **106**, 7748.

7 K. A. Bello and I. A. Bello, Some observations on the visible absorption spectra and stability properties of the silicon phthalocyanine system, *Dyes and Pigments*, 1997, **35**, 261.

8 (a) J. A. Elvidge and A. B. P. Lever, Manganese phthalocyanine as an oxygen carrier, *Proc. Chem. Soc.*, 1959, 195; (b) R. D. Joyner and M. E. Kenney, Germanium phthalocyanines, *J. Am. Chem. Soc.*, 1960, **82**, 5790.

9 R. D. Joyner and M. E. Kenney, A phthalocyaninosiloxane, *Inorg. Chem.*, 1962, **1**, 717.

10 N. S. Hush and I. S. Woolsey, Electronic absorption spectra of phthalocyanine monomers and dimers, *Mol. Phys.*, 1971, **21**, 465.

11 U. Lauter, M. Schulze and G. Wegner, Rigid rod polymers with regularly spaced silicon-centered phthalocyanine units in the backbone, *Macromol. Rapid. Commun.*, 1995, **16**, 239.

12 M. D. Maree and T. Nyokong, Effect of oligomerisation on the photochemical properties of silicon octaphenoxyphthalocyanine, *J. Photochem. Photobiol. A: Chem.*, 2001, **142**, 39.

13 A. R. Kane, J. F. Sullivan, D. H. Kenny and M. E. Kenney, The nuclear magnetic resonance spectra and the electronic spectra of some silicon and germanium phthalocyanines, *Inorg. Chem.*, 1970, **9**, 1445.

14 M. Kasha, H. R. Rawls and M. A. El-Bayoumi, The Exciton Model in molecular spectroscopy, *Pure Appl.Chem.*, 1965, **11**, 371.

15 D. W. DeWulf, J. K. Leland, B. L. Wheeler, A. J. Bard, D. A. Batzel, D. R. Dininny and M. E. Kenney, Isolation, spectroscopic properties and electrochemical properties of two oligomeric silicon phthalocyanines, *Inorg. Chem.*, 1987, **26**, 266.

16 L. Oddos-Marcel, F. Madeore, A. Bock, D. Neher, A. Ferencz, H. Rengel, G. Wegner, C. Kryschi and H. P. Trommsdorff, Electronic states and relaxation dynamics of silicon phthalocyanine dimers, *J. Phys. Chem.*, 1996, **100**, 11850.

17 A. P. Pellicioli, K. Henbest, G. Kwag, T. R. Carvagno, M. E. Kenney and M. A. J. Rodgers, Synthesis and excited state dynamics of μ-oxo group IV metal phthalocyanine dimers: a laser photoexcitation study, *J. Phys. Chem. A*, 2001, **105**, 1757.

18 C. Farren, S. FitzGerald, M. R. Bryce, A. Beeby and A. S. Batsanov, Synthesis, structure and optical characterisation of silicon phthalocyanine bis-esters, *J. Chem. Soc., Perkin Trans. 2*, 2002, 59.

19 J. R. Darwent, I. McCubbin and G. Porter, Photoreduction of methyl viologen sensitized by sulphonated phthalocyanines in micellar solution, *J. Chem. Soc., Faraday Trans. 2*, 1982, **78**, 903.

20 T. Ohno, S. Kato and N. N. Lichtin, Electron transfer in the quenching of triplet states of zinc phthalocyanine and methylene blue by the use of Fe(III), Co(III) and organic oxidants, *Bull. Chem. Soc. Jpn.*, 1982, **55**, 2753.

21 M. E. Daraio, A. Volker, P. F. Aramendia and E. San Roman, Reactions of zinc phthalocyanine excited states with amines in cationic micelles, *Langmuir*, 1996, **12**, 2932.

22 T. Muto, T. Temma, M. Kimura, K. Hanabusa and H. Shirai, A new phthalocyanine derivative having peripheral 2-thienyl substituents, *Chem. Commun.*, 2000, 1649.

23 M. J. Cook and A. Jafari-Fini, Phthalocyanine-related macrocycles: cross cyclotetramerisation products from 3,4-dicyanothiophenes, 2,3-dicyanothiophene and 3,6-dialkylphthalonitriles, *Tetrahedron*, 2000, **56**, 4085.

24 (a) R. A. Marcus, On the theory of oxidation-reduction reactions involving electron transfer, I, *J. Phys. Chem.*, 1956, **24**, 966; (b) R. A. Marcus, Chemical and electrochemical electron transfer theory, *Ann. Rev. Phys. Chem.*, 1964, **15**, 155.

25 D. Rehm and A. Weller, Kinetics of fluorescence quenching by electron and H-atom transfer, *Israel J. Chem.*, 1970, **8**, 259.

26 P. W. Atkins, *Physical Chemistry*, Oxford University Press, Oxford, 1995, Fifth Edition.

27 R. C. Weast (Ed.), *Handbook of Chemistry and Physics*, CRC Press, Inc., Boca Raton, Florida, 61st Edition, 1980.

28 J. Roncall in *Handbook of Conducting Polymers*, Eds. T. J. Skotheim, R. L. Elsenbaumer, J. R. Reynolds, Marcel Dekker, 1998.

29 C. F. Stanley, *Photophysical Investigation of Substituted Zinc Phthalocyanines as sensitisers for Photodynamic Therapy*, Ph.D. Thesis, University of Durham, 1997.

Chapter 5

Properties of Axially Substituted Silicon Phthalocyanines Containing Tetrathiafulvalene Units

5.1 Introduction

5.1.1 Tetrathiafulvalene

Intense scientific interest in tetrathiafulvalene, TTF (Figure 5.1), was prompted by reports in 1972 of the compound's conductor properties,[1] and, in the presence of 7,7,8,8-tetracyano-π-quinodimethane (TCNQ), the formation of the charge transfer salt TTF-TCNQ which showed metallic behaviour down to 54 K - the first example of a true organic metal.[2] Since then, superconducting TTF salts have also been demonstrated.[3] A number of reviews on TTF and its applications have been published.[4]

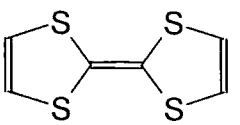

Figure 5.1 Structure of tetrathiafulvalene.

The properties of TTF are such that it is an attractive building block within the chemistry of materials[4c] - for example, oxidation of the ring to form the radical cation and dication is sequential, and occurs at remarkably low oxidation potentials, which can themselves be finely tuned by careful substitution of the TTF ring. In addition the rings readily aggregate, forming dimers, stacks or two dimensional sheets. In light of these properties, Bryce *et al.* have investigated a number of macromolecular TTF systems, including dendritic species and phthalocyanine-TTF hybrids.[5]

TTF displays an intense absorption band (ε_{max}= 1.25 x 10^4 $dm^3 mol^{-1} cm^{-1}$) centred at ~285 nm, with a weak tail stretching into the visible region and affording TTF its orange hue.[6] Oxidation to the radical cation results in strong visible absorption in the region 300-700 nm. Both the parent TTF and its radical cation are non-fluorescent, but further oxidation to the dication results in an emissive species (λ_{max}(em) ≈ 500 nm, Φ_f = 0.04, τ_f < 1 ns).[7]

5.1.2 Phthalocyanines Containing Tetrathiafulvalene

There exists in the literature a small number of reports of phthalocyanine species containing the TTF moiety. A metal free phthalocyanine containing eight peripheral

TTF substituents was reported[8] and subsequently a full photophysical evaluation of this compound and a similar one with four peripheral TTF units gave evidence of extensive TTF-phthalocyanine interactions.[9] Both compounds showed broad absorption bands in the Q band region, indicative of exciton interactions[10,11] - this behaviour was observed even in extremely dilute solutions, suggesting the presence of intramolecular interactions between the phthalocyanine and TTF units. Fluorescence from the compounds was found to be of extremely low intensity, with quantum yields of just 1.7×10^{-3} and $<10^{-4}$ for the phthalocyanines with eight and four TTF units respectively, hypothesised to be due to rapid intramolecular electron transfer quenching. Similar *inter*molecular quenching was observed for the parent metal free tetra-*tert*-butyl phthalocyanine, with a diffusion limited rate constant of 1.1×10^{10} dm^{-3} mol^{-1} s^{-1}. Further investigation of this intermolecular process showed that the rate constant was significantly increased in heterogeneous solution.[12] No quenching of the phthalocyanine triplet state was observed upon addition of TTF.

Two unsymmetrically substituted phthalocyanine containing one and two TTF units in the peripheral α-position also showed spectroscopic evidence of aggregation with some 50% quenching of the phthalocyanine emission. The singly substituted compound was, additionally, shown to exhibit liquid crystalline behaviour.[13]

5.2 Experimental

Dr Chris Farren is thanked for providing the tetrathiafulvalene containing silicon phthalocyanine species discussed herein, which were synthesised by standard methodology, involving the reaction of silicon phthalocyanine dichloride with carboxylic acids in a polyether solvent. Full experimental data is reported elsewhere.[14] The synthesis of the reference bis-(4-*tert*-butyl)benzoate compound, **1**, has been previously described.[15]

5.3 Results and Discussion

5.3.1 Photophysics

The photophysical properties of reference compound **1** (Figure 5.2) were discussed in full in the previous chapter (Section 4.3) but for clarity are briefly repeated here. The bulky axial ligands efficiently prevent aggregation in the concentration range

10^{-4}-10^{-7} mol dm^{-3} and sharply defined absorption and emission peaks are observed. As is typical for silicon phthalocyanines,[16] the lifetime and quantum yield are increased with respect to the more commonly studied zinc and aluminium species (Table 5.1).

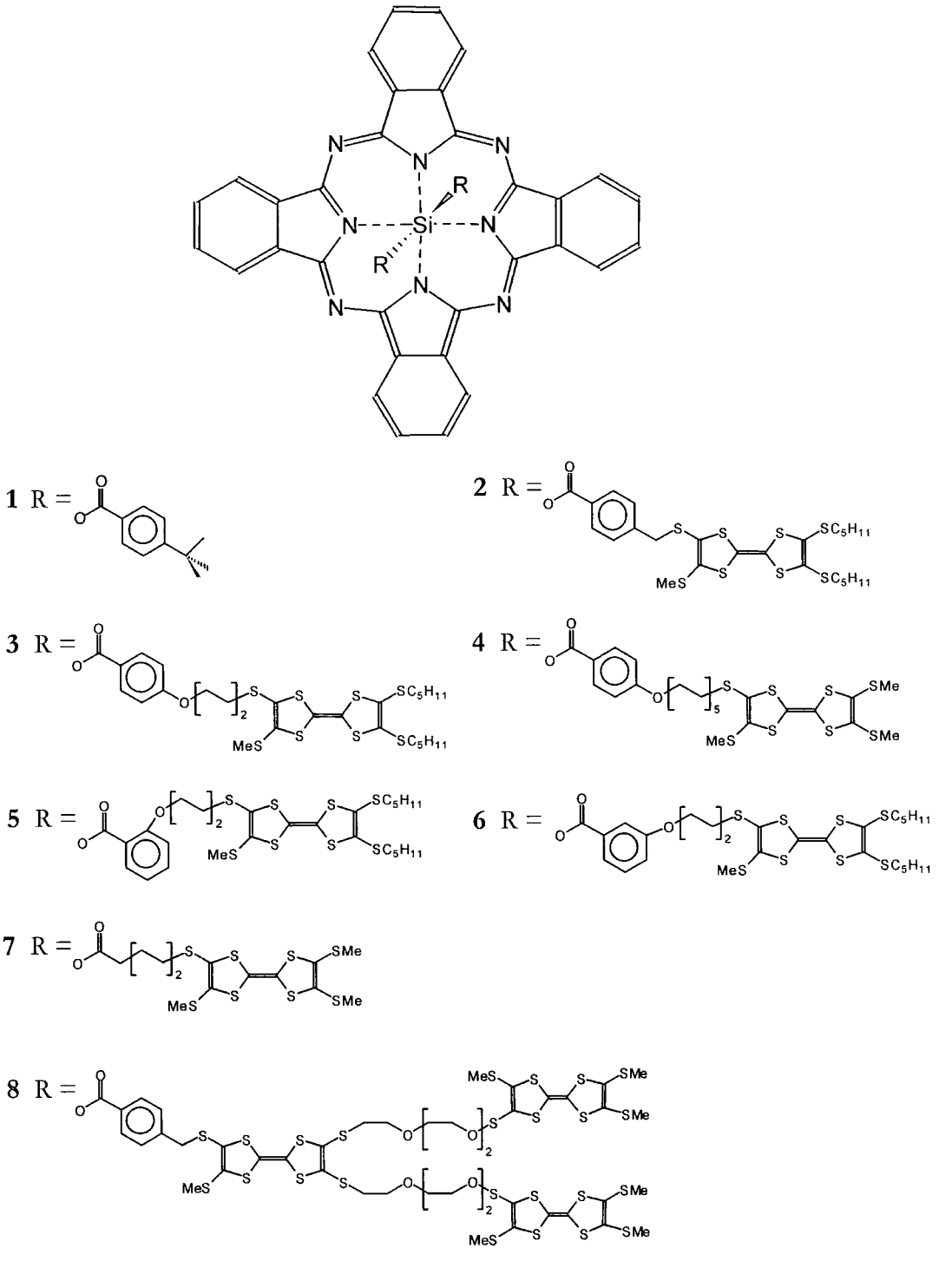

Figure 5.2 Structures of TTF containing silicon phthalocyanine bis-esters, **1**-**8**.

Table 5.1 Photophysical data for TTF containing silicon phthalocyanine bis-esters, **1-8**.

	$\tau_f \pm 0.1$ / ns [a]				$\Phi_f \pm 10\%$ [b]
	dichloromethane		2-methyltetrahydrofuran		
	τ_1 (yield)	τ_2 (yield)	τ_1 (yield)	τ_2 (yield)	
1	6.7 (100%) [c]	-	6.9 (100%) [c] 6.9 (100%) [d]	- -	0.62
2	6.3 (93%) [c]	1.9 (7%) [c]	6.3 (94%) [c] 6.8 (98%) [d]	2.2 (6%) [c] 2.2 (2%) [d]	0.29
3	6.2 (91%) [c]	1.6 (9%) [c]	5.6 (86%) [c] 6.5 (95%) [d]	1.7 (14%) [c] 2.2 (5%) [d]	0.39
4	6.4 (91%) [c]	1.8 (9%) [c]	6.3 (92%) [c] 6.5 (97%) [d]	2.8 (8%) [c] 2.1 (3%) [d]	0.45
5	6.1 (96%) [c]	1.5 (4%) [c]	6.0 (88%) [c] 6.5 (92%) [d]	1.9 (12%) [c] 2.7 (8%) [d]	0.17
6	6.1 (92%) [c]	1.1 (8%) [c]	5.8 (95%) [c] 6.3 (93%) [d]	1.4 (5%) [c] 1.7 (7%) [d]	0.30
7	-	-	6.7 (93%) [d]	1.8 (7%) [d]	0.006
8	-	-	6.6 (92%) [d]	1.8 (8%) [d]	0.04

[a] λ_{ex} = 635 nm, λ_{em} = 690 nm; [b] λ_{ex} = 612 nm, λ_{em} = 640-800 nm, 293 K, dichloromethane; [c] 293 K; [d] 77 K.

The electron rich TTF moiety is known to be an efficient quencher of zinc phthalocyanine emission by electron transfer, by both intermolecular and intramolecular mechanisms, the former with a diffusion limited rate constant.[9] Similarly **1** undergoes intermolecular quenching by TTF in dichloromethane with a rate constant of $k_Q = 1.6 \times 10^{10}$ dm^3 mol^{-1} s^{-1} and quenching reflected by both reduced fluorescence lifetime and quantum yield (Figure 5.3). However, it has previously been shown that the efficiency of the quenching process is strongly dependent upon the emitting species,[12] with a tetra-*tert*-butyl zinc phthalocyanine displaying strong quenching, whilst the emission of a related octasubstituted decyl zinc remained unquenched. Hence the above result provides confirmation that the presence of a silicon atom and axial ligands does not prevent electron transfer quenching by TTF.

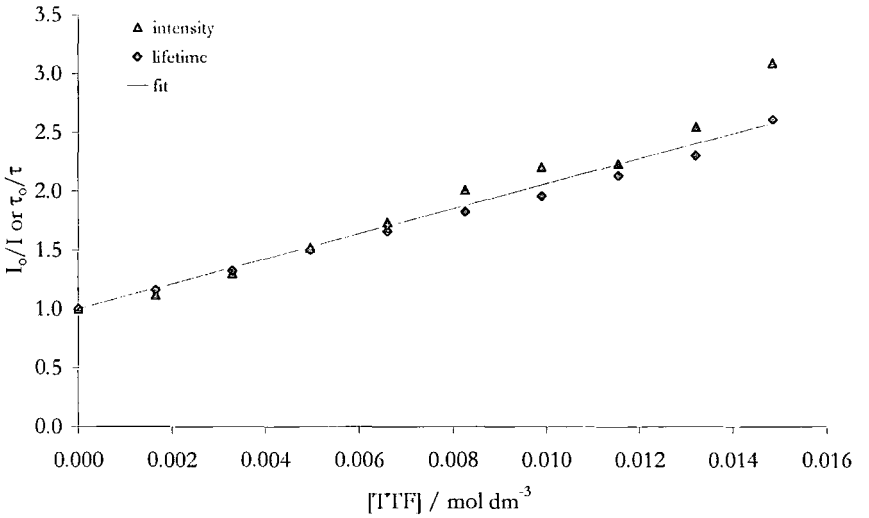

Figure 5.3 Stern Volmer plot for quenching of emission of **1** by tetrathiafulvalene.

The phthalocyanine **2** containing TTF in its axial ligand shows a typical phthalocyanine absorption profile, with no evidence of ring interaction, as was seen for the peripherally substituted zinc species.[9] However a reduced fluorescence quantum yield relative to reference compound **1** is observed, equivalent to 63% quenching of the macrocycle fluorescence by the electron donor. Whilst this is a significant result, in comparison with the 95.5% or greater intramolecular quenching exhibited by zinc phthalocyanines with four or eight peripheral TTF subsituents[9] the reduced efficiency of quenching in **2** is rather surprising. Given that **1** undergoes efficient electron transfer with TTF in an intermolecular fashion it is strange that the *intra*molecular process is not as efficient, particularly when quenching by methoxyphenyl acetic acids discussed in the previous chapter was shown to be strongly distance dependent. However, the crystal structure of **1** clearly shows the rigidity of the benzoate units, which lie perpendicular to the plane of the macrocycle ring,[15] and the two atoms between the benzoate group and the TTF unit in **2** will add only minimal flexibility. Hence the reduced quenching in **2** is explained as being a direct consequence of the TTF moiety being held at a greater than optimum distance from the phthalocyanine core. Interestingly, addition of the TTF containing carboxylic acid ligand to a solution of **2** shows further quenching as a result of *inter*molecular interactions, and this observation confirms that the position of the TTF moiety in **2** relative to the phthalocyanine core is unfavourable for the electron transfer process to occur fully.

Compounds **3** and **4**, with added flexibility in the axial ligands (linking units consisting of 6 and 12 atoms respectively), both display reductions in fluorescence

quenching relative to **2**, with quantum yields of 0.39 and 0.45 respectively. It is apparent that the increase in linker length across the series **2** (2 atoms in flexible unit), **3** (6 atoms) and **4** (12 atoms) has a direct affect upon the efficiency of quenching by TTF. Simple molecular modelling confirms that the increasing degree of flexibility in this series is more than offset by the concomitant increase in phthalocyanine-TTF separation distance (Figure 5.4). A similar effect was seen in the previous chapter in 3,4-methoxybenzene containing axial ligands, with zero, one, two and three methylene units between the macrocycle and benzene units.

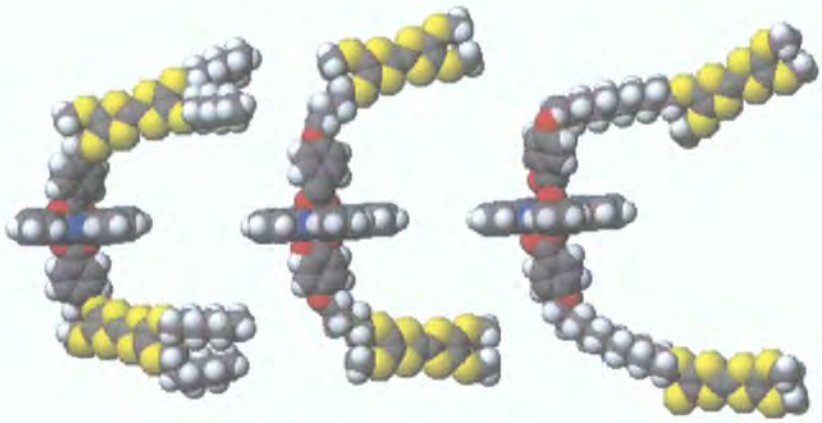

Figure 5.4 Optimised structures of compounds **2**-**4**.

Fluorescence lifetimes for the three hybrids discussed so far display a second minor component; the fluorescence decay of the reference compound **1** exhibits clear single exponential behaviour, and the presence of the quenching moiety in the phthalocyanine-TTF hybrids seems to complicate their behaviour. It is interesting to note that the *lifetimes* show no reduction in line with the reduced quantum yields. Similar behaviour was noted for the thiophene-containing silicon phthalocyanine bis-ester discussed in the previous chapter, and it is again suggested that there are two possible states for these compounds - an "on" state in which fluorescence is observed with a normal lifetime and an "off" state in which fluorescence is rapidly and efficiently quenched, and for which the lifetime is very short. Previous studies with phthalocyanine-TTF quenching systems[9,12] did not report lifetimes so no comparison is possible. With *inter*molecular quenching, as displayed by reference compound **1** in the

presence of TTF, this phenomenon is not observed, and fluorescence lifetime and quantum yield values decrease proportionally as quencher concentration increases. Similar 'normal' behaviour was observed for the *intra*molecular quenching observed for the methoxybenzene containing phthalocyanines.

In a further attempt to increase the quenching of the phthalocyanine emission the 2- and 3-substituted analogues of **3** were synthesised in order to bring the TTF containing part of the ligand in closer proximity to the macrocycle core. Enhanced quenching is observed for these two species relative to **3**, with **6** (3-substituted) and **5** (2-substituted) possessing quantum yields of 0.30 and 0.17 respectively, the latter equivalent to 73% quenching of the phthalocyanine emission by the axial TTF groups. Once again lifetimes were unperturbed by this quenching. The ability to tune the degree of quenching by altering the ligand chain length and substitution pattern has thus been demonstrated, a direct consequence of minimising the TTF phthalocyanine separation distance. However, as with the methoxybenzene species discussed in the previous chapter, the extent of tuneability is small, and the quenching still remains far from that obtained with the peripherally substituted zinc phthalocyanines.[9]

In contrast, compound **7**, without the rigid benzoate ester linkage, shows a dramatic increase in quenching relative to the previous compounds, and has a quantum yield of <0.006 indicating >99% fluorescence quenching. That removal of the benzoate ester results in such a profound change in behaviour emphasises the role of the rigid benzoate ester group in solution. With such efficient quenching there became available a suitable system with which to further investigate the unusual two state quenching model. The possibility of there being distinct "on" and "off" states for fluorescence led to the consideration of the effect of temperature upon the equilibrium between these two states. Cooling a solution of **7** to an optically transparent glass at 77 K resulted in a 300 fold increase in emission intensity, exhibiting a sharp turn on below 140 K, coinciding with the glass point of the solvent[17] (Figure 5.5B). Generally, cooling a solution of phthalocyanine (or indeed, any chromophore) results in the sharpening of both absorption and emission peaks, and the contraction of the solvent results in an additional effective increase in concentration. Further complication can be added by the fact that phthalocyanines often aggregate as the temperature is lowered, but for the axially substituted silicon phthalocyanines there is no spectroscopic evidence of such temperature induced aggregation. Care was taken to avoid errors arising from the

cooling process. The spectra were corrected for changes in absorption at the excitation wavelength, and the reported increases in emission intensity were calculated via integration of the emission spectra. Thus, reported increases in emission additionally represent increases in quantum yield.

As the solvent solidifies the flexible ligand arm is frozen into its thermodynamically favoured configuration, and the dramatic increase in emission indicates this to be with the TTF units held distant to the phthalocyanine macrocycle. Similar temperature dependence of emission was observed for the other phthalocyanine-TTF systems previously described, with the exception of **3** and **4**. These two compounds show the least fluorescence quenching at room temperature (27% and 37% respectively) and it is not unreasonable to suppose that with the TTF moiety already far removed from the phthalocyanine core cooling has no further effect. The increase in emission of the other species can directly be related to their room temperature quantum yields. Thus, **7** with the smallest quantum yield at 293 K, shows the largest increase on cooling, whilst compounds **2**, **6** and **5** show more modest increases (1.5, 2 and 3 fold respectively). Figure 5.5 shows the temperature effect upon the emission of partially quenched **5** and fully quenched **7**. The fluorescence lifetime of **7** was not measurable at room temperature, but was found to be 6.7 ns (plus a minor second component) at 77 K, this being similar to that of the reference compound **1**.

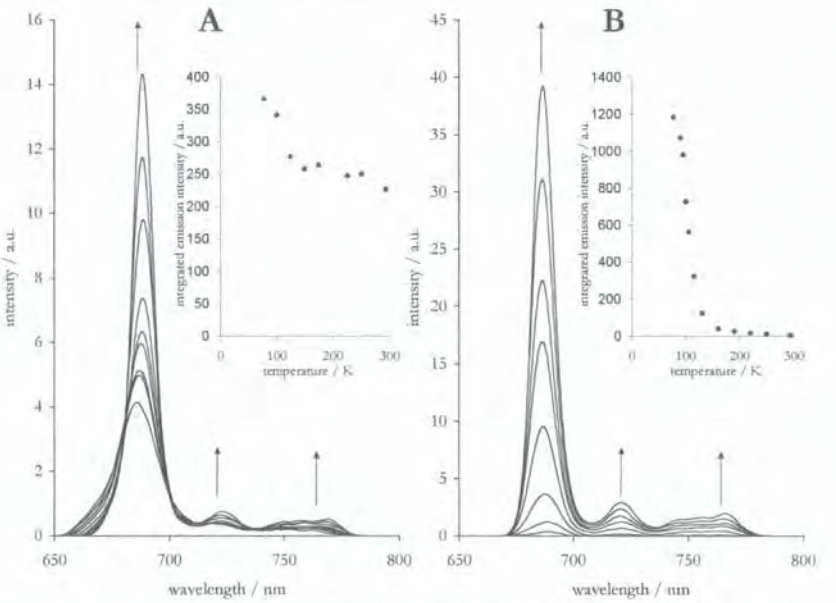

Figure 5.5 Temperature effect on emission spectra of (A) **5** and (B) **7**. Inset: integrated, absorption corrected emission intensity as a function of temperature.

The dendritic species, **8**, despite the presence of the benzoate linker, showed similar emission properties to **7**, with a slightly larger quantum yield of 0.04 and correspondingly reduced effect on cooling to 77 K. This increase in quenching, despite the presence of the rigid benzoate ester linkage, can be attributed to a combination of exceptional flexibility due to the glycol units and the increased local concentration of TTF units. **7** contains six units per molecule, whilst the previously discussed compounds (**2-6**) have just two per molecule. Given the poor extent of quenching observed for **4**, with a flexible linker consisting of 12 atoms, it can perhaps be surmised that it is the increased local TTF concentration in **7** which dominates.

5.3.2 Spectroelectrochemistry

The electrochemistry of TTF is well known, and the reversible formation of the radical cation and dication can be followed spectroscopically.[6,18] Whilst TTF is an excellent electron donor, removal of one or two electrons to form the radical cation or dication species respectively prevents this process. The oxidation potentials for formation of the radical cation and dication are remarkably low, +0.56 V and +1.0 V respectively[4c] (*vs* normal hydrogen electrode in acetonitrile).

The phthalocyanine-TTF hybrids reported here are particularly interesting since the TTF first oxidation potential lies well below that of the phthalocyanine core; hence selective oxidisation of the TTF should be possible, without disturbing the phthalocyanine. The oxidised form of TTF would lose its electron donating properties and the cessation of phthalocyanine emission quenching would be expected. The result would be an electrochemically activated fluorescence switch comprising the non-fluorescent phthalocyanine-TTF and fluorescent phthalocyanine-$TTF^{+\bullet}$ species. Photoswitches are not unknown, and examples in the literature are dominated by porphyrin containing species. For example, a zinc porphyrin containing an axially coordinated phenylazopyridine quenching unit, can be activated by external redox and protonation stimuli.[19] A similarly axially substituted species comprising a phosphorus porphryin with axial azobenzene derivatives displayed luminescence switching by photoisomerisation,[20] whilst an azobenzene linked diporphyrin species with contrasting electron rich and poor porphyrin moieties also showed changes in quantum yield upon photoisomerisation of the linking unit, due to interactions between the two macrocycles. Redox switching in a ruthenium (II) bispyridine complex has also been observed,

involving the electrochemical conversion of a quinone substituent to a hydroquinone.[21] Interest in such photoswitches centres upon their potential use in the performance of switching and gating functions currently undertaken by conventional silicon circuitry.[22]

Spectroelectrochemistry allows the study of the spectroscopic properties of compounds with a variable applied potential. With an optically transparent thin layer electrode (OTTLE) cell[23] developed for absorption and emission spectroscopy, the spectroelectrochemical behaviour of the reference compound **1** was first investigated. Absorption spectra of phthalocyanine radical anions and cations are well known - both display loss of Q band absorption with concomitant growth throughout the visible region. Studies of zinc phthalocyanine radical anions showed three principal regions, all far less intense than the bands in the neutral species - Q band (750-1000 nm); π^*-π^* band (500-750 nm) and Soret band (300-480 nm).[24] Further reduction yields the di-, tri- and tetra-anions, and absorption spectra of these species were presented by Clack and Yandle,[25] with further analysis at a later date.[26] Assignment of bands of the radical cationic species has been slightly more complex. Nyokong *et al.* discussed the observed spectrum for the radical cationic species in terms of four regions - π-π (750-850 nm), Q (centred at 720 nm), π-π (400-650 nm) and Soret (below 400 nm).[27] A later paper by the same group focussing on a magnesium phthalocyanine assigned the 720 nm band to the dimeric radical cation Q band, whilst the region to higher wavelength was proposed to be that of the monomeric radical cation Q band.[28]

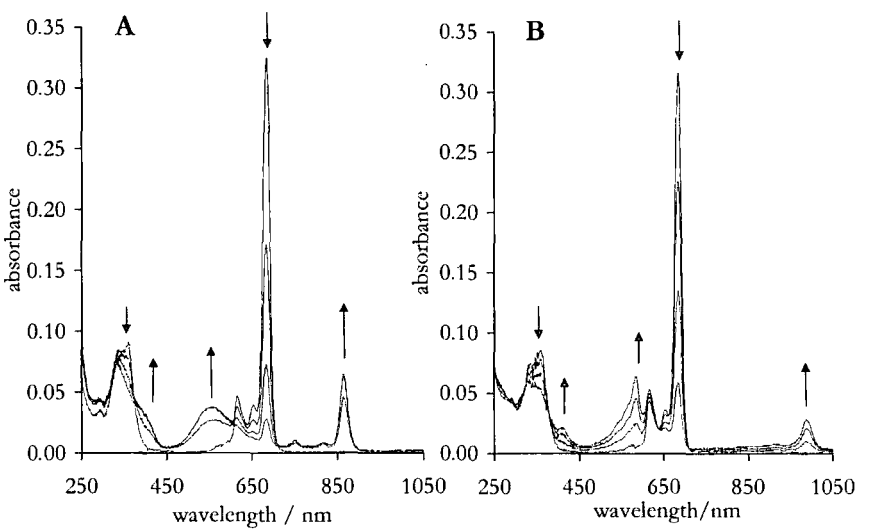

Figure 5.6 Absorption spectra of (A) radical cationic and (B) radical anionic species of **1**. Arrows indicate spectral changes with increased oxidation and reduction potential respectively. Acetonitrile solution, 0.1 mol dm^{-3} $^tBu_4NBF_4$, 293 K; aerated (A) and degassed (B) solution.

Silicon phthalocyanine **1** shows analagous behaviour to the zinc and magnesium species discussed above - reduction to form the radical anion shows a loss of normal Q and Soret band intensity, with new absorption bands at 410 nm, 585 nm and 990 nm, assigned to the Soret, π^*-π^* and Q bands of the radical anion respectively (Figure 5.6A). The radical cation shows similar reduction of Q and Soret band intensity, with a concurrent increase in absorption at 400 nm (broad), 550 nm (broad), and 865 nm (with vibrational satellites at 750 nm and 820 nm), with similar band assignment as for the radical anion, albeit with the central region now due to π-π transitions, and the Q band at slightly higher energy (Figure 5.6B). Note that the previous assignment of a 720 nm band observed for zinc and magnesium species as a dimer radical cation Q band is corroborated by the absence of this band for this silicon species. As previously observed **1** shows a complete absence of ring interactions due to the bulky, orthogonal axial substituents, so the observation of just monomeric radical cation species is not unexpected.

For the phthalocyanine-TTF compounds it was possible to achieve selective oxidation of the TTF group, apparent by new, broad absorption bands centred at 450 nm and 850 nm. These are assigned to the $TTF^{+\bullet}$ monomer species.[18,29] The selectivity of oxidation was indicated by the phthalocyanine Q bands, which retained their shape and intensity throughout the reversible electrochemical process (Figure 5.7). The Soret envelope does show a reduction in absorption, but this is due to removal of the overlapping TTF absorption (310 nm).

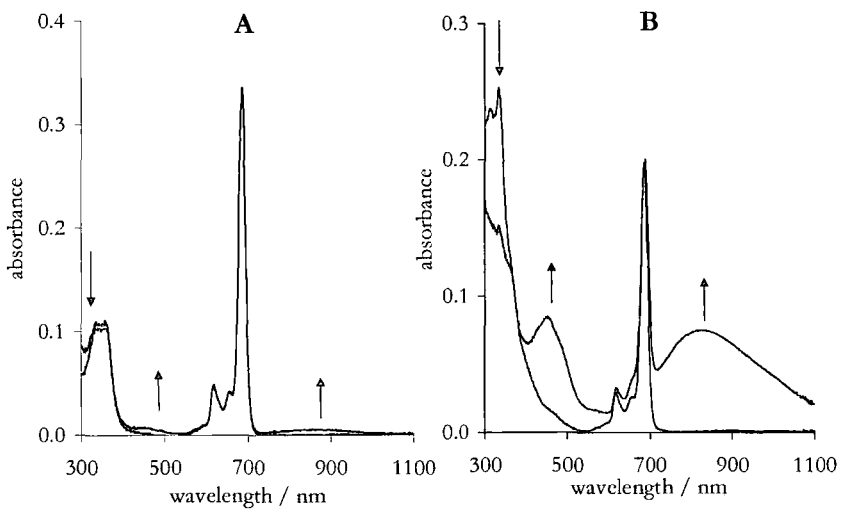

Figure 5.7 Absorption spectra of (A) **2** and (B) **8** under oxidative conditions. Arrows indicate spectral changes with increased oxidation potential. Acetonitrile solution, 0.1 mol dm^{-3} $^tBu_4NBF_4$, 293 K; aerated solution.

Emission spectra of the phthalocyanine-TTF species were recorded in the OTTLE cell, but despite the selective oxidation of the TTF (as monitored by absorption spectroscopy) the phthalocyanine emission spectrum remained unchanged. In theory, the observed quenching of the phthalocyanine emission in the phthalocyanine-TTF hybrids occurs via a simple electron transfer process, from the TTF to the HOMO of the previously ground state phthalocyanine (Scheme 5.1, Route A).

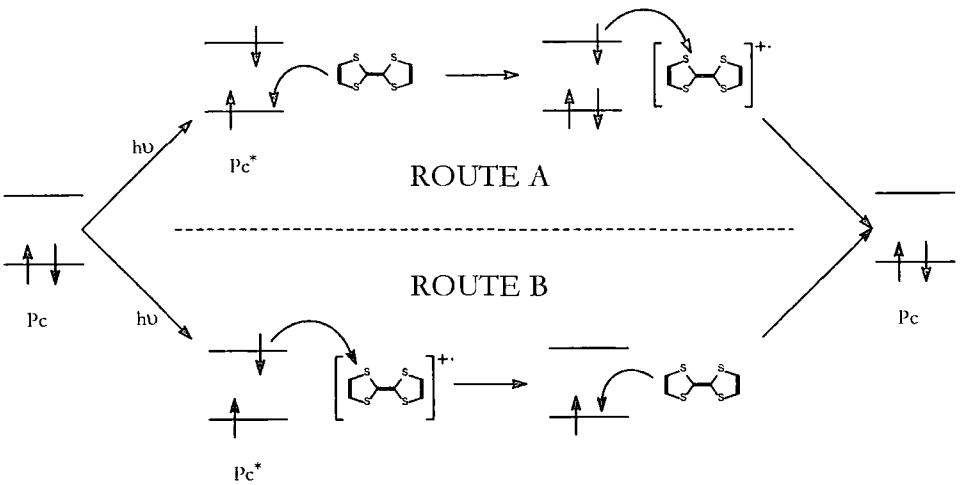

Scheme 5.1 Electron transfer process between phthalocyanine and TTF species. Route A shows the 'normal' quenching by TTF, involving donation of an electron from the TTF quencher to the phthalocyanine (Pc) excited state. Route B shows the reversed process in the presence of $TTF^{+\bullet}$, involving donation of an electron *to* the quencher *by* the phthalocyanine excited state.

Calculations based on Rehm-Weller theory[30] for electron transfer predict this to be a thermodynamically feasible process, both inter- and intramolecularly, and this is reflected in the observed and calculated rate constants (Table 5.2; Rehm-Weller theory and its application to silicon phthalocyanines is discussed in full in the previous chapter). Photoexcitation of the phthalocyanine increases its acceptor strength by an amount equal to the excitation energy (in this case 1.81 eV) and hence electron transfer from TTF to Pc* proceeds readily and results in emission quenching. However, this increase in phthalocyanine acceptor strength upon excitation is accompanied by an equal increase in *donor* strength, and so Pc* can readily donate electrons to electron deficient species. The TTF radical cation is just such an electron deficient species, and hence there exists a new, *reversed*, electron transfer path, from Pc* to $TTF^{+\bullet}$ (Scheme 5.1, Route B). Thus oxidation of TTF in the phthalocyanine-TTF hybrids does not result in the

increase of fluorescence (reduction of quenching) initially predicted, and the Rehm-Weller calculations concur, yielding a rate constant of quenching for this reverse process of 1.26 $dm^3 mol^{-1} s^{-1}$. A similar phenomenon was recently observed involving quenching of anthracene fluorescence by tetrathiafulvalene, although the results were not specifically interpreted in terms of a reversal of electron transfer.[31]

Table 5.2 Rehm-Weller calculations for phthalocyanine tetrathiafulvalene electron transfer processes.

Acceptor (E_{A/A^-} / V)	Donor ($E_{D^+/D}$ / V)	a [a] (nm)	ΔG (kJ mol^{-1})	ΔG# (kJ mol^{-1})	k_Q (calc.) [b] ($dm^3 mol^{-1} s^{-1}$)	k_Q (expt) [c] ($dm^3 mol^{-1} s^{-1}$)
Pc (-0.69)	TTF (+0.59)	1	-66.4	1.47	1.14×10^{10}	1.6×10^{10}
		0.34	-96.1	1.03	1.20×10^{10}	-
$TTF^{+\bullet}$ (+0.59)	Pc (+1.04)	0.34	-176	0.57	1.26×10^{10}	-

[a] encounter distance – 1 nm for an intermolecular process, 0.34 nm for an intramolecular process (calculated via models generated in CAChe); [b] rate constant for quenching of phthalocyanine emission by TTF obtained via Rehm-Weller calculations; [c] obtained via a Stern-Volmer plot.

With one exception, all of the phthalocyanine-TTF hybrids discussed in this chapter shows identical behaviour, that is, no change in the extent of quenching upon oxidation of the TTF moiety. Compound **4** however, with its highly flexible linker, displays an unusual difference - a *decrease* in emission intensity upon oxidation of the TTF units (Figure 5.8). This in fact concurs with behaviour seen for the previously mentioned anthracene-TTF systems[31] where oxidation yielded stronger quenching, explained as being due to increased binding between π-rich anthracene and π-deficient $TTF^{+\bullet}$ units. It is suggested that oxidation results in increased phthalocyanine-TTF interaction, and with the flexible axial ligands in **4** the fluorophore-quencher separation distance is reduced, allowing enhanced quenching by electron transfer from the phthalocyanine to the electron poor $TTF^{+\bullet}$.

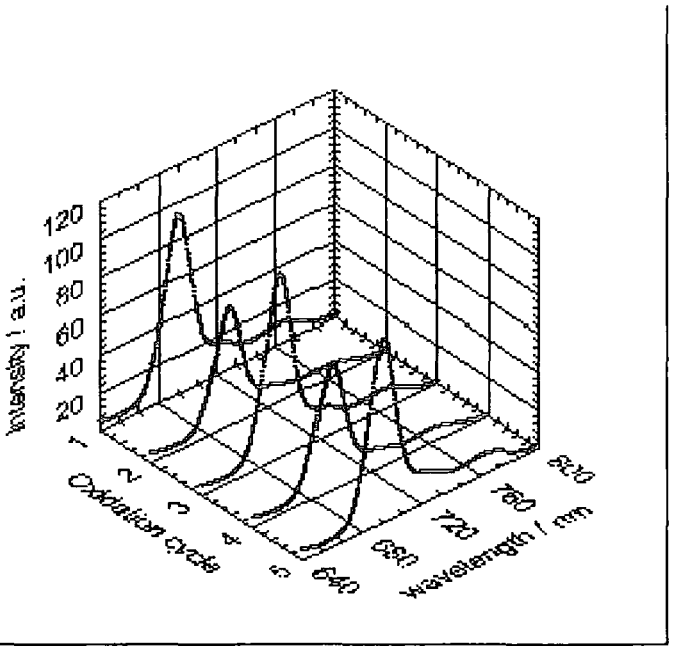

Figure 5.8 Emission spectra of **4** with cycled oxidation potential. (1) 0.0 V, (2) 0.6 V, (3) 0.0 V, (4) 0.6 V and (5) 0.0 V applied potential.

5.4 Conclusions

The photophysics of a number of new axially substituted silicon phthalocyanines containing the tetrathiafulvalene (TTF) functionality have been studied.[14] The extent of quenching by electron transfer from the electron rich TTF to the phthalocyanines is shown to depend strongly upon the flexibility and substitution pattern of the TTF containing axial substituent - removal of the rigid benzoate moiety from the axial ligand allows strong quenching, and a fluorescence quantum yield of <0.006 results. Oxidation and reduction of the bis(4-*tert*-butyl)benzoate reference compound results in the expected spectral changes indicative of the formation of cation and anion radicals of the phthalocyanine ring. The oxidation potentials of phthalocyanine and TTF allow the selective oxidation of the TTF moiety in the phthalocyanine-TTF hybrids, but the expected reduction in quenching was not observed. This is due to a facile *reversal* of the electron transfer direction, such that it occurs from phthalocyanine to $TTF^{+\bullet}$ in the oxidised species. The most flexible compound shows an *increase* in quenching upon oxidation, due to the enhanced interaction between the fluorophore and quencher, resulting in a reduced separation distance.

5.5 References

1 F. Wudl, D. Wobschall and E. J. Hufnagel, Electrical conductivity by the bis-1,3-dithiole-bis-1,3-dithiolium system, *J. Am. Chem. Soc.*, 1972, **94**, 670.

2 J. Ferraris, D. O. Cowan, V. V. Walatka and J. H. Perlstein, Electron transfer in a new highly conducting donor-acceptor complex, *J. Am. Chem. Soc.*, 1973, **95**, 948.

3 A. M. Kini, U. Geiser, H. H. Wang, K. D. Carlson, J. M. Williams, W. K. Kwok, K. G. Vandervoot, J. E. Thompson, D. L. Stupka, D. Jung and M.-H. Whangbo, A new ambient-pressure organic superconductor, κ-$(ET)_2Cu[N(CN)_2]Br$, with the highest transition temperature yet observed (inductive onset T_c = 11.6K, resistive onset = 12.5K), *Inorg. Chem.*, 1990, **29**, 2555.

4 (a) G. Schukat and E. Fanghänel, *Sulfur Rep.*, 1993, **13**, 254; (b) M. R. Bryce, Current trends in tetrathiafulvalene chemistry: towards increased dimensionality, *J. Mater. Chem.*, 1995, **5**, 1481; (c) M. R. Bryce, Tetrathiafulvalenes as π-electron donors for intramolecular charge-transfer materials, *Adv. Mater.*, 1999, **11**, 11.

5 M. R. Bryce, W. Devonport, L. M. Goldenberg and C. Wang, Macromolecular tetrathiafulvalene chemistry, *Chem. Commun.*, 1998, 945.

6 S. Hünig, G. Kiesslich, H. Quast and D. Scheutzow, Two-step redox systems. X. Tetrathioethylenes and their higher oxidation levels, *Liebigs Ann. Chem.*, 1973, 310.

7 P. R. Ashton, V. Balzani, J. Becher, A. Credi, M. C. T. Fyfe, G. Mattersteig, S. Menzer, M. B. Nielsen, F. M. Raymo, J. F. Stoddart, M. Venturi and D. J. Williams, A three-pole supramolecular switch, *J. Am. Chem. Soc.*, 1999, **121**, 3951.

8 M. A. Blower, M. R. Bryce and W. Devonport, Synthesis and aggregation of a phthalocyanine symmetrically-functionalized with eight tetrathiafulvalene units, *Adv. Mater.*, 1996, **8**, 63.

9 C. Wang, M. R. Bryce, A. S. Batsanov, C. F. Stanley, A. Beeby and J. A. K. Howard, Synthesis, spectroscopy and electrochemistry of phthalocyanine derivatives

functionalised with four and eight peripheral tetrathiafulvalene units, *J. Chem. Soc., Perkin Trans. 2*, 1997, 1671.

10 M.Kasha, H.R.Rawls and M.A.El-Bayoumi, The Exciton Model in molecular spectroscopy, *Pure Appl.Chem.*, 1965, **11**, 371.

11 M.J.Stillman and T.Nyokong in *Phthalocyanines – Properties and Applications, Vol.1*, Eds. C.C.Leznoff and A.B.P.Lever, VCH Publishers, Inc., New York, 1989.

12 C.F.Stanley, *Photophysical evaluation of substituted zinc phthalocyanines as sensitisers for photodynamic therapy*, Ph.D. Thesis, University of Durham, 1997.

13 M. J. Cook, G. Cooke and A. Jafari-Fini, A liquid crystalline tetrathiafulvalenephthalocyanine, *Chem. Commun.*, 1996, 1925.

14 C. Farren, C. A. Christensen, S. FitzGerald, A. Beeby and M. R. Bryce, Synthesis of novel phthalocyanine-tetrathiafulvalene hybrids; intramolecular fluorescence quenching related to molecular geometry, *J. Org. Chem.*, submitted April 2002.

15 C. Farren, S. FitzGerald, M. R. Bryce, A. Beeby and A. S. Batsanov, Synthesis, structure and optical characterisation of silicon phthalocyanine bis-esters, *J. Chem. Soc., Perkin Trans. 2*, 2002, 59.

16 C. C. Leznoff and A. B. P. Lever (Eds.), *Phthalocyanines – Properties and Applications*, VCH Publishers, Inc., New York, (a) Volume 1, 1989 (b) Volume 2, 1993 (c) Volume 3, 1994, (d) Volume 4, 1996.

17 H. Greenspan and E. Fischer, Viscosity of glass-forming solvent mixtures at low temperature, *J. Phys. Chem.*, 1965, **69**, 2466.

18 J. B. Torrance, B. A. Scott, B. Welber, F. B. Kaufman and P. E. Seiden, Optical properties of the radical cation tetrathiafulvalenium (TTF^+) in its mixed-valence and monovalence halide salts, *Phys. Rev. B*, 1979, **19**, 730.

19 J. Otsuki, K. Harada and K. Araki, Supramolecular electro- and proto-photoswitch, *Chem. Lett.*, 1999, 269.

20 D. R. Reddy and B. G. Maiya, A molecular photoswitch based on an 'axial-bonding' type phosphorus (V) porphyrin, *Chem. Commun.*, 2001, 117.

21 V. Goulle, A. Harriman and J.-M. Lehn, An electro-photoswitch: redox switching of the luminescence of a bipyridine metal complex, *J. Chem. Soc., Chem. Commun.*, 1993, 1034.

22 P. Day, Future molecular electronics, *Chem. Br.*, 1990, **26**, 52.

23 P. A. Christensen and A. Hammett, *Techniques and mechanisms in electrochemistry*, Blackie Academic and Professional, Glasgow, 1994.

24 J. Mack and M. J. Stillman, Photochemical formation of the anion radical of zinc phthalocyanine and analysis of the absorption and magnetic circular dichroism spectral data. Assignment of the optical spectrum of $[ZnPc(-3)]^-$, *J. Am. Chem. Soc.*, 1994, **116**, 1292.

25 D. W. Clack and J. R. Yandle, Electronic spectra of the negative ions of some metal phthalocyanines, *Inorg. Chem.*, 1972, **11**, 1738.

26 J. Mack and M. J. Stillman, Assignment of the optical spectra of metal phthalocyanine anions, *Inorg. Chem.*, 1997, **36**, 413.

27 T. Nyokong, Z. Gasyna and M. J. Stillman, Phthalocyanine π-cation-radical species: photochemical and electrochemical preparation of $[ZnPc(-1)]^{\bullet+}$ in solution, *Inorg. Chem.*, 1987, **26**, 548.

28 E. Ough, Z. Gasyna and M. J. Stillman, Photochemical, electrochemical, and chemical formation of the π-cation-radical species of magnesium phthalocyanine. Analysis of the absorption and MCD spectra of $[MgPc(-1)]^{\bullet+}$, *Inorg. Chem.*, 1991, **30**, 2301.

29 V. Khodorkovsky, L. Shapiro, P. Krief, A. Shames, G. Mabon, A. Gorgues and M. Giffard, Do π-dimers of tetrathiafulvalene cation radicals really exist at room temperature, *Chem. Commun.*, 2001, 2736.

30 D. Rehm and A. Weller, Kinetics of fluorescence quenching by electron and H-atom transfer, *Israel J. Chem.*, 1970, **8**, 259.

31 H. Augiers de Cremiers, G. Clavier, F. Ilhan, G. Cooke and V. M. Rotello, Tuneable electrochemical interactions between polystyrenes with anthracenyl and tetrathiafulvalenyl sidechains, *Chem. Commun.*, 2001, 2232.

Chapter 6

The Photophysics of Fluorescent Phthalocyanine Dimers

6.1 Introduction

Phthalocyanines have a rich and diverse chemistry,[1] and their propensity to form aggregates is well known. The spectroscopic behaviour of phthalocyanine dimers and higher aggregates is of considerable interest both as a study of the fundamental spectroscopy of the compounds and from an industrial point of view, where aggregation can lead to changes in the colour/appearance of a dyestuff, and loss of efficacy in therapeutic agents.[2]

Kasha's Exciton Theory[3] predicts that the spectroscopic behaviour of macrocycle aggregates depends strongly upon the relative geometry of the rings, and hence a wide range of behaviour is to be expected (discussed more fully in Chapter 1, Section 1.4.1). This is equally true for phthalocyanines, and the most commonly encountered interaction is when the two adjacent phthalocyanines are in a slipped co-facial conformation, where, depending upon the degree of slippage, such an aggregate can exhibit either blue or red shifted absorption. Most aggregates described to date are of the blue shifted type, and selection rules are such that these species are non-fluorescent. Another possible geometry is the clamshell arrangement, whereby the phthalocyanine molecules are no longer parallel. The selection rules are relaxed for such aggregates and both red and blue shifted absorption bands are predicted, and emission (red shifted) is not categorically excluded. However, although theoretically predicted, actual examples of fluorescent phthalocyanine dimers are exceedingly rare.

Most initial reports of fluorescent dimers have since been demonstrated to arise from artefacts. For example, a report of red shifted absorption and emission bands in a tetrasulfonated aluminium phthalocyanine suggested to be a result of a slipped face-to-face dimer[4] was later reinterpreted as effects of reabsorption.[5] Similarly, spectral characteristics assigned to a novel dimer of tetrasulfonated zinc phthalocyanine[6] have since been shown to arise from ring protonation[7] - this particular case is discussed more fully in Chapter 3.

Binuclear systems have been demonstrated to show genuine fluorescence from exciton coupled rings, fluorescence which is strongly red shifted as theory[3] predicts. For example, at 77 K certain metal free binuclears displayed a weak band centred at 750 nm.[8] The strongest emission was observed for a neopentoxy peripherally substituted compound, with an O-CH_2-C(Me)(Et)-CH_2-O linker, and was attributed to a

dimer with an oblique or clamshell conformation. Silicon phthalocyanine dimers containing μ-oxo bridges allow much stronger interaction between the macrocycles, and certain of these species have been reported to exhibit weak emission in the near infra-red region. One such compound with octa-alkoxy substituents was shown[9] to have a dimer emission quantum yield of just 10^{-3}. Hybrid dimers containing germanium and tin in addition to silicon behave similarly.[10]

Despite these reports of *binuclear* species showing fluorescence from exciton coupled rings, examples of genuine *mononuclear* compounds showing such emission are extremely rare. The principal example involves the 1,4,8,11,15,18,22,25-octadecylated zinc phthalocyanine C10, which showed unusual aggregation behaviour at low temperature.[11] Lowering the temperature to 77 K resulted in five peaks appearing in the absorption spectrum (relative to the single Q band at 293 K) and the change was reversed by raising the temperature. Increasing the concentration of C10 resulted in increased structure at low temperature, in particular, the central 693 nm peak was seen to increase in intensity dramatically. The length of the peripheral substituents was critical – methyl groups instead of decyl showed small effect when the temperature was lowered, whilst butoxy ligands showed no change whatsoever, despite being isoelectronic with pentyl ligands which showed a definite spectral change with temperature. The emission spectrum also showed temperature dependence, with the appearance at low temperature of an additional peak to the red of the normal monomer emission band. Again, increase in C10 concentration resulted in increased intensity of the red shifted band. Excitation studies showed the two emission peaks to arise from different emitting species with the normal monomer emission (at 718 nm) originating from the monomer absorption peak at 698 nm, which showed definite splitting into x and y components at low temperature. The red shifted emission peak (centred at 760 nm) was shown to originate from the five peaked low temperature absorption profile. The strange splitting of the monomer band at low temperature was assigned to interactions between the alkyl chains reducing the symmetry of the molecule. It was tentatively suggested that exciton coupling of the monomer units results in a splitting of the energy level into five equally spaced levels, E_1-E_5, thus explaining the presence of five dimer absorption bands, but only one dimer emission peak (760 nm). Absorption to any of the five levels would, as stipulated by Kasha's Rule,[12] result in emission from

the lowest level only. No definitive explanation of this five-fold splitting was given, although similar behaviour has also been observed for a binuclear silicon species.[13]

The dimer emission of C10 was reported to have a quantum yield of 0.35 relative to that of the monomer, and the fluorescence lifetime showed a fractional decrease relative to that of the monomer at the same temperature. Time resolved nanosecond flash photolysis of the fluorescent dimers showed complex behaviour, particularly in cold, fluid solution, and evidence was presented for disaggregation of the dimers upon absorption of excitation light at intermediate temperatures.

This current work investigates the behaviour of a family of zinc phthalocyanines based upon a solketal substituted compound, all of which exhibit emission due to dimer species with clamshell conformations. Detailed time resolved studies reveal complex behaviour of these dimers following absorption of excitation light.

6.2 Experimental

The syntheses of tetra-(±)-2,2-dimethyl-1,3-dioxane-4-methanol (solketal) substituted phthalocyanine, **1**, and tetra-neopentoxy zinc phthalocyanine, **2**, are described elsewhere.[14,15] Acid catalysed hydrolysis of **1** to the derived octa-alcohol followed by treatment with an excess of acid chloride allowed the preparation of compounds **3**, **4** and **5**, for which full preparative and characterisation details have recently been reported.[16] Dr Chris Farren is thanked for the synthesis of all these compounds.

6.3 Results and Discussion

6.3.1 Steady State Spectroscopy

The solketal substituted phthalocyanine **1** (Figure 6.1) shows a strong susceptibility to aggregation, and at room temperature deviates from the Beer-Lambert equation throughout the concentration range 10^{-4}-10^{-7} mol dm^{-3} (Figure 6.2). Spectral evidence for aggregation at high concentrations is not unusual for phthalocyanines, but the particular strength with which this phenomenon occurs in solutions of **1** is unusual - behaviour of **1** at room temperature is otherwise typical for a zinc phthalocyanine (Table 6.1). A very dilute solution (5 x 10^{-8} mol dm^{-3}) of **1** at room temperature shows an absorption spectrum typical of a monomeric phthalocyanine. Assuming that at low temperature there are only two species present, the major being aggregated

phthalocyanine, the minor the monomeric species, it is possible to determine the absorption spectrum of the aggregate by subtraction of a fraction of the monomeric spectrum from spectra observed at high concentrations (10^{-4} mol dm^{-3}). Spectral decomposition in this fashion allows the calculation of the pure monomer and dimer extinction coefficients, and these take values of 1.1 x 10^5 dm^3 mol^{-1} cm^{-1} and 4.5 x 10^4 dm^3 mol^{-1} cm^{-1}. Further treatment of these data, as described by Wilkinson *et al.*[17] using a simple fitting routine, yields a value for the equilibrium constant, K_D, of 1.8 x 10^6 dm^3 mol^{-1} at room temperature. However, changes in spectral profile and extinction coefficients upon cooling preclude the extension of this technique to determine K_D at low temperature.

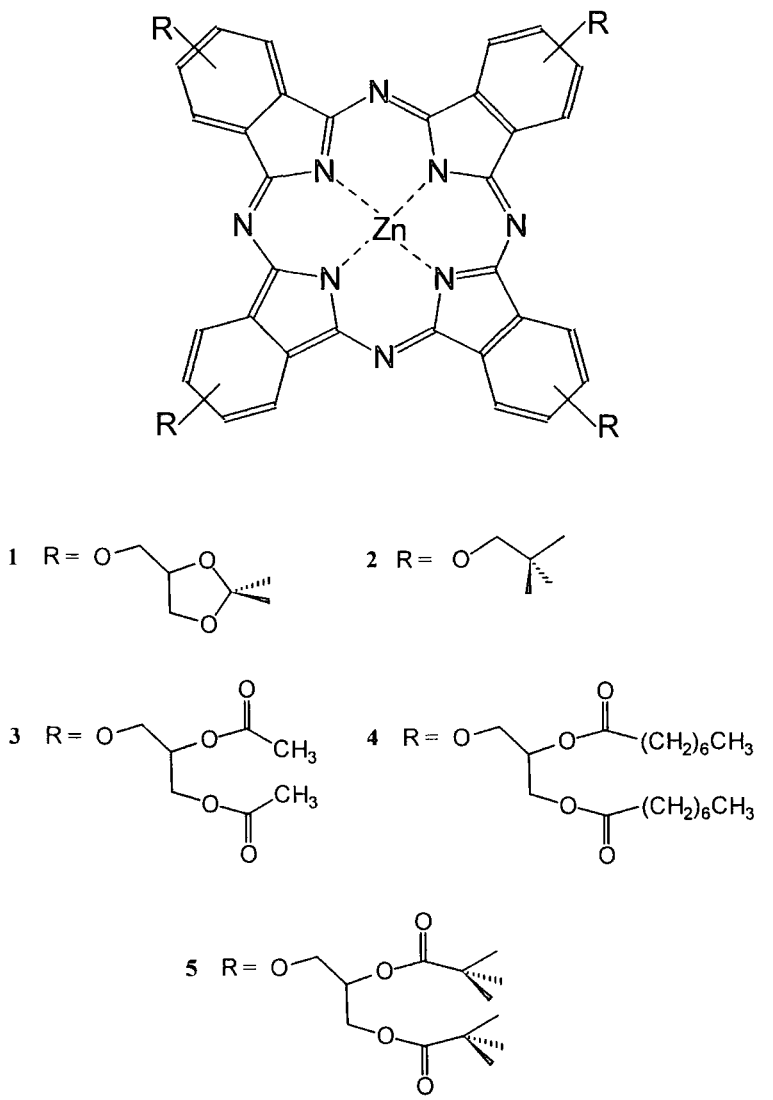

Figure 6.1 Structures of zinc phthalocyanines **1-5**.

Table 6.1 Photophysical data for zinc phthalocyanines **1-5**.

	λ_{max} / nm [a,c] (absorbance)	λ_{max} / nm [a,c] (emission)	Φ_f (±10%) [a,c]	τ ±0.1/ ns [d] (yield)	$I_f^{750nm} : I_f^{690nm}$ [b,d]
1	680	691	0.28	3.5 (100%) [a,e] 3.5 (100%) [a,f] 3.7 (96%), 1.6 (4%) [b,e] 4.2 (85%), 2.4 (15%) [b,f]	1.7
2	682	686	0.30	3.1 (100%) [a,c,e]	-
3	679	691	0.32	3.5 (100%) [a,e] 3.5 (100%) [a,f] 3.8 (93%), 2.2 (7%) [b,e] 4.8 (31%), 3.0 (69%) [b,f]	3.0
4	679	691	0.32	3.5 (100%) [a,e] 3.5 (100%) [a,f] 3.7 (100%) [b,e] 4.3 (50%), 2.9 (50%) [b,f]	7.0
5	679	691	0.26	3.4 (100%) [a,e] 3.4 (100%) [a,f] 3.6 (100%) [b,e] 4.6 (37%), 3.1 (63%) [b,f]	0.6

[a] 293 K; [b] 77 K; [c] dichloromethane; [d] EPA (5:5:2 v/v/v diethylether/2-methylbutane/ethanol); [e] λ_{em}=680 nm; [f] λ_{em}=750 nm. Concentrations throughout were ~1x10^{-6} mol dm^{-3}

On cooling the solution to an optically transparent glass, the extent of aggregation increases greatly, as evidenced by the reduction of monomeric Q band absorption at 675 nm and concomitant growth of a new absorption band centred at 625 nm but tailing into the near infra red (Figure 6.3A). Below the freezing point of the solution (140 K),[18] little further change to the spectrum is observed with the exception of slight band sharpening.

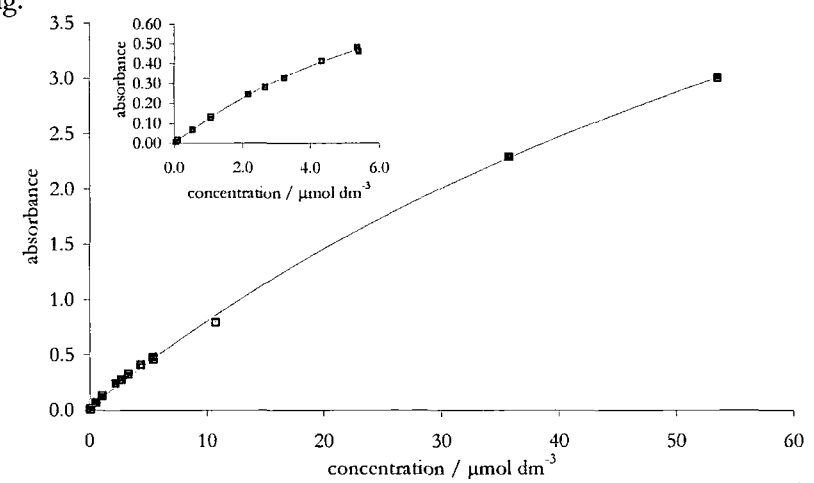

Figure 6.2 Beer-Lambert plot for **1** at 293 K, in range 0-60 μmol dm^{-3}. Inset: expanded range, 0-6 μmol dm^{-3}.

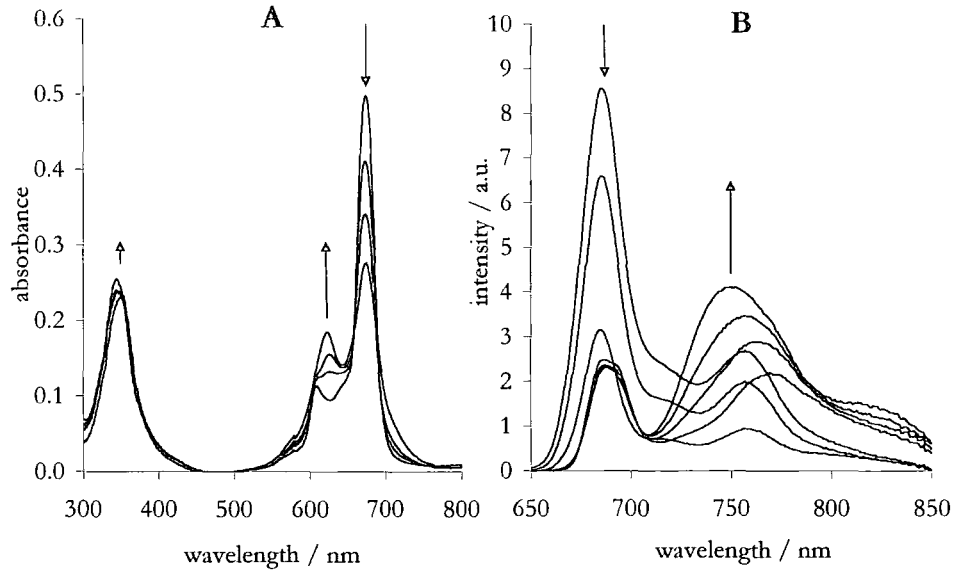

Figure 6.3 (A) Absorption and (B) emission spectra of **1** in EPA with varied temperature. Arrows indicate changes in absorbance/intensity in the direction 293 K→77 K.

At room temperature **1** shows the characteristic emission spectrum of a metallophthalocyanine, with Q band λ_{max} = 691 nm (Table 6.1). As the temperature is lowered, the emission intensity centred at 685 nm decreases, and below the glass transition temperature of the solvent a new red shifted peak is observed, $\lambda_{max} \approx 750$ nm, its intensity continuing to grow as the temperature is decreased to 77 K (Figure 6.3B). Excitation spectra for these two bands obtained with λ_{em} = 850 nm and λ_{em} = 710 nm, respectively, indicate the two emission bands arise from different species. The latter is typical of monomeric phthalocyanine with a clearly defined Q band profile, whilst the former shows the broadening and strong absorbance at 625 nm typical of an aggregated phthalocyanine species.

The tetra-neopentoxy zinc phthalocyanine **2** shows superficial structural similarities to **1**, and Table 1 shows that at room temperature the photophysical properties of **2** are also similar. However, as seen in the absorption spectrum (Figure 6.4A), cooling of a solution containing **2** results in no apparent aggregation, the only observation upon cooling is a sharpening of the absorption peaks. Such sharpening is also observed in the emission spectrum (Figure 6.4B), and the lack of any red shifted emission at 77 K is notable. This provides clear evidence that **2** does not undergo aggregation, even at low temperature, and for this reason **2** is used in this work as a non-aggregating reference compound.

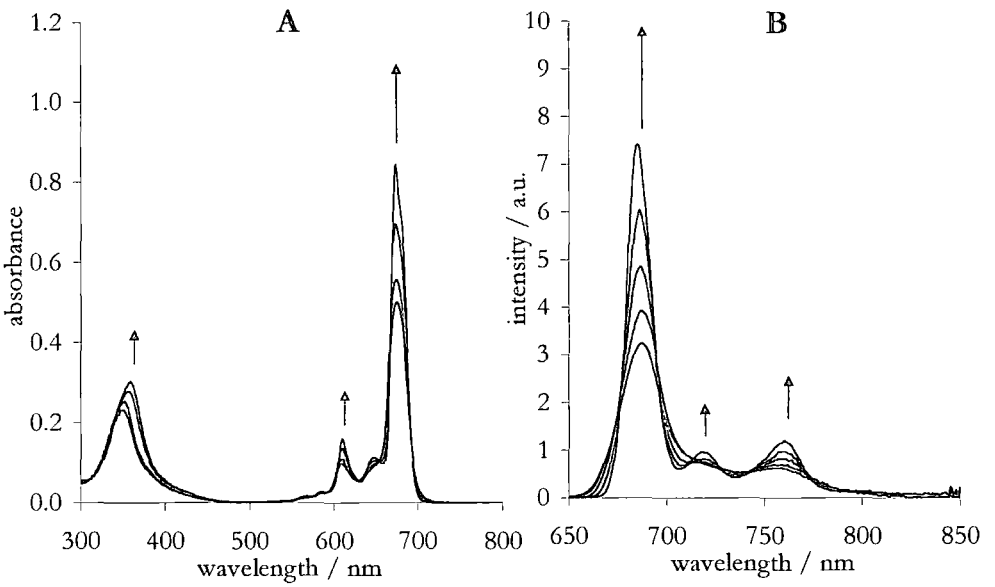

Figure 6.4 (A) Absorption and (B) emission spectra of **2** in EPA with varied temperature. Arrows indicate changes in absorbance/intensity in the direction 293 K→77 K.

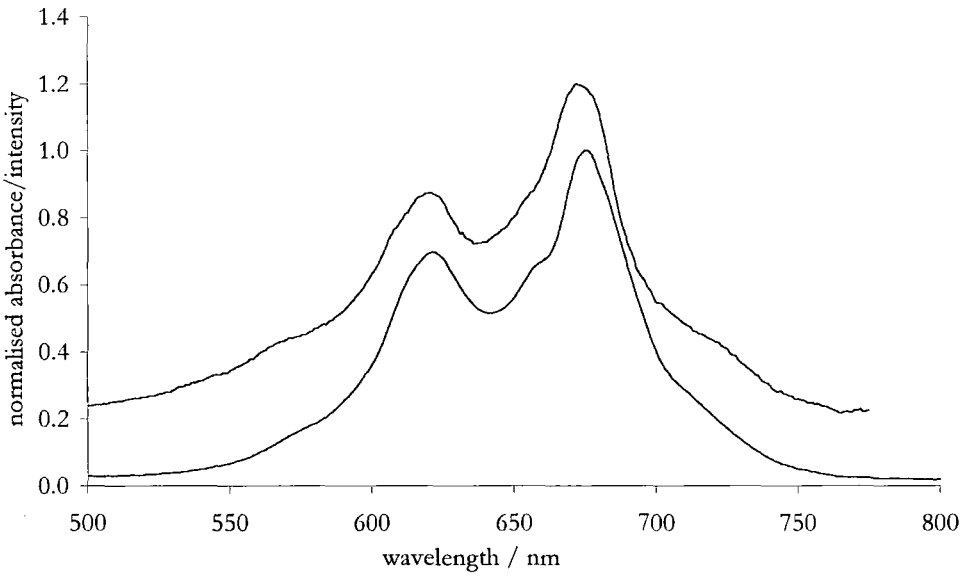

Figure 6.5 Absorption and excitation spectra of **1** in EPA at 77 K, λ_{em} = 850 nm. The excitation spectrum is offset for clarity.

Comparison of the absorption spectrum of **1** obtained at 77 K with the excitation spectrum of the red shifted emission band (Figure 6.5), obtained with λ_{em} = 850 nm (at which wavelength contribution from monomeric **1** becomes negligible) shows excellent correlation. This match provides good evidence that greater than 95% of **1** exists as dimer at low temperature.

The method of spectral subtraction discussed above can also be used to calculate the dimer quantum yield relative to that of the monomer.[11] The individual absorbances due to the monomer and dimer species at the excitation wavelength can be calculated, and with integration of the resulting emission spectrum between 640-715 nm and 716-800 nm (corresponding to monomer and dimer emission respectively) it is possible to construct emission *vs* absorbance graphs for the monomer and dimer species. The gradients of these graphs are proportional to the fluorescence quantum yield of each species. For **1** Φ_{dimer} was found to be $0.4\Phi_{monomer}$ at 77 K (Figure 6.6), which agrees well with the ratio of 0.35 obtained for the octadecyl zinc phthalocyanine, C10.[11]

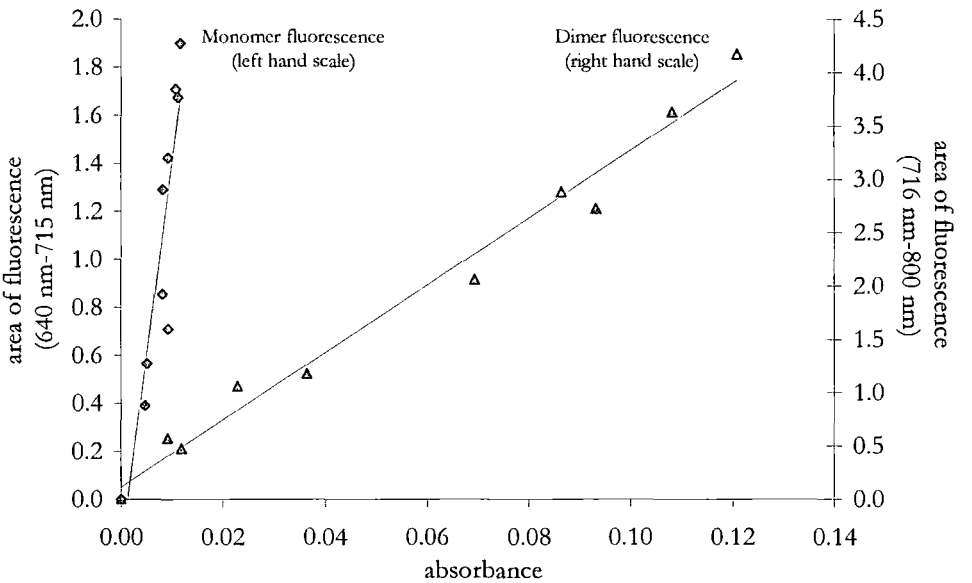

Figure 6.6 Emission intensity *vs* absorbance due to monomer and dimer species of **1** at 77 K.

Compounds **3**-**5** (Figure 6.1) show room temperature behaviour which is comparable with that of **1** and other zinc phthalocyanines (see Table 6.1). As with **1** these materials show spectra characteristic of the monomeric phthalocyanine at room temperature whilst below 140 K unusual behaviour is observed. Figure 6.7 shows the change of absorption and emission spectra for **4** - once again the absorption spectrum shows extensive changes upon cooling to 140 K, but thereafter only minimal perturbation to the spectral profile is observed. Conversely, the red shifted emission peak attributed to dimer species only becomes significant *below* 140 K.

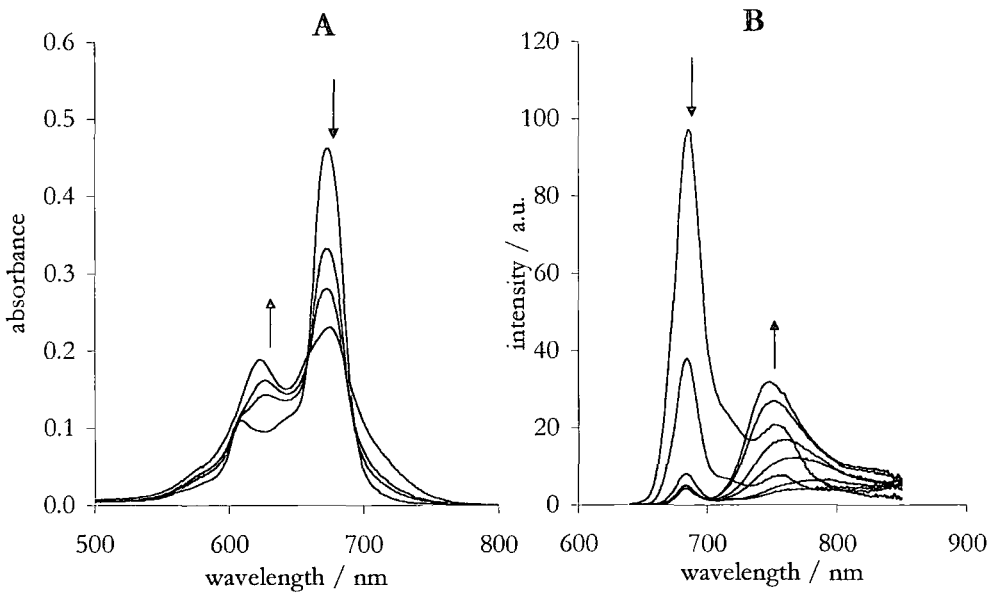

Figure 6.7 (A) Absorption and (B) emission spectra of **4** in EPA with varied temperature. Arrows indicate changes in absorbance/intensity in the direction 293 K→77 K.

With all these compounds (**1**, **3**-**5**) which exhibit dimmer formation there remains at 77 K a small contribution of monomer emission, and comparison of the ratio of dimer ($\lambda_{max} \approx 750$ nm) to monomer ($\lambda_{max} \approx 690$ nm) emission intensities affords an idea of the extent of aggregation in the compounds. The parent compound **1** shows a ratio of 1.7, whilst **3**, with altered peripheral substituent, shows an increased dimer to monomer emission ratio of 3.0. The emission ratio of 7.0 for compound **4** is larger still, perhaps due to enhancement of aggregation through interdigitation of the alkyl chains (such behaviour has been observed for aromatic molecules in the solid state[19]). Conversely, a reduced ratio of 0.6 is observed for compound **5** with *tert*-butyl groups at the periphery, most likely a result of the increased bulk of the substituents preventing close interaction of the macrocycle rings. The lifetimes observed for compounds **1** and **3**-**5** in monomer and dimer form are all similar (see below), and this confirms that the changes in relative emission ratios are not due to changes in lifetimes of the compounds.

As with **1** the excitation spectra (recorded for the red shifted emission) and low temperature absorption spectra of compounds **3**-**5** are closely matched. They indicate, for all the fluorescent dimers, that the emitting species possesses both blue and red shifted absorption, indicating the dimers to be of a clamshell conformation. Exciton Theory[3] predicts red shifted absorption and emission for a parallel, co-facial

conformation - however if the phthalocyanine rings become angled the distinction between the exciton levels becomes blurred and both red and blue shifted absorption is observed. Since the transition to and from the lower level is no longer formally forbidden red shifted fluorescence can be observed for a dimer with a clamshell conformation. Figure 6.8 shows the excellent agreement between excitation and absorption spectra for **4** and **5**.

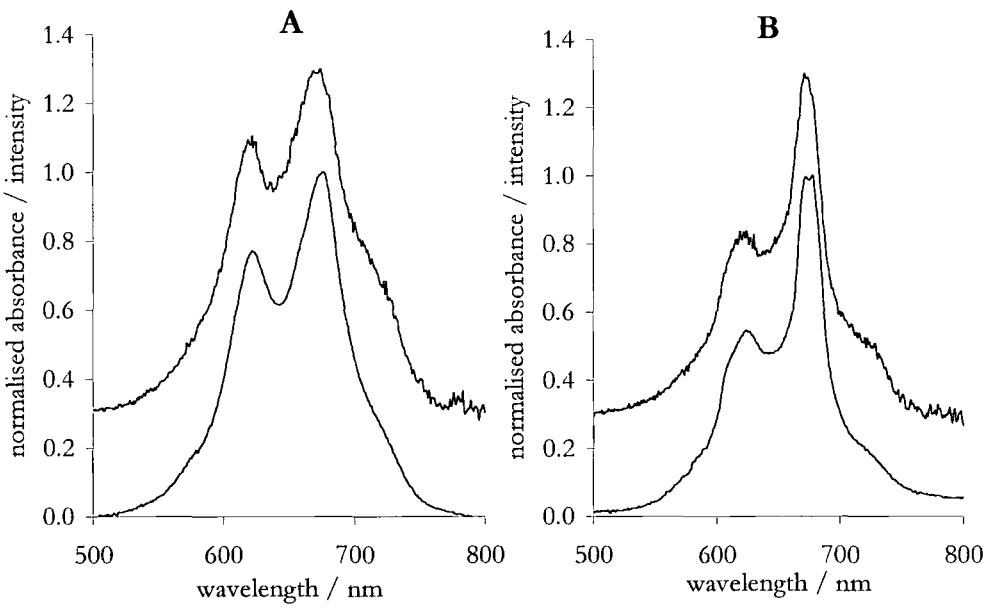

Figure 6.8 Absorption and excitation spectra of (A) **4** and (B) **5** in EPA at 77 K, λ_{em} = 850 nm. The excitation spectra are offset for clarity.

The precise mechanism for aggregation in these unusual systems is currently not understood, but it is interesting to note that Tai and Hayashi[20] saw similar propensity for aggregation in novel naphthalocyanines containing four peripheral alkoxycarbonyl substituents. The alkoxycarbonyl substituted species were observed to have a much stronger tendency for aggregation than was seen for related alkyl and alkoxy substituted naphthalocyanines - sadly no fluorescence studies were carried out so the possibility of fluorescent aggregrates was not addressed. The increased aggregation was attributed to possible steric effects of the substituents binding to the macrocyclic ring or to an electronic inductive effect of the substituent. The structural similarity between these naphthalocyanines and compounds **3**-**5** is striking, and it is likely that the behaviour in both cases is due to a related mechanism of aggregation.

The characteristics of the emission observed for the dimer species discussed here are similar to those observed both by Leznoff and Lever in their metal free binuclear

species,[8] and by Stanley with mononuclear octadecyl substituted phthalocyanine.[11] In these cases the emissive species was hypothesised to be of a clamshell orientation, and the present work concurs with these conclusions.

6.3.2 Fluorescence Lifetimes

The fluorescence lifetime of reference compound **2** recorded at either 293 K or 77 K is typical of a zinc phthalocyanine (Table 6.1). Lifetimes for **1** and **3**-**5**, monitored at 680 nm (monomer) or 750 nm (dimer), show, at room temperature, no significant deviation from that of **2**. However, on cooling to 77 K values obtained by monitoring the red shifted 750 nm emission become more complex, whilst the lifetimes of the residual monomer emission at 680 nm remain unchanged. A good fit using a single exponential model could not be achieved for the dimer lifetimes (that is, monitoring at 750 nm), but when fitted to a simple double exponential equation of the form $I(t) = A_1\exp(-t/\tau_1) + A_2\exp(-t/\tau_2)$ good fits were obtained, yielding two lifetimes, one larger and one smaller (or equal) to that of the monomer, in varying proportions (Table 6.1).

With the proposed clamshell arrangement of the phthalocyanine rings it is not unreasonable to assume there will exist a distribution of conformations, so that complex lifetime behaviour is not unexpected. As a result an alternative method of analysing the decay data was considered, making use of a Gaussian distribution of lifetimes controlled by τ_{av} and σ (corresponding to the average lifetime and the standard deviation of the distribution respectively).[21] The fluorescent lifetime distributions of the dimer species obtained by this method of analysis are broader (larger σ) and/or longer lived (larger τ_{av}) than those of monomer phthalocyanines.

Studies of α-substituted octasubstituted decyl zinc phthalocyanine showed a small *decrease* in lifetime for the dimer species, and this was rationalised to be a result of increased deactivation pathways available to the aggregate. However, the transition from a parallel co-facial conformation to that of a clamshell sees the lowest energy level (from which emission originates) become increasingly allowed - thus the allowed nature of the transition resulting in fluorescence will depend upon exact conformation. A partially forbidden transition would be expected to display an elevated lifetime, and thus the increase in lifetime observed for the compounds discussed herein is not unreasonable. Nonetheless, the behaviour is extremely complex and a simple explanation for the changes seen cannot be provided.

6.3.3 Laser Flash Photolysis

The technique of laser flash photolysis[22] allows the study of transient species on the nanosecond and sub-nanosecond timescale.[23] The short lived transient species are generated by an intense excitation pulse, the "flash", and subsequently monitored. The probe technique used for this work is that of white light absorption, allowing both transient absorption spectra and lifetimes to be obtained. Previous studies of phthalocyanines[1,10,24] using this technique have yielded some general results: the long lived species probed by this method is the triplet species, ^{3}Pc*, which has a broad, featureless absorption band across the visible region, with its maximum at ~480 nm. The triplet lifetime, τ_T, is of the order of 10^{-4} s in degassed solution at room temperature (this value being dependent on solvent and temperature), whilst the triplet-triplet absorption coefficient, ε_{TT}, typically takes values of the order of 18,000 to 36,000 $dm^3\ mol^{-1}\ cm^{-1}$.[25]

The transient spectrum of reference compound **2** clearly shows these generic characteristics (Figure 6.9). The transient difference spectrum features a broad triplet-triplet absorption, and, above 600 nm, the ground state bleach with its monomeric phthalocyanine profile, whilst the addition of a small fraction of the ground state absorption to this difference spectrum yields the total triplet-triplet absorption spectrum, in this case a structureless band stretching across the entire visible region. The value of 250 μs for the triplet lifetime τ_T at 293 K is in broad agreement with other studies,[24] and this value is independent of λ_{probe}. The reduction of relaxation pathways as a result of cooling the solution to 77 K results in an increased lifetime of 620 μs, and the monomer bleach shows considerably sharpening, agreeing with the observed changes in the ground state absorption spectrum. Intermediate lifetimes are observed at temperatures between 293 K and 77 K.

Table 6.2 Transient lifetimes for **1**-**5**. All data were recorded in EPA, λ_{ex} = 615 nm. Lifetimes τ_1-τ_3 relate to processes shown in Scheme 6.1 below.

	293 K		175 K			77 K
	τ_1 / μs	τ_2 / μs	τ_1 / μs	τ_2 / μs	τ_3 / μs	τ / μs
1	250	-	400	30	4	500
2	250	-	390	-	-	620
3	145	28	290	60	6	645
4	200	45	260	60	6	625
5	220	-	360	50	5	610

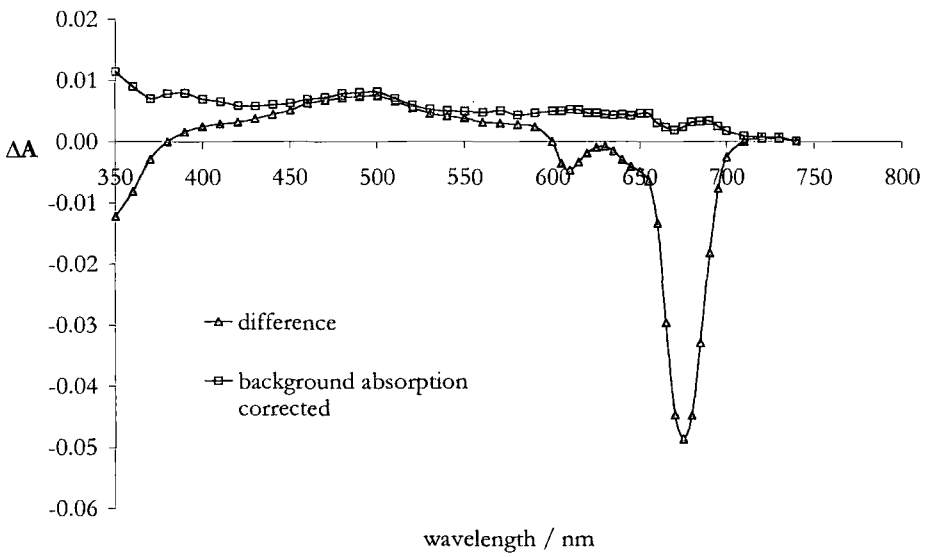

Figure 6.9 Difference and transient absorption spectra of **2** in EPA at 293 K (λ_{ex} = 615 nm).

The behaviour of **1** at room temperature is analagous to that of **2**, the triplet lifetime taking a value of 180 μs, and typical monomer bleach is visible (Figure 6.10A). At 77 K the triplet-triplet absorption remains similar to that of monomeric zinc phthalocyanine is observed, and a broadened bleach profile is also seen (Figure 6.10B). At this temperature the majority of the material is present as dimer which means the observed transient absorption arises from dimer phthalocyanine. The triplet state of rhodamine B has been shown to experience exciton splitting of less than 2 cm^{-1} upon aggregation,[26] so similarity in profile between the monomer and dimer transient absorption spectra observed here is not surprising. A previous study of μ-oxo silicon phthalocyanine dimers concurs with these findings.[13] The triplet lifetime of **1** at 77 K is

500 μs, showing a similar increase upon cooling to that observed for **2**. Below 600 nm the ground state absorption corrected transient spectrum shows little difference to that at room temperature, but in the phthalocyanine Q band region above this wavelength a strongly positive ΔA centred at 680 nm is visible (Figure 6.10B) - a feature not observed in the low temperature spectrum of **2**.

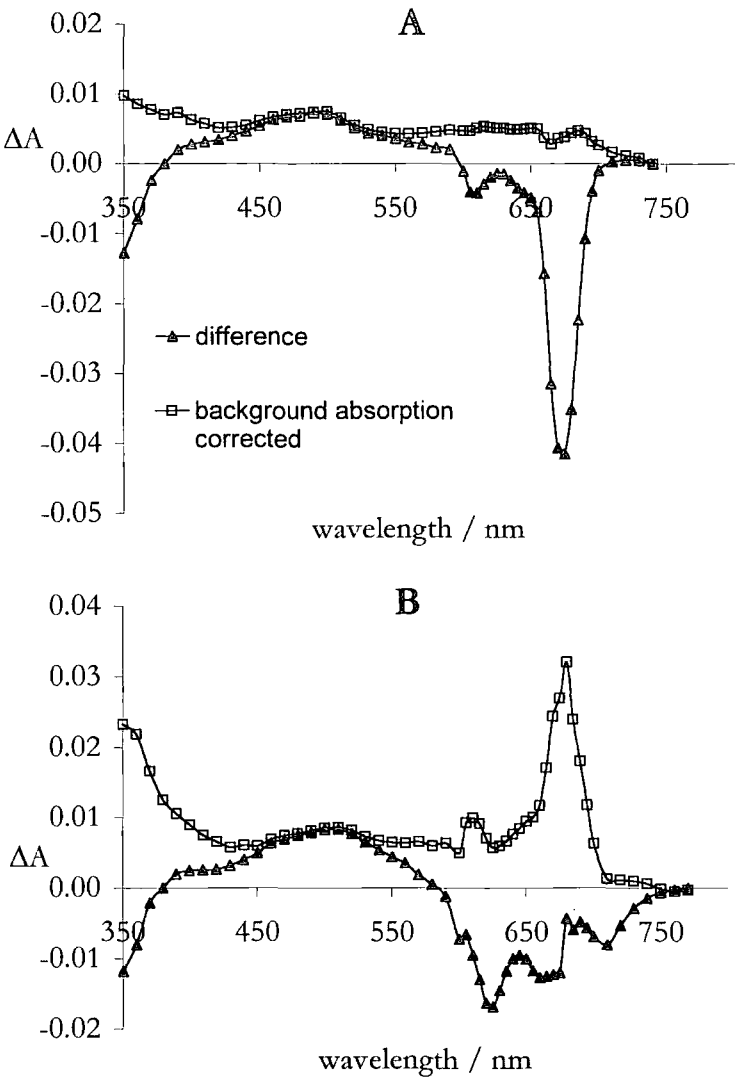

Figure 6.10 Difference and transient absorption spectra of **1** at (A) 293 K and (B) 77 K (λ_{ex} = 615 nm).

This feature coincides exactly in position and band shape with the monomeric ground state absorption of **1** (as observed at room temperature), and provides evidence for an additional deactivation pathway for the dimer, that is, disaggregation upon absorption of an exciting photon (see Scheme 6.1). Typically the energy imparted to a molecule by absorption of a photon gives rise to an electronically excited state - however, in this particular case, that energy can also result in fast separation of the

dimer to give the monomeric units. The resulting increase in absorption of ground state monomer is clearly seen in in the positive ΔA region of the graph. Whilst useful to be able to compare the relative yields of the monomer and triplet dimer species, it is not possible since the extinction coefficient, ε, is not known for the triplet dimmer state, nor for the monomer at 77 K. Establishing these data would require further work.

Thus there are two expected processes - triplet formation and dimer separation - and each has an associated decay pathway, depicted by $^3Pc^* \rightarrow {}^1Pc$ (τ_1) and $2\,{}^1Pc \rightarrow {}^1(Pc)_2$ (τ_3) respectively. However, throughout the spectrum, excellent fits can be achieved using just a single lifetime despite the presence of at least two processes. It may be that at this temperature the two rate constants k_1 and k_3 are comparable (and hence inseparable), or alternatively it is possible that the rigidity of the EPA glass prevents full diffusional separation and irradiation results in a 'dimer' with enlarged internuclear separation and an absorption spectrum representative of a monomeric species.

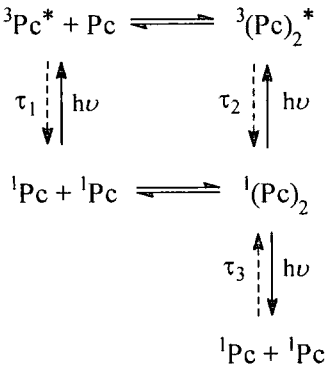

Scheme 6.1 Ground and excited state equilibria of **1**. Full arrows indicate photoexcited processes, whilst dashed arrows indicate relaxation pathways with rate constant $1/\tau_n$.

At temperatures between 77 K and 100 K the behaviour of **1** shows little change, but as the temperature is raised to, and above, the glass transition temperature of the solvent (~140 K)[11] diffusion becomes easier because of the reduced viscosity, and hence further complexities in the behaviour of the transient species become apparent. At 175 K adequate fits for decays obtained with λ_{probe} = 400–600 nm can be achieved using a model with just two lifetimes, but a third, much shorter, component becomes apparent above 600 nm. Analysis of the pre-exponential factors for the long lifetime component (τ_1) yields a bleach with a typical ground state monomeric phthalocyanine absorption profile, indicating τ_1 (with a value of 400 μs at this temperature) to be the

lifetime for the decay of excited triplet phthalocyanine to ground state monomer, $^3Pc^* \rightarrow {}^1Pc$. Compound **2** showed lifetimes of 650 μs and 250 μs at 77 K and 293 K respectively, and the value for τ_1 of 400 μs (for **1** at 175 K) lies inbetween these two extremes, as expected. The second component observable throughout the spectrum (τ_2) has a broadened dimer phthalocyanine bleach profile, with a faster decay (τ_2 = 30 μs) corresponding to the decay of triplet dimer to ground state dimer, $^3(Pc)_2^* \rightarrow {}^1(Pc)_2$.

Above 600 nm the third component becomes apparent, characterised by a positive pre-exponential factor; this spectral region is dominated by the *bleach* of ground state species, and the bleach is observed with negative pre-exponential factors. The opposite sign of the third pre-exponential factor indicates that the additional lifetime measures the decay of a process yielding an *increase* in absorption (positive ΔA) upon irradiation. As shown in Scheme 6.1 the decay process is described by the recombination of two monomeric units to form a ground state dimer. The separation of the dimer into two constituent ground state monomer entities is caused by irradiation, resulting in the positive ΔA value. Similar dissociation/re-association behaviour has been observed in dimeric copper and cobalt phthalocyanine species, albeit as a result of photoinduced redox chemistry forming monomeric radical species.[27] The value for τ_3 is 4 μs, indicating recombination is extremely fast compared with the triplet relaxation of monomer and dimer (τ_1 and τ_2 respectively). Example fits obtained in this region are shown in Figure 6.11.

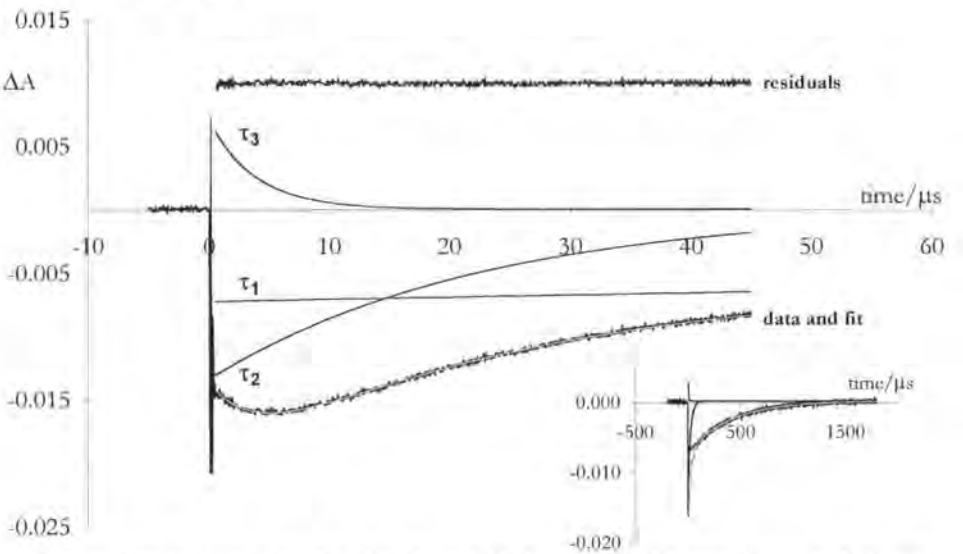

Figure 6.11 Transient decay with fits for **1** at 175 K (λ_{ex} = 615 nm, λ_{probe} = 670 nm). Lifetimes refer to those defined in Scheme 6.1. Inset: decay with fit over long timescale showing full decay of τ_1.

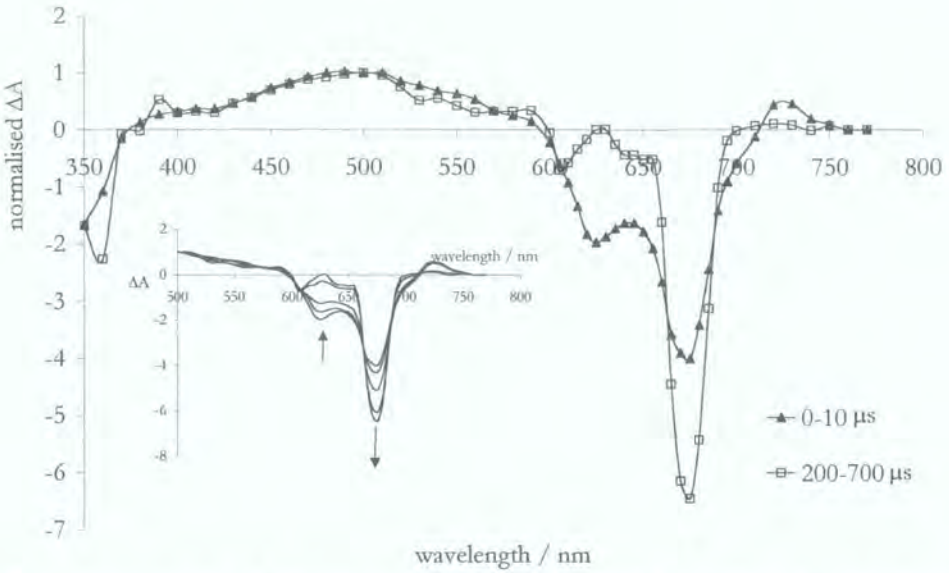

Figure 6.12 Time resolved difference spectrum of **1** in EPA at 175 K (λ_{ex} = 615 nm). Transient decays were integrated between 0-10 μs and 200-700 μs to obtain the spectra shown. Inset: full evolution of bleach area of spectrum with 0-10 μs, 10-20 μs, 20-50 μs, 50-200 μs and 200-700 μs integration times. Arrows indicate spectral changes in direction 0-10 μs → 200-700 μs. All spectra have been normalised to 500 nm.

The spectral separation of the processes with lifetimes τ_1 and τ_2 for **1** at 175 K is possible by using transient difference spectra obtained by integration of the decays between carefully chosen limits (Figure 6.12). The ground state bleach above 600 nm has a broad aggregated profile with strong intensity at 635 nm when monitored at early times after the excitation pulse. This bleach profile becomes increasingly monomeric in character as more time elapses, such that beyond 200 μs it is reminiscent of pure monomer. The magnitudes of τ_1 and τ_2 are in excellent agreement with the observed spectral time dependence - τ_1 is relatively long lived (representing the monomeric triplet-singlet process), whilst τ_2, relating to the dimer triplet-singlet process, is much shorter. Thus the transient spectrum observed at long time delays is that of the monomer triplet state, whilst that of the dimer becomes increasingly apparent at shorter time delays.

The monomer and dimer triplet-singlet processes are represented by the long lifetime (τ_1) and intermediate lifetime (τ_2) components respectively, when monitored at relatively high temperatures (Figure 6.13). As the temperature is lowered beneath the solvent's glass transition temperature, τ_2 shows a dramatic increase in magnitude, such

that at 77 K the lifetime for the dimer process is 500 μs. Below 175 K the concentration of monomer rapidly diminishes, and so the corresponding lifetime, τ_1, becomes increasingly insignificant, such that at 137.5 K τ_1 and τ_2 become difficult to resolve.

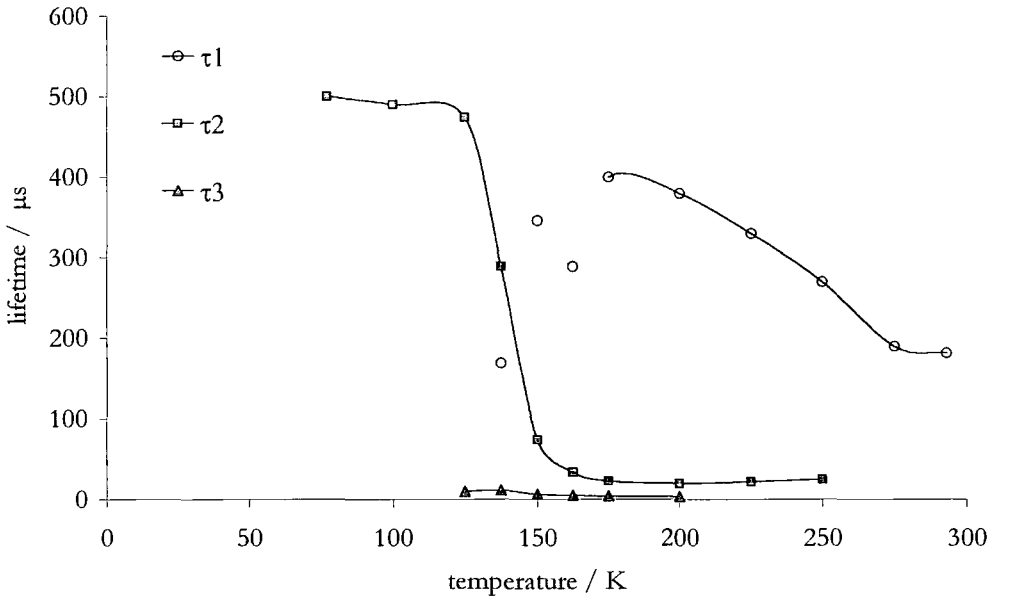

Figure 6.13 Temperature variation in the transient lifetime values obtained for **1**. Lifetimes refer to those defined in Scheme 6.1.

Spectra obtained by analysis of the pre-exponential factors for the monomer-monomer recombination process (with lifetime τ_3) show an interesting dependence upon temperature. At 175 K the profile is broadened and featureless, and apart from its position shows little resemblance to a typical monomeric phthalocyanine absorption band (Figure 6.14). However, upon cooling (to 125 K) the band sharpens considerably, and a vibrational overtone to the blue of the main peak becomes clearly visible - a typical feature of a monomeric phthalocyanine. At intermediate temperatures the band shows broadening to varied extent, the overall profile lying between the two extremes obtained at 175 K and 125 K. It is hypothesised that the featureless profile observed at 175 K results from monomer units which have indistinct and non-static separation. Hence, as a direct consequence of the reduced solvent viscosity, the macrocycle rings oscillate through an equilibrium separation distance, and a time averaged spectrum results. The increased viscosity caused by cooling prevents this dynamic conformation, and so the spectral profile becomes increasingly representative of a true monomeric phthalocyanine.

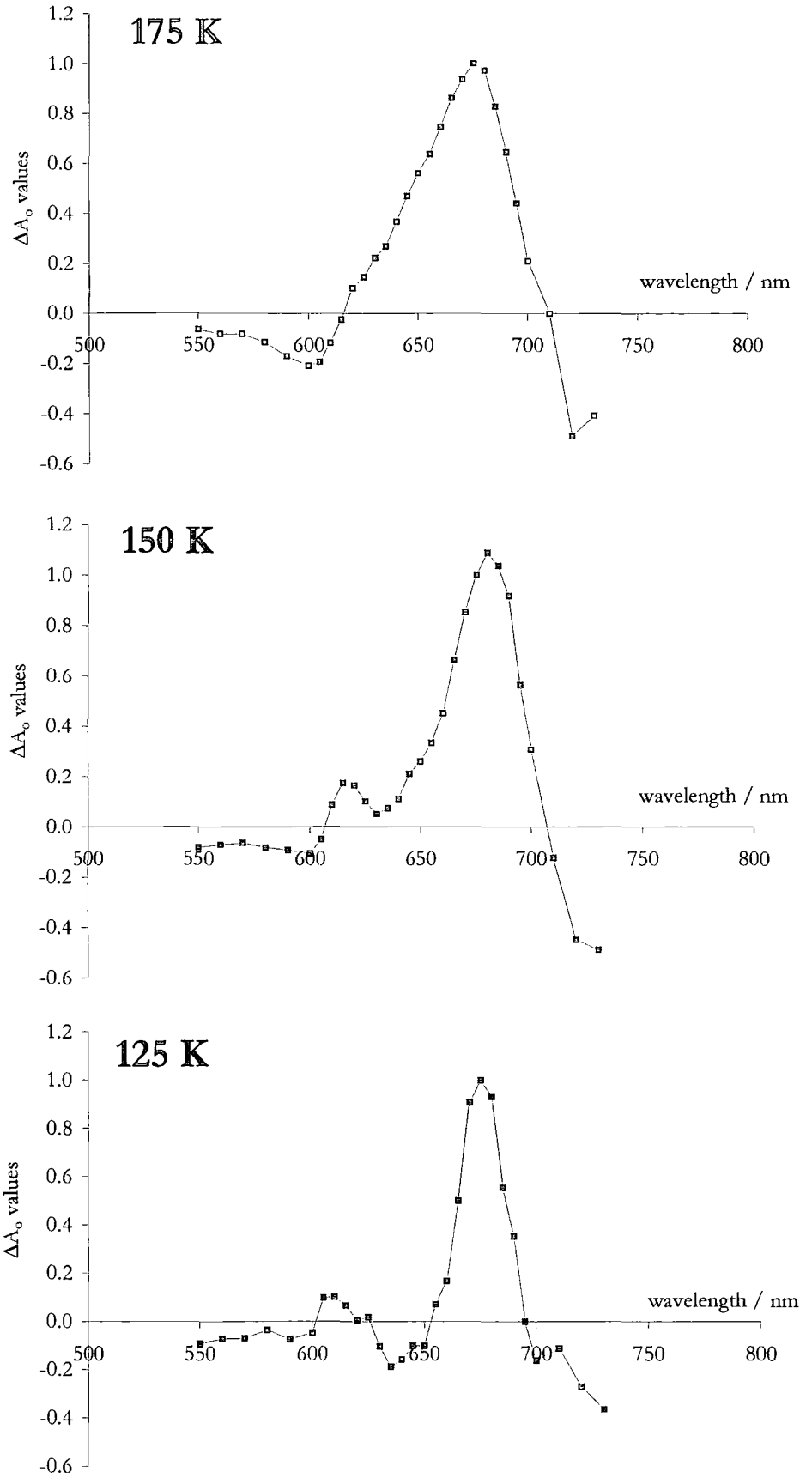

Figure 6.14 Triplet-triplet ΔA_o values for τ_3 as a function of wavelength. Measurements have been made on **1** in EPA at 175 K, 150 K and 125 K.

Compounds **3**-**5** behave similarly to **1** such that at intermediate temperatures three transient processes can be observed, relating to the monomer triplet-singlet, dimer triplet-singlet and monomer-monomer recombination processes described above. However, it is interesting to note that unlike parent compound **1**, **3** and **4** show double exponential behaviour even at 293 K, which is observable in the time resolved difference spectra at that temperature. This relates directly to the degree of aggregation seen in these compounds, their ratios of dimer to monomer emission intensity being higher than the other species studied herein (Table 6.1), and hence there is a more significant dimer contribution at room temperature. This is also reflected in the time resolved difference spectra at 175 K, where there is less monomer bleach contribution, such that even at long time intervals the bleach remains decidedly dimer-like (Figure 6.15).

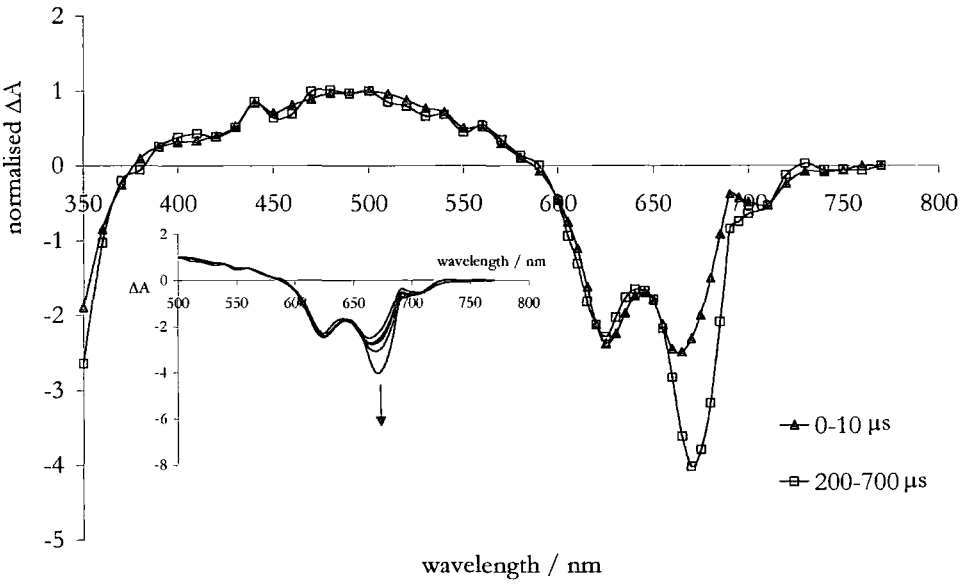

Figure 6.15 Time resolved difference spectrum of **4** in EPA at 175 K (λ_{ex} = 615 nm). Transient decays were integrated between 0-10 μs and 200-700 μs to obtain the spectra shown. Inset: full evolution of bleach area of spectrum with 0-10 μs, 10-20 μs, 20-50 μs, 50-200 μs and 200-700 μs integration times. Arrows indicate spectral changes in direction 0-10 μs → 200-700 μs. All spectra have been normalised to 500 nm.

6.4 Conclusions

A zinc phthalocyanine with peripheral solketal substituents and its derivatives have been demonstrated to form fluorescent dimers in low temperature glasses.[16] At room temperature these species show a strong propensity for aggregation, but otherwise their

behaviour is typical of zinc phthalocyanines. Cooling the solutions results in red and blue shifted absorption and a new emission band centred at 750 nm, which indicates the formation of dimers with a clamshell conformation. The degree of aggregation in each species has been related to its structure - for example, the bulky *tert*-butyl substituents of **5** result in reduced dimer formation relative to the other compounds, whilst **4** shows increased aggregation, possibly as a result of tangling of its long alkyl chains.

The dimer species possess fluorescence lifetimes which show little significant difference from those of the monomer species at room temperature, although a lifetime distribution analysis shows the dimer species to have broader distributions than the monomers. The excitation spectra for the dimer emission show excellent matches with the absorption profiles, and indicate that greater than 95% of the material is in the dimer form. Spectral decomposition for **1** has allowed the estimation of the dimer quantum yield, shown to be 40% that of the monomer at low temperature.

Flash photolysis studies have shown that both the monomer and dimer phthalocyanine species form transient triplet species with very similar spectral profiles. In cold fluid solution (125-175 K) it is possible to observe three processes - monomer triplet formation (and subsequent decay to the singlet state), dimer triplet formation (and subsequent decay to the singlet state) and dimer disaggregation (and subsequent monomer-monomer recombination), each with a characteristic lifetime. Time resolved difference spectra show a change in bleach profile from aggregated to monomeric with increasing time interval between pump and probe, agreeing with the relative magnitudes of the lifetimes observed for these two processes. At the solvent's glass transition temperature the lifetime of the dimer triplet state increases dramatically.

This work provides an in depth study of the extremely rare phenomenon of the formation of fluorescent phthalocyanine dimers. It is generally held that formation of phthalocyanine aggregates results in loss of their beneficial photophysical properties, and in particular their cytotoxicity - however, this current study shows that formation of dimer triplet states is possible, and hence the role of dimers in photodynamic therapy should not be ignored.

6.5 References

1 C. C. Leznoff and A. B. P. Lever (Eds.), *Phthalocyanines – Properties and Applications*, VCH Publishers, Inc., New York, (a) Volume 1, 1989 (b) Volume 2, 1993 (c) Volume 3, 1994, (d) Volume 4, 1996.

2 M. Paardekooper, A. E. V. van Gompel, H. J. G. M. de Bont, J. F. Nagelkerke, J. V. Stevenick and P. J. A. van den Broek, Photodynamic treatment of yeast with chloroaluminium phthalocyanine: role of the monomeric form of the dye, *Photochem. Photobiol.*, 1994, **59**, 161.

3 M. Kasha, H. R. Rawls and M. A. El-Bayoumi, The Exciton Model in molecular spectroscopy, *Pure Appl.Chem.*, 1965, **11**, 371.

4 M. Yoon, Y. Cheon and D. Kim, Absorption and fluorescence spectroscopic studies on dimerisation of chloroaluminum (III) phthalocyanine tetrasulfonate in aqueous alcoholic solutions, *Photochem. Photobiol.*, 1993, **58**, 31.

5 S. Dhami, A. J. de Mello, G. Rumbles, S. M. Bishop, D. Phillips and A. Beeby, Phthalocyanine fluorescence at high concentration: dimers of reabsorption? *Photochem. Photobiol.*, 1995, **61**, 341.

6 Y. Kaneko, T. Arai, K. Tokumaru, D. Matsunaga and H. Sakuragi, Observation of a novel fluorescent dimer of zinc tetrasulphonatophthalocyanine, *Chem. Lett.*, 1996, 345.

7 A. Beeby, S. FitzGerald and C. F. Stanley, Protonation of tetrasulfonated zinc phthalocyanine in aqueous acetonitrile, *Photochem. Photobiol.*, 2001, **74**, 566.

8 E. S. Dodsworth, A. B. P. Lever, P. Seymour and C. C. Leznoff, Intramolecular coupling in metal-free binuclear phthalocyanines, *J. Phys. Chem.*, 1985, **89**, 5698.

9 L. Oddos-Marcel, F. Madeore, A. Bock, D. Neher, A. Ferencz, H. Rengel, G. Wegner, C. Kryschi and H. P. Trommsdorff, Electronic states and relaxation dynamics of silicon phthalocyanine dimers, *J. Phys. Chem.*, 1996, **100**, 11850.

10 A. P. Pellicioli, K. Henbest, G. Kwag, T. R. Carvagno, M. E. Kenney and M. A. J. Rodgers, Synthesis and excited state dynamics of μ-oxo group IV metal phthalocyanine dimers: a laser photoexcitation study, *J. Phys. Chem. A*, 2001, **105**, 1757.

11 C. F. Stanley, *Photophysical evaluation of substituted zinc phthalocyanines as sensitisers for photodynamic therapy*, Ph.D. Thesis, University of Durham, 1997.

12 M. Kasha, Characterization of electronic transitions in complex molecules, *Disc. Faraday Soc.*, 1950, **9**, 14.

13 A. Ferencz, D. Neher, M. Schulze, G. Wegner, L. Viaene and F. C. De Schryver, Synthesis and spectroscopic properties of phthalocyanine dimers in solution, *Chem. Phys. Lett.*, 1995, **245**, 23.

14 C. Farren, S. FitzGerald, A. Beeby and M. R. Bryce, The first genuine observation of a mononuclear fluorescent phthalocyanine aggregate, *Chem. Commun.*, 2002, 572.

15 C. C. Leznoff, S. M. Marcuccio, S. Greenberg, A. B. P. Lever and K. B. Tomer, Metallophthalocyanine dimers incorporating 5-atom covalent bridges, *Can. J. Chem.*, 1985, **63**, 623.

16 S. FitzGerald, C. Farren, C. F. Stanley, A. Beeby and M. R. Bryce, Fluorescent phthalocyanine dimers - a steady state and flash photolysis study, *Photochem. Photobiol. Sci.*, 2002, **1**, 581.

17 F. Wilkinson, D. R. Worrall and L. F. Vieira Ferreira, Photochemistry on surfaces: fluorescence emission of monomers and dimers and triplet state absorption of acridine orange adsorbed on microcrystalline cellulose, *Spectrochim. Acta*, 1992, **48A**, 135.

18 H. Greenspan and E. Fischer, Viscosity of glass-forming solvent mixtures at low temperature, *J. Phys. Chem.*, 1965, **69**, 2466.

19 G. Saito, Tetrachalcogenafulvalenes with outer chalcogeno substituents. Precursors of organic metals, superconductors, LB films, etc. *Pure Appl. Chem.*, 1987, **59**, 999.

20 S. Tai and N. Hayashi, Strong aggregation properties of novel naphthalocyanines, *J. Chem. Soc., Perkin Trans. 2*, 1991, 1275.

21 J. R. Lakowicz, *Principles of Fluorescence Spectroscopy*, Kluwer Academic/Plenum Publishers, New York, 2nd Edition, 1999.

22 G. Porter (ed.), *Chemistry in Microtime*, Imperial College Press, London, 1997.

23 N. J. Turro, *Modern Molecular Photochemistry*, University Science Books, Sausalito, California, 1991.

24 D. A. Fernández, J. Awruch and L. E. Dicelio, Photophysical and aggregation studies of *t*-butyl-substituted Zn phthalocyanines, *Photochem. Photobiol.*, 1996, **63**, 784.

25 (a) S. M. Bishop, A. Beeby, H. Meunier, A. W. Parker, M. S. C. Foley, D. Phillips, The photophysics of disulfonated metallophthalocyanines upon complexation with fluoride, *J. Chem. Soc., Faraday Transactions*, 1996, **92**, 2689. (b) M. Aoudia, G. Cheng, V. O. Kennedy, M. E. Kenney and M. A. J. Rodgers, Synthesis of a series of octabutoxy- and octabutoxybenzophthalocyanines and photophysical properties of two members of the series, *J. Am. Chem. Soc.*, 1997, **119,** 6029.

26 R. W. Chambers, T. Kajiwara and D. R. Kearns, Effect of dimer formation of the electronic absorption and emission spectra of ionic dyes. Rhodamines and other common dyes, *J. Phys. Chem.*, 1974, **78**, 380.

27 G. Ferraudi and E. V. Srisankar, Photochemical redox activity of dimeric and monomeric copper (II) and cobalt (II) sulfophthalocyanines, *Inorg. Chem.*, 1978, **17**, 3164.

SUMMARY

The spectroscopic behaviour of tetrasulfonated zinc phthalocyanine in aqueous acetonitrile has been shown to be pH sensitive, which arises due to protonation on the bridging azomethine units. Protonation causes a decrease in the LUMO energy, resulting in red shifted absorption and emission profiles, and a reduced fluorescence lifetime. Other workers have previously assigned the red shifted bands to a novel fluorescent dimer, but this current work proves this not to be the case.

A detailed study of silicon phthalocyanines with axial methoxybenzene substituents has shown fluorescence quenching through an electron transfer mechanism. The extent of quenching is strongly dependent upon the flexibility and length of the linker which connects the quenching unit and phthalocyanine core Additionally the oxidation potential of the quencher is an important factor in the quenching mechanism - calculations according to Rehm's and Weller's method for electron transfer show good agreement with experimental data.

Related silicon phthalocyanines with pendant tetrathiafulvalene (TTF) units also show quenching by electron transfer, with a similar dependence on linker structure. Interestingly, fluorescence lifetimes remain unperturbed, despite, in some cases, greatly reduced fluorescence quantum yields - a similar phenomenon was also observed with a thiophene substituted phthalocyanine. At low temperature, 77 K, the flexible linkers are frozen into conformations unfavourable for quenching, and dramatic increases in fluorescence quantum yields are seen. Electrochemical oxidation of the TTF units (which occurs selectively, without perturbing the phthalocyanine) results in a reversed electron transfer mechanism, and the macrocycle fluorescence remains quenched.

A solketal substituted zinc phthalocyanine and a number of its derivatives show a strong propensity for aggregation. At 77 K, the absorbance spectrum is greatly broadened, and a new red shifted emission band (~750 nm) is observed, due to a clamshell dimer. The excitation spectra provide excellent matches with the absorption profiles. Flash photolysis studies at intermediate temperatures have highlighted the dynamic nature of the dimer - absorption of a photon causes disaggregation, followed by rapid recombination. Additional observation of monomer and dimer singlet-triplet processes yields up to three observable decay processes, depending upon temperature.

Appendix A

LabVIEW Computer Programming

A.1 Introduction

In 1976 Dr James Truchard began work (in his garage in Austin, Texas, USA) on a product to connect scientific instruments to microcomputers, and within a year had produced and sold the first GPIB (General Purpose Interface Bus) unit.[1] By 1981 the company National Instruments[2] had moved three times to ever larger premises, and saw annual sales in excess of $1 million.

In 1983 Jeff Kodosky started research into a graphical development software, and in 1986 LabVIEW was announced - a software which has revolutionised the way engineers and scientists work. In conjunction with this software development, National Instruments continued to develop new hardware, including plug-in data acquisition (DAQ) boards. At the time of writing National Instruments presents a comprehensive hardware/software catalogue for data acquisition and analysis, industrial automation, vision and motion control, and ready-to-run test executives.

In conjunction with National Instruments DAQ boards, LabVIEW is extensively used for the measurement and acquisition of such spectroscopic data as presented in this thesis. Although LabVIEW comes complete with a wide host of functioning VIs (Virtual Instruments), the power of LabVIEW lies in the ease with which such programmes can be adapted, and new programmes written - with sufficient equipment and hardware almost any application becomes possible.

This appendix contains an overview of LabVIEW programmes developed by the author for use within the Time Resolved Spectroscopy Group at Durham University, together with a detailed study of software allowing complex analysis of flash photolysis data. All virtual instruments were designed to be simultaneously efficient, effective and user friendly.

A.2 A Library of Virtual Instruments

A.2.1 LabVIEW Virtual Instruments

LabVIEW is a graphical programming medium with two levels. The first is the front panel, with a host of switches, buttons, controls and indicators at the disposal of the programmer. The front panel is the user interface. The second level is the diagram panel - each item on the front panel is represented by an icon in the diagram, and data

flow is represented through wires, coloured according to data type (ie, number, string, array, Boolean). The programming takes place through the wiring and the use of mathematical functions represented by icons and a comprehensive library of sub-VIs. Loops (For-Next, While, Case) and controlled sequences are routinely available, allowing programming on many levels.

A.2.2 Triax_190.VI and Triax_320.VI

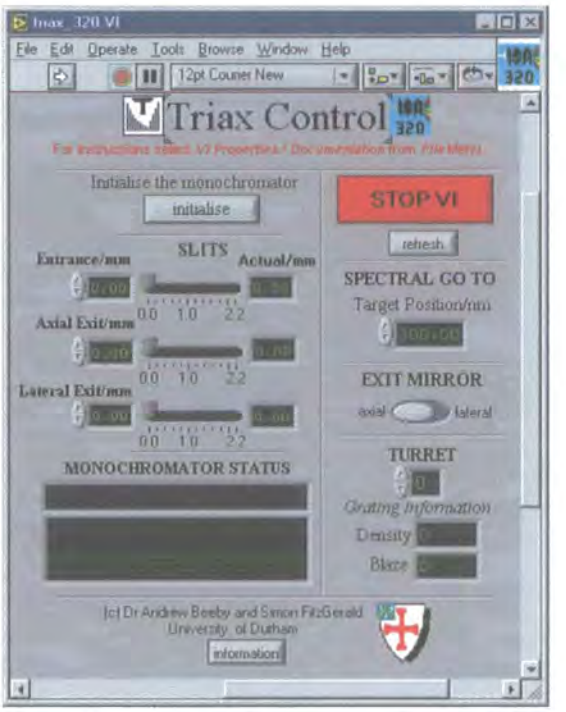

Figure A.1 Front panel of Triax_320.VI.

These two similar programmes allow a complete control interface for the Triax 190 and 320 monochromators (Jobin Yvon, Ltd.[3]). The monochromators are provided with LabVIEW instrument drivers, individual programmes which control one specific function of the monochromator (for example, slits, grating, wavelength, port), but use of these in an experimental setting is cumbersome and time consuming. As a result the Triax control programmes were written to draw together these individual parts into one unit which would allow facile control of the monochromators. Once activated the programmes run continuously - any user implemented change in parameter is immediately detected and acted upon. When the monochromator is in the desired state the programmes assume a 'resting state' in which they merely monitor the user controls

for any change - as a result the CPU requirements in the 'resting state' are negligible, and presents no drain on the computer's resources. The Triax 320 also receives control signals from other software (for example, spectrum acquisition programmes) - changes to the monochromator status implemented by such programmes are undetected by Triax_320.VI when in its 'resting state' (since it monitors its own controls for changes, and not the monochromator hardware). In light of this, a refresh function is provided which causes the programme to interrogate the monochromator, read its current hardware status and update the front panel display. Figure A.1 shows the front panel of Triax_320.VI.

A.2.3 Fluorolog_Integration_and_Correction.VI

Fluorescence quantum yield measurements require repetitive spectral acquisition and analysis, and this programme allows increased efficiency in the analysis of the data. Its main function is to integrate a spectrum recorded on a Fluorolog or Fluoromax spectrofluorimeter (Jobin Yvon, Ltd.[3]) and present a numerical value equivalent to the total emission intensity. By recording a number of spectra with sequential file names it is possible to use this programme to open each sequential file, integrate between chosen wavelength limits, and present the value on screen. Each new calculation on the next file is done at the touch of just one key. In addition, when working with the group's Fluorolog 3 spectrofluorimeter additional spectral correction (at wavelengths greater than 550 nm, not included in the Fluorolog's self correction software) can be incorporated into the calculation.

A.2.4 A Time Resolved Emission Spectroscopy Library

This complete suite of programmes allows the acquisition and analysis of data by the technique of time resolved emission spectroscopy (TRES) on the home built laser pumped fluorimeter (details of which can be found in the experimental chapter, Section 2.5.2 - note that the description provided there is for flash photolysis - TRES was carried out by monitoring the emission rather than the white probe light, but otherwise details remain the same).

The functioning of the acquisition programme is as follows:

1. Set emission wavelength, $\lambda_{em}(1)$, at which to record emission decay.
2. Acquire data on oscilloscope.
3. Wait for a chosen time period to allow averaging on oscilloscope.
4. Read data from Channels 1 and 2 of oscilloscope (note that monochromator settings such as slits, grating and port are all controlled by this programme).
5. Analyse data from oscilloscope. The oscilloscope has different vertical scales on Channels 1 and 2, such that Channel 1 is intended for low intensity readings, and Channel 2 for high intensity readings. According to parameters inputted prior to running the programme, the software takes intensity values at a particular time point of the decay - if that of Channel 1 is greater than the inputted threshold value, Channel 1 is rejected, and data from Channel 2 will be accepted. If that of Channel 1 is less than the threshold, data from that channel will be accepted.
6. Write data to 2D array.
7. Set next emission wavelength, $\lambda_{em}(2)$.
8. Reset oscilloscope.
9. Repeat steps 2-6 until full spectrum (according to input values - start wavelength, stop wavelength and wavelength interval) has been acquired.

The resulting 2D array contains a full emission decay (intensity *vs* time) for each emission wavelength. For a full spectral window with reasonable wavelength step size the array can contain data corresponding to many hundreds of decays - such an array is too large for analysis by conventional spreadsheet software, and so further LabVIEW virtual instruments are required for analysis. Three such programmes allow the user to obtain a full 3D representation of the data, a 2D representation of the emission spectrum at a chosen time point of the decay, and a 2D representation of the emission decay at a chosen emission wavelength.

A.2.5 Flash_Photolysis_Time_Resolved_Analysis.VI

This programme, the design of which is discussed in detail in the next section, provides a full analysis solution for the large data set which the flash photolysis experiment produces. Spectral and temporal analysis is possible, providing insight into the transient

difference and absorption spectra in a time resolved fashion, and calculation of triplet lifetimes, with a variety of fitting models, at any chosen wavelength.

A.3 A Detailed Study - Flash Photolysis

The flash photolysis experiment involves monitoring the transient changes in absorption of white light, as described in Chapter 2. At a given probe wavelength a transient decay of the absorption is acquired, and - as with TRES - a full transient spectrum across a reasonable wavelength range involves the capture and handling of considerable amounts of data. The resulting array of data contains decays at each probe wavelength, across the wavelength range - temporal and spectral analysis is thus desired. Flash_photolysis_time_resolved_analysis.VI has been designed to assist in full analysis of the data at the post acquisition stage (Figure A.2). Features include:

- Automatic reading of sequentially numbered data files.
- Plotting of difference spectrum between chosen time (or channel) limits.
- Spectral addition of ground state absorption to difference spectrum (monitored by first and second derivatives).
- Ability to save difference spectrum after each alteration if required.
- Fitting of transient decays between cursor limits at any chosen probe wavelength.
- A variety of fitting solutions (single, double, triple exponential).

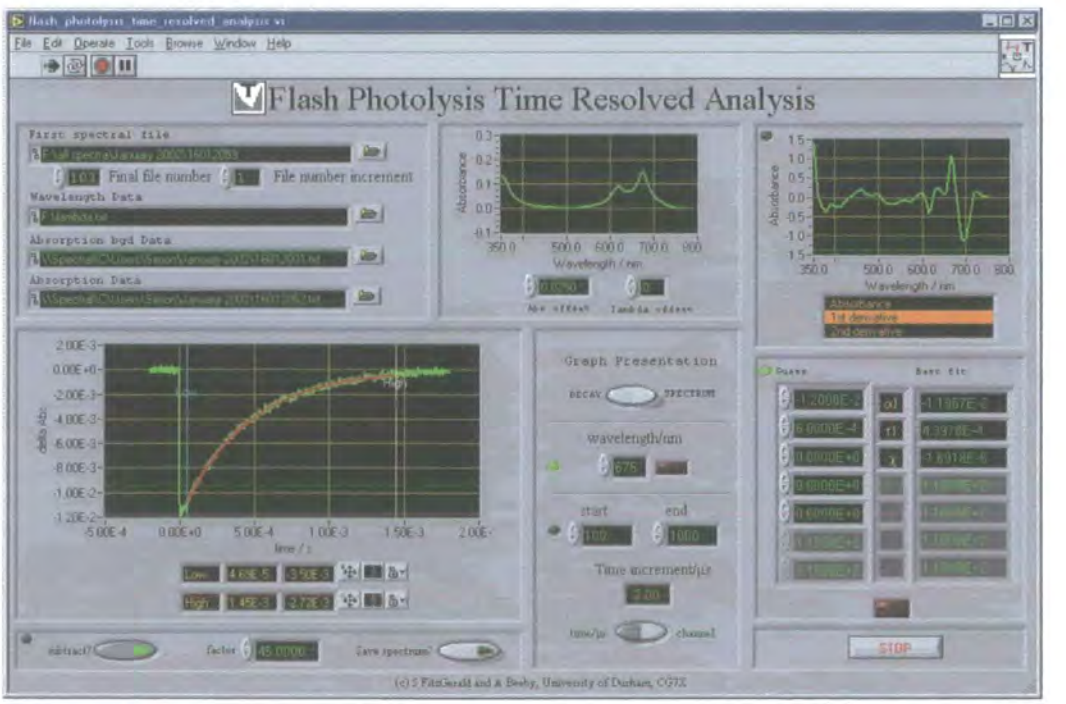

Figure A.2 Front panel of flash_photolysis_time_resolved_analysis.VI.

A.3.1 File Read

The first sequence (Figure A.3) is responsible for reading in all the data files required for analysis.

- Transient decay files - the user browses for the first of the sequentially numbered data files and inputs the number of the final file and the numeric increment. The files must be named in the format: ABCDE$$$ where $$$ represents the sequential numbering of the files (the text description ABCDE can be of unlimited characters length).
- Wavelength data - a 1D array of the probe wavelengths.
- Absorption background file - a 2D array of wavelength and absorption data, corresponding to the solvent background.
- Absorption file - a 2D array of wavelength and absorption data, corresponding to the solution under investigation.

The transient decay files are read in through a loop, each file being individually read, converted to transient absorption units (according to Equation 2.6 in the experimental chapter) and added to a 2D array. Once complete this 2D data array is passed to the next loop, together with the absorption and wavelength data.

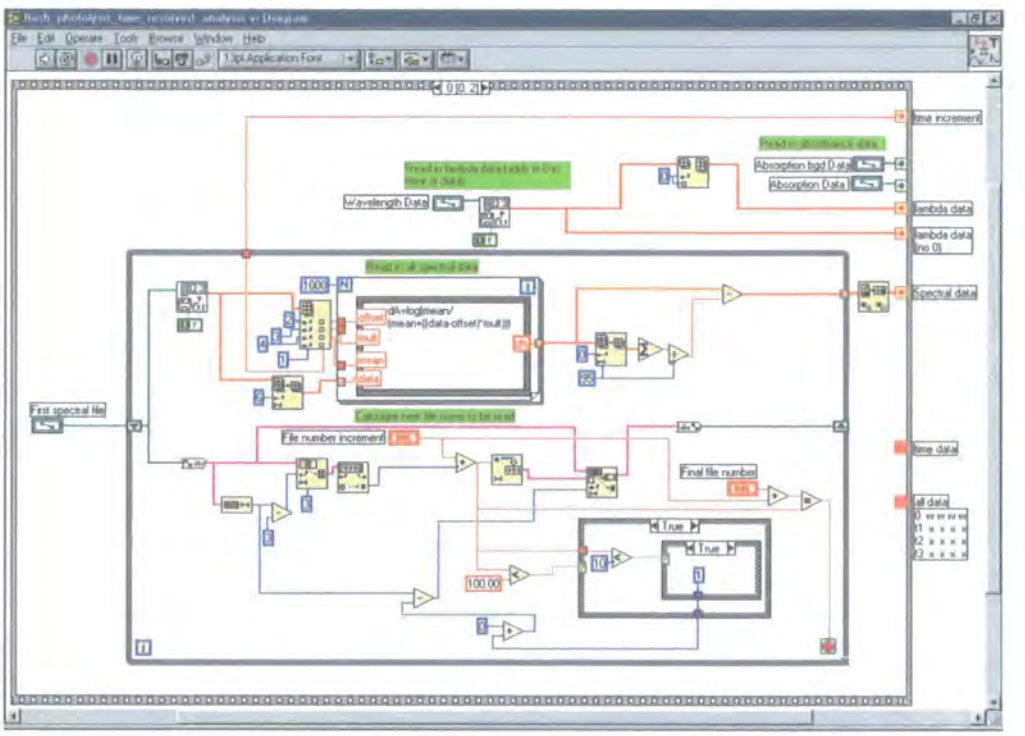

Figure A.3 Sequence 0 of flash_photolysis_time_resolved_analysis.VI.

A.3.2 Array Manipulation

This small sequence (Figure A.4) creates a time scale and adds this and the wavelength data to the transient absorption decay 2D array, resulting in an array of the form:

	Wavelength 1	Wavelength 2 →
Time 1	Data 1.1	Data 1.2
Time 2	Data 2.1	Data 2.2
Time 3	Data 3.1	Data 3.2
↓		↘

The time interval between data points is included within the decay file header read in the first sequence, and this is used to create the time scale for all the data. This time scale comprises 100 pre-trigger data points, plus 900 post-trigger points. The laser pulse occurs at time zero.

Once the array is completed it is passed to the next sequence.

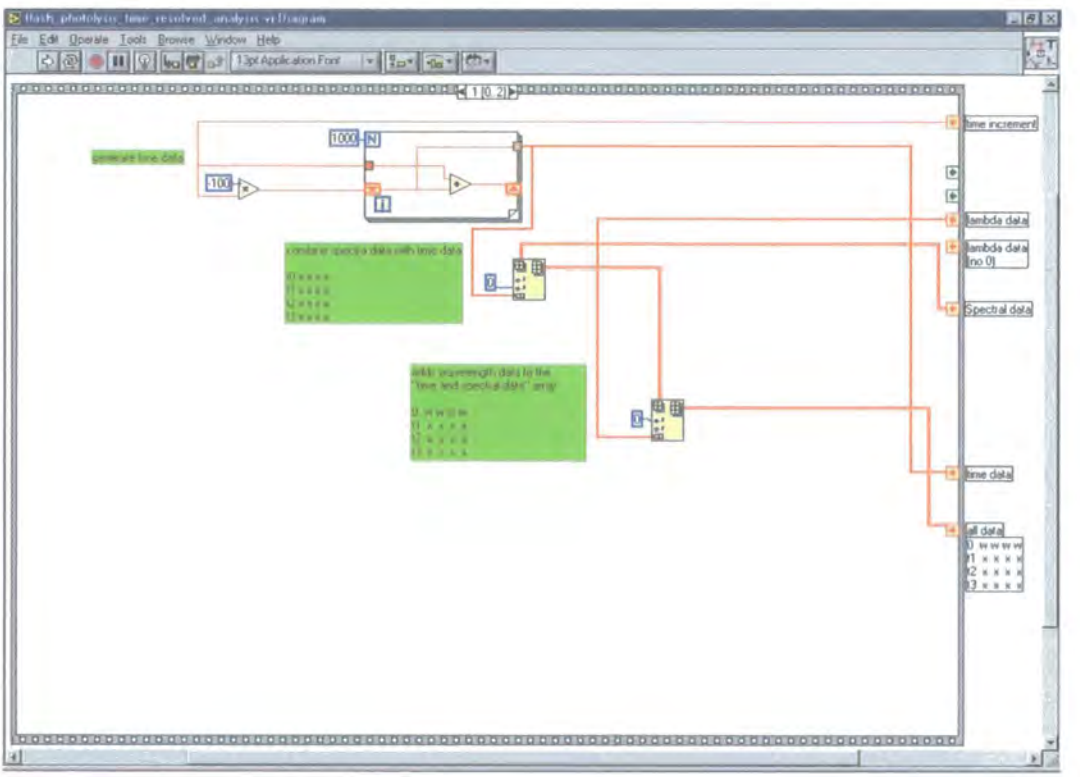

Figure A.4 Sequence 1 of flash_photolysis_time_resolved_analysis.VI.

A.3.3 Analysis

The user can view the data in either spectral or temporal format at any given time, controlled by a simple toggle switch. The analysis functions present in this sequence run in a While Loop, the loop repeating every 2000 ms. This allows continual refinement of analysis without having to reload data each time.

To aid the user in switching between the two functions (spectral or temporal analysis) there are a number of indicators to highlight which controls are operable within the given function. The properties of the shared graph window are similarly function dependent such that axes titles, number format, and line format automatically change upon moving from spectral to temporal analysis and vice versa.

A.3.3.1 Spectral

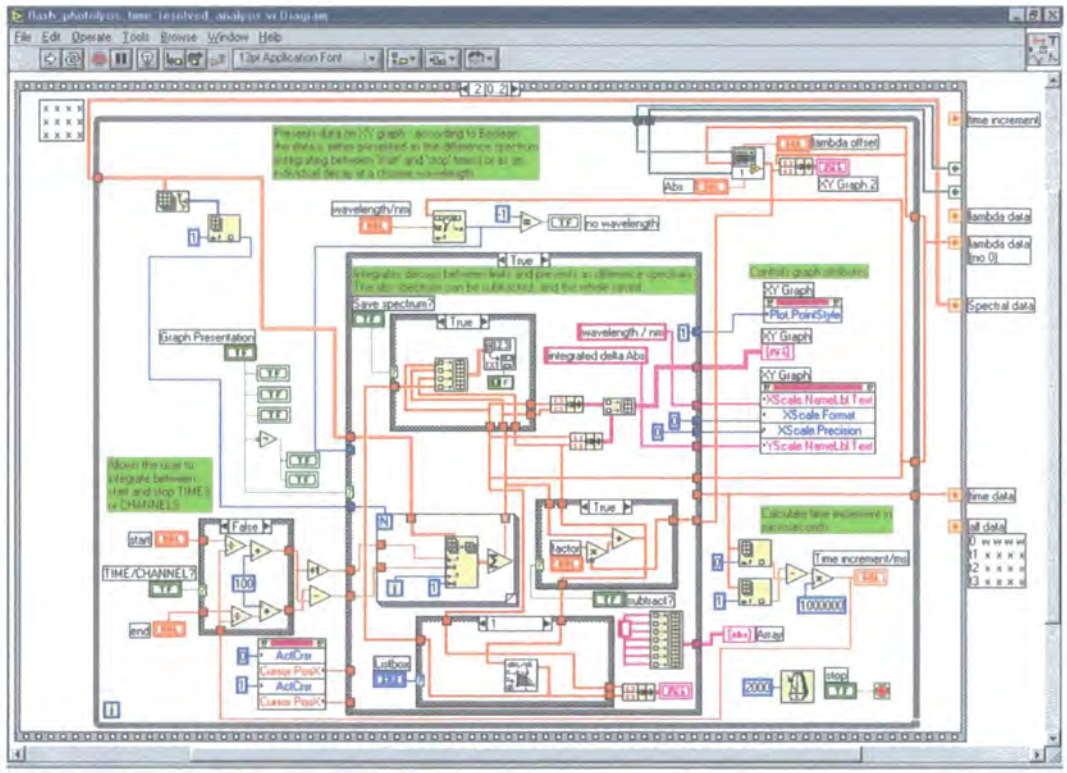

Figure A.5 Sequence 2 (spectral) of flash_photolysis_time_resolved_analysis.VI.

The spectral analysis section of the programme (Figure A.5) performs the following functions:

- Manipulation of the sample and background absorption data to yield a background corrected sample absorption spectrum, with optional X and Y offsets. For clarity in the diagram this manipulation is carried out through a simple sub-VI. Offsets are controlled by user controls on the front panel. The Y offset allows for small correction due to shifted baselines between sample and background. The X offset will be discussed more fully below.
- Graphical presentation of the Δabsorbance *vs* wavelength data. This is achieved by integrating each transient decay at every probe wavelength - the integration takes place between user chosen limits on the decay (either in channels or time units), allowing time resolved spectral presentation, of the form depicted in Figures 6.12 and 6.15 in Chapter 6.

  The graph window shows two concurrent representations of this data, the first the raw difference spectrum, the second the background corrected difference spectrum. Background correction is achieved by adding a small fraction of the ground state sample absorption to the raw difference spectrum. It is vital at this stage that the ground state absorption data is correctly baselined, hence the presence of the Y offset discussed above. The proportion of ground state absorption added to the difference spectrum is defined by a user control.

  Since the ground state absorption spectrum is acquired on a standard UV-visible spectrometer, the bandpass and precise wavelength calibration may differ slightly from that of the flash photolysis spectrometer on which the difference spectrum is recorded. As a result the match of the two spectra in terms of wavelength position may not be perfect, and this becomes particularly noticeable in the Q band region of phthalocyanines, due to the sharpness of this peak. Hence, the X offset for the absorption spectrum is included to allow the user to counter this potential mismatch by shifting the absorption spectrum horizontally, in both a positive and negative fashion.
- First and second derivative calculation. As discussed in Chapter 2, Section 2.5.2, the addition of ground state absorption can be monitored by studying the first and second derivatives of the resulting background corrected difference spectrum. The user has the option of seeing the plain spectrum, its first derivative or its second derivative.

- Data save. The user can, at any point of the spectral analysis, save the graphical data as a 2D array, comprising wavelength, difference and background corrected difference data. The user is prompted for a file name. Once the file is saved the user can continue with further analysis (and further saves if so desired).

A.3.3.2 Temporal

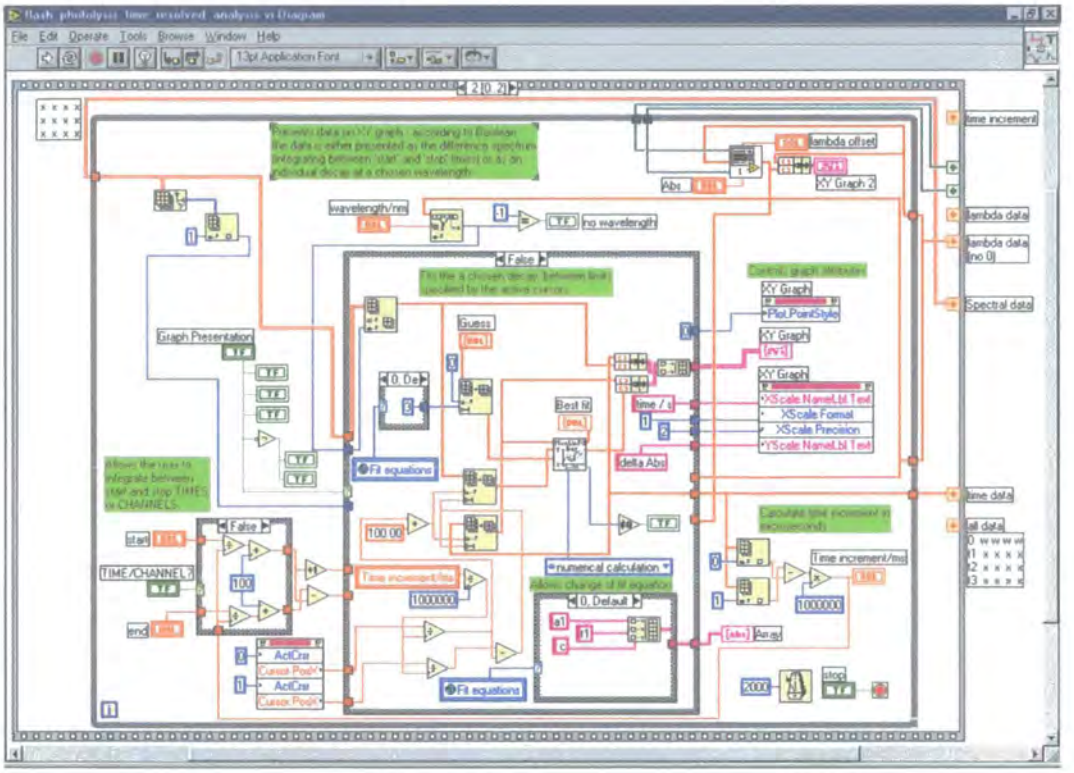

Figure A.6 Sequence 2 (temporal) of flash_photolysis_time_resolved_analysis.VI.

The temporal analysis section of the programme (Figure A.6) performs the following functions:

- Graphical presentation of transient decay of the form intensity *vs* time, at any given probe wavelength chosen by the user.
- Fit of the decay to a chosen model function. The non-linear fitting routine is carried out according to the Levenberg-Marquardt algorithm, provided as part of the standard LabVIEW analysis sub-VIs. This programme requires the input of the model equation and guess parameters, and, if a solution is found, outputs the

fit parameters and data. The fitting model equations are chosen according to a Global Virtual Instrument (Fitting_Global.VI) which contains a selection of different model equations. These equations are written into an inner section of the fitting sub-VI, and the global fitting VI governs which equation the fitting sub-VI uses. As the equation changes, the number of guess parameters also changes, so the user's input controls for the guess parameters include labels. If the fitting model is changed these labels will update. The fitting occurs between user chosen limits, according to cursor positions on the graph.

A.4 Programming Considerations

To produce an effective virtual instrument there are a number of general considerations which are important. The first relates to the actual functioning of the programme, and the computer requirements for this. To minimise the memory requirements for running a particular instrument (and hence, maximise its efficiency) care needs to be taken over data manipulation within loops and sequences. Loops by their nature are repetitive, and unnecessary repetitive functioning is time consuming and memory intensive. Hence, with thought, functions within loops can be reduced to a minimum, and functions not requiring repetitive execution can be kept without the loop.

To be effective, an instrument must be easily approachable by the user. To this effect, all the LabVIEW virtual instruments discussed above have been provided with organised front panels and clear labelling, and, where necessary, instructions for use. It must be remembered that whilst the developer of the programme will know how to run it, others may not. This consideration also applies to the coding behind the front panel - the diagram and its wiring.

In the future, others may need to troubleshoot a particular virtual instrument, or may desire to adapt it for their particularly needs. For this to be possible the diagrams must be organised, logical and clear. As can be seen in Figures A.3 to A.6 the wiring of diagrams within the virtual instruments developed by the author is carefully arranged, and sections are clearly labelled to aid identification of their function.

A.5 Conclusions

LabVIEW provides scientists with an easy to use programming medium with diverse applications, as demonstrated within this Appendix. Its particular strengths lie in its adaptability, allowing new experiments to be made possible, old experiments to be improved, and time to be saved in complex data analysis.

All the programmes written by the author and discussed above are in frequent use within the Time Resolved Spectroscopy Group at Durham, and, additionally, certain instruments have been forwarded to other academic users, both within the United Kingdom and abroad.

A.6 References

1 http://www.ni.com/company/history.htm

2 UK Office: Measurement House, Newbury Business Park, London Road, Newbury, Berkshire, RG14 2PS. http://www.ni.com

3 UK Office: 2 Dalston Gardens, Stanmore, Middlesex, HA7 1BQ. http://www.jyhoriba.co.uk

Appendix B

Visual Basic and Excel Computer Programming

B.1 Introduction - A Deconvolution Spreadsheet

The fitting of a luminescence decay to an exponential decay and hence obtain the lifetime is easily achieved in an Excel programme by using the non-linear fitting routine available within the Solver function. However, such a process is complicated when the lifetime becomes comparable to the width of the excitation pulse – in this case, the measured signal becomes a convolution of both the decay and the excitation profile.[1] Subsequent deconvolution of the measured signal followed by standard fitting represents the obvious solution to this, but true deconvolution is mathematically complex and often unreliable. An easier method is to use a reconvolution and iterative fitting protocol, in which the excitation profile and a theoretical decay function are convoluted, and then compared with the measured practical data. The decay paremeters are changed to find the best fit or correlation between observed and calculated data. It is this method that is used in the deconvolution spreadsheet which is the focus of this Appendix.

The deconvolution software presents a single platform upon which to carry out all the standard fitting routines required in analysing the fluorescence decays obtained from the phthalocyanines discussed in this thesis (Figure B.1).

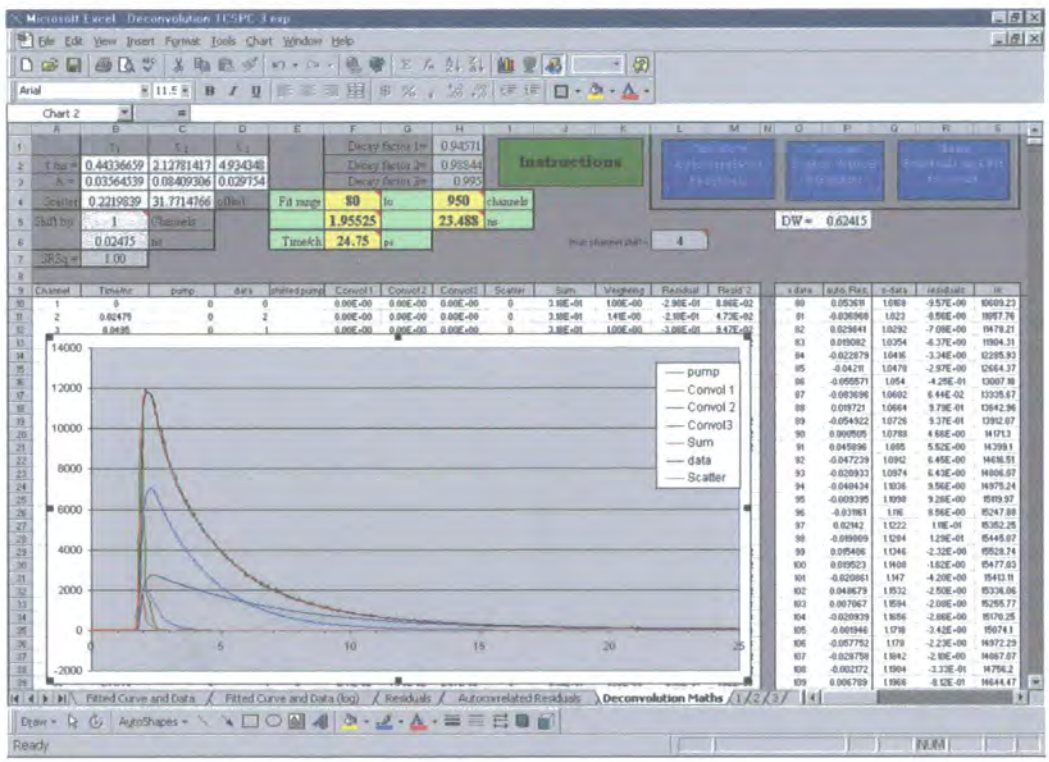

Figure B.1 Analysis page of the deconvolution spreadsheet.

The excitation and decay data are inputted into the sheet, and are then presented on the main graph window. The user must input the 'time per channel' value, in ps, and define the fitting region – all subsequent manipulation of data, fitting and analysis occurs on data lying within this region only. The non-linear fitting process, occurring through the Solver function, allows the user a number of options for the fit:

- Number of exponential decays – provision is made within the sheet for up to three exponential components to be used, with individual lifetimes (τ) and amplitudes (A).
- Scatter – scattered excitation light present in the measured decay can be modelled by adding a small fraction of signal with identical profile to the excitation pulse.
- Offset – a vertical baseline shift; generally only required when obtaining lifetimes with very long acquisition times, in order to remove contribution from low levels of light leakage.
- Shift – the excitation profile is recorded by using a dilute scattering sample, monitoring the excitation wavelength, λ_{ex}, whilst the sample decay is generally monitored at a different wavelength. The different wavelengths will take slightly differing paths through the monochromator (see Chapter 2 for details of equipment used) which can result in a slight shift in the 'zero' position for excitation pulse and sample decay. As a result, the excitation pulse can be shifted by a number of channels (usually up to ±3, but potentially up to ±10) to counter this.

Through the Solver user interface, these functions can be incorporated within the fitting process, or left unaltered, as the user desires. Following a successful fit routine, the user has a number of means of assessing the quality of the fit – the reduced χ^2, the weighted residuals, the Durbin Watson parameter, and the autocorrelated residuals. The first two methods are trivial, and immediately apparent on screen. The reduced χ^2 is obtained according to the equation

$$\chi_R^2 = \frac{\chi^2}{n-p} \qquad \textbf{(B.1)}$$

where

$$\chi^2 = \sum_{i=1}^{n} \frac{[N(t_i) - N_c(t_i)]^2}{N(t_i)} \qquad \textbf{(B.2)}$$

and n is the number of data points, p is the number of floating parameters, $N(t_i)$ is the data, and $N_c(t_i)$ is the calculated decay.[2] The value of the reduced χ^2 tends to unity for a good fit. The weighted residuals are represented simply by

$$r(j) = \frac{N(t_i) - N_c(t_i)}{\sqrt{N(t_i)}} \qquad \textbf{(B.3)}$$

However, the calculation of the Durbin Watson parameter and the autocorrelated residuals require more complex mathematical analysis, and within the spreadsheet this data manipulation is carried out via two dedicated macros (written in Visual Basic) which are discussed in sections B.2 and B.3 below. Finally, the user can present the decay, fit and residuals with improved clarity by use of a third macro, discussed in section B.4.

B.2 The Durbin Watson Parameter

The Durbin Watson parameter was first introduced in the 1950s, and provides a test for serial correlation in linear regression analysis.[3] It is defined as

$$DW = \frac{\sum_{i=n_1+1}^{n_2} [r(t_i) - r(t_{i-1})]^2}{\sum_{i=n_1}^{n_2} [r(t_i)]^2} \qquad \textbf{(B.4)}$$

where $r(t_i)$ and $r(t_{i-1})$ are the residuals at channels i and i-1, and n_1 and n_2 are the first and last channels of the chosen region for the fit.[1] Typically, for a single and double exponential fit, if the Durbin Watson parameter takes values less than 1.70 and 1.75 respectively the quality of fit can be judged as poor.

The Visual Basic coding to calculate this parameter is now presented.

```
Sub DurbinWatson()
'
'Residual AutoCorrelation Calculation obtains Start and Finish
'points in terms of Row number, using the "fit to" range and
'the time per channel(n3 is the total number of cells which are
'be to worked upon)
'
Start = Cells(4, 6) + 9
Finish = Cells(4, 8) + 9
n3 = Finish - Start + 1
'
'the For Next loop obtains sum:R(i)^2 (denominator)
'
total = 0
For i = Start To Finish
    a = Cells(i, 12) ^ 2
    total = total + a
Next i
'
'This For Next loop calculates each individual sum for
'a particular j value
'
total2 = 0
For i = Start + 1 To Finish
    b = (Cells(i, 12) - Cells(i - 1, 12)) ^ 2
    total2 = total2 + b
Next i
'
'Writes the Durbin Watson Parameter to the given cell
'
Cells(5, 16).Select
ActiveCell.Value = total2 / total
Cells(7, 4).Select
End Sub
```

B.3 Autocorrelated Residuals

The autocorrelation function[4] provides a more sensitive means of judging the residuals, according to the equation

$$cr(j) = \frac{\frac{1}{m}\sum_{i=n_1}^{n_1+m-1} r(t_i)r(t_{i+j})}{\frac{1}{n_3}\sum_{i=n_1}^{n_2}[r(t_i)]^2} \qquad \textbf{(B.5)}$$

where $n_3=n_2-n_1+1$, cr(j) is the correlation between the residual in channel i and the residual in channel i+j, where j_{max} is fixed to $n_3/2$ to allow proper averaging. Thus, if there are a 100 fitting channels, j can extend to 50, and i runs from 1 to 50. m is defined as n_3-j.[1]

For a good fit, the autocorrelated residuals shows high frequency low amplitude oscillations about zero.

The Visual Basic routine calculates each cr(j) value individually, and writes this value into a temporary data column on the sheet. Once all the cr(j) values have been calculated, the data is then transferred back into the main user window of the spreadsheet, where it can be viewed within a prepared graph window.

The Visual Basic coding to calculate the autocorrelated residuals is now presented.

```
Sub Autocorrelation()
'
'Residual AutoCorrelation Calculation
'Clears results column prior to adding new data
'
Range("Graph").ClearContents
'
'obtains Start and Finish points in terms of Row number, using
'the "fit to" range and the time per channel
'(n3 is the total number of cells which are be to worked upon)
'
Start = Cells(4, 6) + 9
Finish = Cells(4, 8) + 9
n3 = Finish - Start + 1
'
```

```
'the For Next loop obtains sum:R(y)^2 (denominator)
'
For i = Start To Finish
    a = Cells(i, 12) * Cells(i, 12)
    total = total + a
Next i
'
'obtains jmax
'
jmax = n3 / 2
'
'the For Next loop contains the calculation for various j values
'(numerator)
'
For j = 1 To jmax
   '
   'obtains m
   '
   m = n3 - j
   '
   'This For Next loop calculates each individual sum for a
   'particular j value
   '
    total2 = 0
    For i = Start To (Start + m - 1)
        b = Cells(i, 12) * Cells(i + j, 12)
        total2 = total2 + b
    Next i
    '
    'Writes each particular Cr(j) value into the given cell in
    'column AX
    '
    Cells(j + 9, 50).Select
    ActiveCell.Value = (total2 / m) / (total / n3)
Next j
'
'Copies the required channels from column A and pastes into the
'"x-data" column
'
```

```
Range(Cells(Start, 1), Cells(Start + (Int(n3 / 2) - 1), 1)).Select
Selection.Copy
Range(Cells(10, 15), Cells(10 + (Int(n3 / 2) - 1), 15)).Select
Selection.PasteSpecial Paste:=xlValues
Application.CutCopyMode = False
'
'Copies the autocorrelated residuals in column AX and pastes into
'Auto. Res. column
'
Range(Cells(10, 50), Cells(10 + Int((n3 / 2) - 1), 50)).Select
Selection.Copy
Range(Cells(10, 16), Cells(10 + Int((n3 / 2) - 1), 16)).Select
Selection.PasteSpecial Paste:=xlValues
Application.CutCopyMode = False
Cells(1, 1).Select
End Sub
```

B.4 Graphical Presentation

The graph window within the main user page of the spreadsheet is necessarily complex, with presentation of excitation, experimental, convolutions one to three, scatter and fit data on the one graph. To improve the clarity, two additional graph pages are provided which present just the excitation and experimental data across the full wavelength range, and the fit and residuals within the chosen region of fit only. The first graph presents the data with a normal intensity scale, whilst the second has a logarithmic scale (see Figure B.2).

The data for the fit and residuals, together with the accompanying x data (time), is copied from the main data columns, according to the start and stop limits for the fit region, and pasted into new columns. The graphs then take their data from these new columns, allowing the presentation of the fit and residuals from within the fit region only.

The Visual Basic code required to do this is trivial, and is not presented within this appendix.

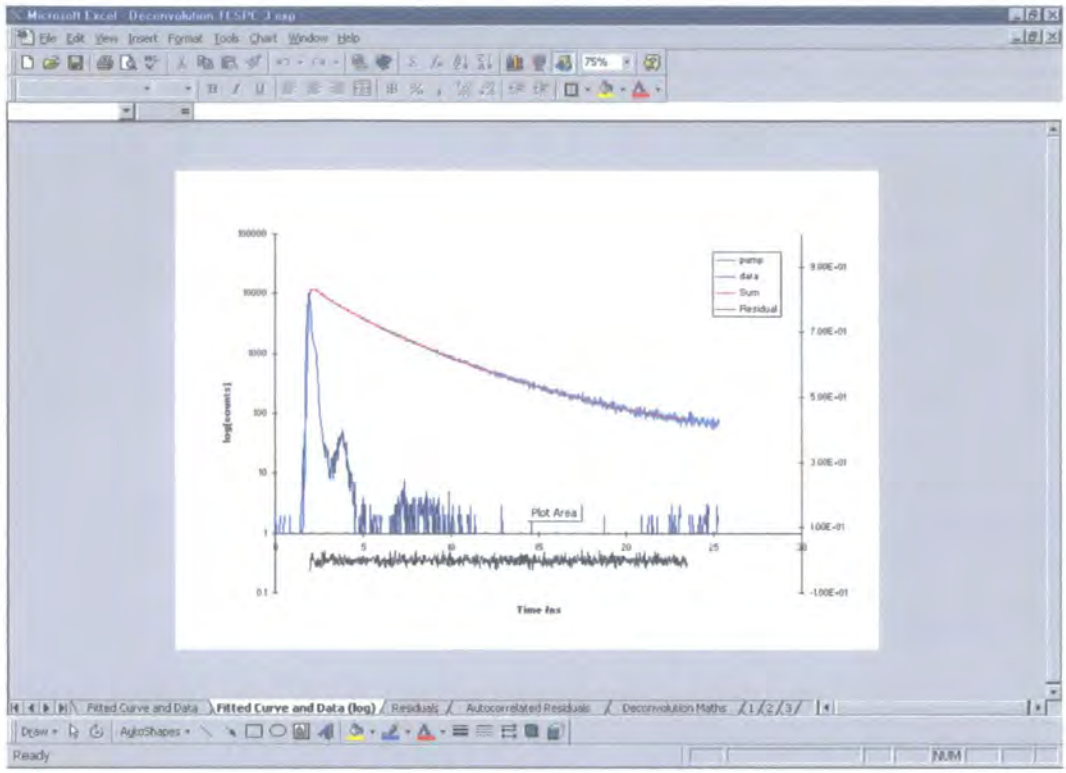

Figure B.2 Logarithmic graphical presentation of data, fit and residuals.

B.5 Spreadsheet Design Considerations

As with the LabVIEW programmes discussed in Appendix A, it was desired that this spreadsheet would allow effective, efficient and user friendly analysis of fluorescence decays. To this end, three help pages have been included, linked to the main user page by buttons controlling simple macros – in particular, these pages provide information concerning the more complex parts of the spreadsheet, that is, the calculation and interpretation of the Durbin Watson parameter and autocorrelated residuals. Additionally, a number of important cells have had labels added, such that hovering the mouse icon above those cells will give information about their use.

B.6 Conclusions

A spreadsheet has been designed which allows the comprehensive analysis of fluorescence decays, including the calculation of the Durbin Watson parameter and autocorrelated residuals, which are vital in judging the goodness of fit. All the phthalocyanine lifetimes presented within this thesis have been obtained using this spreadsheet.

B.7 References

1 D. V. O'Connor and D. Phillips, *Time Correlated Single Photon Counting*, Academic Press, London, 1984.

2 J. R. Lakowicz, *Principles of Fluorescence Spectroscopy*, Kluwer Academic/Plenum Press, New York, 1999, Second Edition.

3 (a) J. Durbin and G. S. Watson, Testing for serial correlation in least squares regression, I, *Biometrika*, 1950, **37**, 409; (b) J. Durbin and G. S. Watson, Testing for serial correlation in least squares regression, II, *ibid.*, 1951, **38**, 159.

4 A. Grinvald and I. Z. Steinberg, On the analysis of fluorescence decay kinetics by the method of least-squares, *Anal. Biochem.*, 1974, **59**, 583.

Appendix C

Publications, Posters Presented, Conference and Seminars Attended

C.1 Publications

- **Synthesis of novel phthalocyanine-tetrathiafulvalene hybrids; intramolecular fluorescence quenching related to molecular geometry**
  C. Farren, C. A. Christensen, S. FitzGerald, A. Beeby and M. R. Bryce
  Journal of Organic Chemistry, submitted April 2002.
- **Fluorescent phthalocyanine dimers: a steady state and flash photolysis study**
  S. FitzGerald, C. Farren, C. F. Stanley, A. Beeby and M. R. Bryce
  Photochemical and Photobiological Sciences, 2002, **1**, 581
- **The first genuine observation of mononuclear fluorescent phthalocyanine aggregates**
  C. Farren, S. FitzGerald, M. R. Bryce and A. Beeby
  Chemical Communications, 2002, 572
- **Visible to infra-red luminescence from 28 atom gold clusters**
  S. Link, A. Beeby, S. FitzGerald, M. El Sayed, M. G. Schaaf and R. L. Whetten
  Journal of Physical Chemistry B, 2002, **106**, 3410
- **Generation of cytotoxic singlet oxygen via phthalocyanine-stabilized gold nanoparticles: a novel vehicle for photodynamic therapy**
  D. C. Hone, P. I. Walker, R. Evans-Gowing, S. FitzGerald, A. Beeby, M. J. Cook and D. A. Russell
  Langmuir, 2002, **18**, 2985
- **Synthesis, structure and optical characterisation of silicon phthalocyanine bis-esters**
  C. Farren, S. FitzGerald, M. R. Bryce, A. Beeby and A. Batsanov
  Journal of the Chemical Society, Perkin Transactions 2, 2002, 59
- **Octaalkynyltetra[6,7]quinoxalinoporphyrazines: a new class of photosensitisers with potential for photodynamic therapy**
  F. Mitzel, S. FitzGerald, A. Beeby and R. Faust
  Chemical Communications, 2001, 2596
- **A photophysical study of the protonation of tetra-tert-butyl phthalocyaninato zinc**

A. Beeby, S. FitzGerald and C. F. Stanley

Journal of the Chemical Society, Perkin Transactions 2, 2001, 1978

- **Protonation of tetrasulfonated zinc phthalocyanine in aqueous acetonitrile solution**

  A. Beeby, S. FitzGerald and C. F. Stanley

  Photochemistry and Photobiology, 2001, **74**, 566

- **Porphyrin sensitization of circularly polarised near-IR lanthanide luminescence: enhanced emission with nucleic acid binding**

  A. Beeby, R. S. Dickins, S. FitzGerald, L. J. Govenlock, C. L. Maupin, D. Parker, J. P. Riehl, G. Siligardi, J. A. G. Williams

  Chemical Communications, 2000, 1183

C.2 Posters Presented

- **The first genuine observation of a fluorescent phthalocyanine dimer**

  S. FitzGerald, C. Farren, A. Beeby and M. R. Bryce

  ICI Postgraduate Poster Competition, Department of Chemistry, University of Durham, December 2001

- **Protonation of tetrasulfonated zinc phthalocyanine**

  A. Beeby and S. FitzGerald

  Fast Reactions in Solutions 2000, University of Durham, August 2000

C.3 Conference Attended

- **Fast Reactions in Solutions 2000**

  University of Durham

  27th-30th August 2000

C.4 Seminars Attended

C.4.1 2001/2002

- **Photonic crystals in a flash**
  Professor B. Denning, University of Oxford
- **Towards benign supramolecular chemistry: synthesis and self-organisation**
  Professor C. Raston, University of Leeds
- **Size is everything**
  Doctor I. Fallis, University of Cardiff
- **Control over polymeric materials at the nanometer level**
  Professor W. T. S. Huck, University of Cambridge
- **Chemistry in a spin - effects of magnetic fields on chemical reactions**
  Doctor P. J. Hore, University of Oxford
- **Phthalocyanine containing new materials**
  Doctor N. McKeown, University of Manchester
- **Laser probing the gas phase chemistry involved in diamond CVD**
  Professor M. Ashfold, University of Bristol

C.4.2 2000/2001

- **Recent developments in organic LED technology: organolanthanide phosphors**
  Doctor V. Christou, University of Oxford
- **Science, art and drug discovery - a personal perspective**
  Doctor S. F. Campbell, formerly of Pfizer
- **Cosmic: a universal DNA based language**
  Doctor J. Cox, University of Bath
- **Life, death and the carotenoids**
  Professor T. G. Truscott, University of Keele
- **Dual activation approaches to electroanalysis: ultrasound, microwave and laser activation**
  Professor R. Compton, University of Oxford

- **"Why should we bother with science anyway?"**
  Professor C. Stirling, University of Sheffield
- **Chemical integrated circuits: organic synthesis and analysis on a small scale**
  Doctor A. de Mello, Imperial College, London
- **The measurement revolution**
  D. Baker, National Instruments UK
- **Liquid crystals of all shapes and sizes**
  Professor R. Richardson, University of Bristol
- **Photonic switch technology**
  G. Henshall, Nortel Networks
- **Luminescent transition metal complexes for chemical sensing**
  Doctor J. A. G. Williams, University of Durham
- **Escapades with arenes and transition metals: from laser spectroscopy to synthetic applications**
  Professor R. Perutz, University of York

C.4.3 1999/2000

- **Tailor made cage molecules for the selective bindings of metal ions**
  Professor K. Gloe, TU Dresden, Germany
- **Aspects of complexation and supramolecular chemistry**
  Professor S. Lincoln, University of Adelaide, Australia
- **Conjugated polymers in the market place**
  Professor A. Holmes, University of Cambridge
- **An introduction to circular dichroism - probing bimolecular interactions**
  Doctor G. Siligardi, King's College, London
- **Atomic and molecular control of inorganic and organic semiconductor thin films**
  Professor T. Jones, Imperial College, London
- **Fireworks - principles and practice**
  Reverend R. Lancaster
- **Shape and stereoselectivity in polymers**
  Doctor S. Moratti, University of Cambridge

- **Measurement and Automation**

  G. McNaught, National Instruments UK
- **A little light relief**

  Professor D. Phillips, Imperial College, London
- **Asymmetric synthesis using planar chiral π-allyl cationic complexes**

  Professor Kocienski, University of Glasgow
- **The flow of polymer blends**

  Doctor N. Clarke, UMIST
- **Computer simulation of interfaces: fact or friction?**

  Professor D. Tildsley, Unilever
- **Curiosity and simplicity - essential ingredients for new reactions**

  Professor W. Motherwell, University College, London
- **Chiral analysis using chiral liquid crystal NMR solvents**

  Professor J. Cortieau, Paris-Sud University
- **Design of molecules for two-photon absorption and their application to 3D polymerisation and imaging**

  Professor S. Marder, University of Arizona, USA
- **Carbon toys**

  Doctor P. Low, University of Durham
- **Advanced materials by acetylenic scaffolding: rods, rings and structures**

  Professor F. Diederich, ETH, Zurich